DECONVOLUTION OF VARIABLE RATE RESERVOIR PERFORMANCE DATA USING B-SPLINES

A Thesis

by

DILHAN ILK

Submitted to the Office of Graduate Studies of
Texas A&M University
in partial fulfillment of the requirements for the degree of

MASTER OF SCIENCE

December 2005

Major Subject: Petroleum Engineering

DECONVOLUTION OF VARIABLE RATE RESERVOIR PERFORMANCE DATA USING B-SPLINES

A Thesis

by

DILHAN ILK

Submitted to the Office of Graduate Studies of
Texas A&M University
in partial fulfillment of the requirements for the degree of

MASTER OF SCIENCE

Approved by:

Co-Chairs of Committee,	Thomas A. Blasingame
	Peter P. Valko
Committee Member,	Ali Beskok
Head of Department,	Stephen A. Holditch

December 2005

Major Subject: Petroleum Engineering

ABSTRACT

Deconvolution of Variable Rate Reservoir Performance Data Using B-Splines. (December 2005)
Dilhan Ilk,
B.S., Istanbul Technical University
Co-Chairs of Advisory Committee: Dr. Thomas A. Blasingame
Dr. Peter P. Valko

This work presents the development, validation and application of a novel deconvolution method based on B-splines for analyzing variable-rate reservoir performance data. *Variable-rate deconvolution is a mathematically unstable problem* which has been under investigation by many researchers over the last 35 years. While many deconvolution methods have been developed, few of these methods perform well in practice — and the importance of variable-rate deconvolution is increasing due to applications of permanent downhole gauges and large-scale processing/analysis of production data. Under these circumstances, our objective is to create a robust and practical tool which can tolerate reasonable variability and relatively large errors in rate and pressure data without generating instability in the deconvolution process.

We propose representing the derivative of unknown unit rate drawdown pressure as a weighted sum of B-splines (with logarithmically distributed knots). We then apply the convolution theorem in the Laplace domain with the input rate and obtain the sensitivities of the pressure response with respect to individual B-splines after numerical inversion of the Laplace transform. The sensitivity matrix is then used in a regularized least-squares procedure to obtain the unknown coefficients of the B-spline representation of the unit rate response or the well testing pressure derivative function. We have also implemented a physically sound regularization scheme into our deconvolution procedure for handling higher levels of noise and systematic errors.

We validate our method with synthetic examples generated with and without errors. The new method can recover the unit rate drawdown pressure response and its derivative to a considerable extent, even when high levels of noise are present in both the rate and pressure observations. We also demonstrate the use of regularization and provide examples of under and over-regularization, and we discuss procedures for ensuring proper regularization.

Upon validation, we then demonstrate our deconvolution method using a variety of field cases. Ultimately, the results of our new variable-rate deconvolution technique suggest that this technique has a broad applicability in pressure transient/production data analysis. The goal of this thesis is to demonstrate that the combined approach of B-splines, Laplace domain convolution, least-squares error reduction, and regularization are innovative and robust; therefore, the proposed technique has potential utility in the analysis and interpretation of reservoir performance data.

DEDICATION

This work is dedicated:

To my family — my mother, Yuksel Ilk, my father, Aytac Ilk, and my brother, Noyan Ilk, for their unlimited love — and for all they have done for me;

To my mentors, Dr.Thomas A.. Blasingame, and Dr. Peter.P. Valko for their influence on me;

To my friends, Feyza Berber, Ayse Nazli Demiroren, and Cansin Yaman Evrenosoglu;

To the researchers who are trying to find a solution to the "inverse problem" which is never going to be solved.

"*Opening all the windows to the sea so that the written word flies off*"

— Pablo Neruda

ACKNOWLEDGEMENTS

The author would like to thank the following for their contributions to this work:

Dr. Thomas A. Blasingame, co-chair of my advisory committee, for his influence, guidance, full support, and providing me the financial support to pursue my M.S. degree at Texas A&M University;

Dr. Peter P. Valko, co-chair of my advisory committee, for his creativity, intelligence, and efforts to help me to bring this thesis into completion;

Dr. Ali Beskok, for his advice and suggestions; and for his service as a member of my graduate advisory committee;

Fekete Associates and Louis Mattar for their enthusiasm; and providing me the opportunities to improve this research;

My friends in 611: Shahram Amini, Caroline Huet, Mansur Zhakupov, and Nima Hosseinpour-Zoonozi, for their support.

TABLE OF CONTENTS

Page

Page

LIST OF FIGURES

FIGURE Page

FIGURE Page

FIGURE Page

LIST OF TABLES

CHAPTER I

INTRODUCTION

1.1 Introduction

The constant-rate drawdown pressure behavior of a well/reservoir system is the primary signature used to classify/establish the characteristic reservoir model. Transient well test procedures are typically designed to create a pair of controlled flow periods (a pressure drawdown/buildup sequence), and to convert the last part of the response (the pressure buildup) to an equivalent constant-rate drawdown via special time transforms. However, the presence of wellbore storage, previous flow history, and rate variations may mask or distort characteristic features in the pressure and rate responses.

With the ever increasing ability to observe downhole rates, it has been long recognized that variable-rate deconvolution should be a viable option to traditional well testing methods because deconvolution can provide an equivalent constant-rate response for the entire time span of observation. This potential advantage of variable-rate deconvolution has become particularly obvious with the appearance of permanent down-hole instrumentation.

In this work we provide a new deconvolution technique using B-splines for representing the derivative of unknown constant-rate drawdown pressure and numerical inversion of the Laplace transform is utilized in our formulation. When significant errors and inconsistencies are present in the data functions, the direct and indirect regularization methods (*i.e.*, mathematical "uniformity" processes) are used. We validate our method with synthetic examples generated with and without errors. For cases of zero noise, the new technique recovers the unit rate drawdown pressure response and its derivative very accurately — in an essentially exact manner. We note that this methodology performs very well in the presence of high levels of noise in the rate and pressure observations. Upon validation, we then demonstrate our deconvolution method using a variety of field cases — including traditional well tests, permanent downhole gauge data as well as production data.

1.2 Objectives

The primary objectives of this work are:

- To develop and validate a new deconvolution method based on B-spline representations of the derivative of unknown constant rate drawdown pressure response (*i.e.*, the undistorted pressure response).

This thesis follows the style and format of the *SPE Journal*.

- To create a practical and robust deconvolution tool that can tolerate relatively large (random) errors in the input rate and pressure functions. The proposed process should also be capable of tolerating small systematic errors in the input functions (via calibrated regularization).
- To apply this new method to traditional variable-rate/ pressure problems, such as wellbore storage distortion, long-term production data, permanent downhole (pressure) gauge data, and well tests having multiple flow sequences.

1.3 Statement of the Problem

Duhamel's principle states that the observed pressure drop is the convolution of the input rate function and the derivative of the constant-rate pressure response — at t=0 the system is assumed to be in equilibrium (*i.e.*, $p(r,t=0) = p_i$). In the petroleum engineering literature, the variable rate well/reservoir pressure response is defined as the "convolution" integral by the following:

$$\int_0^t q(t-\tau)\,p_u'(\tau)\,d\tau = \Delta p(t) \quad \text{.....(1.1)}$$

The goal of variable-rate deconvolution is to estimate the unit (*i.e.*, constant) rate reservoir response using observed measurements of pressure drop and flowrate. This objective leads us to the *inverse problem* in which the time dependent "input signal" (constant-rate pressure response) must be extracted from the output signal (pressure drop response distorted by the specified variable-rate profile). To reconstruct the unknown function (*i.e.*, the derivative of the unit rate reservoir pressure response ($K(t) = p_u'(t)$), we require the solution of the Volterra integral equation of the first kind (*i.e.*, the convolution integral), where the role of the *convolution kernel* is represented by the sandface rate.

Essentially, *variable-rate deconvolution is mathematically ill-conditioned* — while numerous methods have been developed and applied to deconvolve "ideal" data — very few deconvolution methods perform well in practice. The ill-conditioned nature of the deconvolution problem means that small changes in the input data cause large variations in the deconvolved constant-rate pressures. Mathematically, we are attempting to solve a first-kind Volterra equation, that is ill-posed[1]. However, in our case the kernel of the Volterra-type equation is the flowrate function (*i.e.*, the generating function) and it is not known analytically, but rather, is approximated from the observed flowrates, and in practical terms, this issue adds to the complexity of the problem.

In the literature related to variable-rate deconvolution we find the development of two basic concepts. One concept is to incorporate an *a priori* knowledge regarding the properties of the deconvolved constant-rate response. The second concept is to use a certain level of regularization — where "regularization" is

defined as the act/process of making a system regular or standard (smoothing or eliminating non-standard/irregular response features). Regularization can be performed indirectly by representing the desired solution using a restricted number of "elements" — or directly by *penalizing* the "non-smoothness" of the solution.

In addition to these main features, individual deconvolution algorithms may have other distinctive features. From a numerical standpoint, recent deconvolution methods tend to use advanced techniques to solve the underlying system of linear equations. One class of approaches makes extensive use of transformations (*i.e.*, the Laplace transform, the Fourier transform, etc.).

Formally, it would be easy to place our proposed method into existing categories. Our proposed approach uses B-splines, numerical inversion of the Laplace transform is also used for certain components of the solution, regularization is provided indirectly (*i.e.*, by the number of knots used in the selected B-spline) and directly (by penalizing the non-smoothness of the logarithmic derivative of the reconstructed constant-rate response).

However, in detail our approach is radically different from any of the the existing methods — in contrast to previous methods our approach does not fit B-splines to observed data. Rather, B-splines are used to represent the unknown response solution (*i.e.*, as a linear combination of B-splines). With respect to the Laplace transform, our approach does not use the Laplace transform to transform the *observed* pressure data series nor does our approach use numerical inversion to provide the objective response (*i.e.*, the constant rate response) as do other spectral methods. In our approach, the application of numerical inversion of the Laplace transform is restricted to the construction of the sensitivity matrix for the least-squares problem.

Our new technique represents the derivative of the *unknown constant-rate drawdown pressure response* as a weighted sum of B-splines, using logarithmically-distributed knots. For the discrete flowrate function, we use piecewise constant, piecewise linear, or any other appropriate representation for which the Laplace transform can be easily obtained. Taking the Laplace transform of the B-splines, we then apply the convolution theorem in the Laplace domain and we calculate the sensitivities of the *observed pressure response* with respect to the B-spline weights by numerical inversion of the Laplace transform.

Finally, the sensitivity matrix is used in conjunction with a least-squares criterion to yield the sought B-spline weights and the unit-rate response (the spline formulation) — which then yields the well testing derivative functions in the real domain. The combined approach of B-splines, Laplace domain convolution, and the least-squares procedure are innovative and robust — and should find numerous

applications in the petroleum industry (production and well test data analysis, inversion of water influx behavior, etc.).

1.4 Validation and Application

We provide an inclusive validation procedure that makes use of a simulated reservoir model (*i.e.*, case where we know the input and output responses), as well as field data obtained from the petroleum literature and industry sources. Our validation includes the cases where we corrupt the data generated by simulation with high levels of error (up to 40 (forty) percent). In addition, we demonstrate the various applications of our method with validation examples. We discuss the procedures of eliminating noise in the input data by direct/indirect regularization methods.

As mentioned before, we generate pressure drop response data distorted by variable rate data using analytical simulation by selecting a reservoir model — dual porosity reservoir model for its strong characteristic features for our purposes. Upon validation without errors in the input data, we then corrupt the generated data with error levels up to 40 (forty) percent and validate the method with error presence in the input data. For field applications we use; 1 (one) case for removing wellbore storage effects, 2 (two) cases having multiple flow sequences, 1 (one) case for analyzing permanent downhole gauge data and 3 (three) cases having long term production history. Furthermore, we present additional field examples in Appendix F.

1.5 Summary and Conclusions

We have achieved a unique deconvolution technique using B-splines, Laplace domain convolution and weighted least squares. We have also implemented a regularization scheme in our deconvolution technique for handling higher levels of noise in the input data.

We use the linear combination of B-splines for representing the derivative of unknown constant rate pressure response function. Taking the Laplace transform of the convolution integral, we reduce the deconvolution problem into a linear system of equations where we are solving for the B-spline coefficients. The sensitivity matrix in the linear system of equations is computed by taking the inverse Laplace transform of the product of the B-splines and rate function. No functions are fitted (*i.e.* no spectral transformation is required) to the observed (measured) pressure data — distorted by variable rate effects. The resulting linear system of equations is solved by means of weighted least squares. When the level of noise is high in the input data, additional regularization is performed by imposing constraints on the change of logarithmic derivative of the B-splines between the knot locations.

We have validated this approach with synthetic examples generated with and without errors (errors level up to 40 percent) of increasing complexity. Upon validation, we then demonstrate our deconvolution

method using a variety of field cases — including traditional well tests, permanent downhole gauge data as well as production data. It is seen that for field applications a regularization scheme is required to ensure a stable deconvolution.

Our work suggests that the new deconvolution method has broad applicability in variable rate/pressure problems — and can be implemented in typical well test and production data analysis applications.

1.6 Future Efforts

The following future efforts are recommended:

- Regularization: Continue efforts using regularization for "noisy" data.
- Rate Deconvolution: By rate deconvolution (variable pressure deconvolution instead of variable rate deconvolution) constant pressure rate response function can be obtained for production data analysis. Our future efforts will include establishing a stable rate deconvolution algorithm.
- Wellbore Storage: Direct deconvolution of wellbore storage data when the sandface rates are not available.
- Computational Purposes: Use alternatives for B-splines for decreasing computational time (*e.g.* linear combination of exponential functions).

1.7 Organization of the Thesis

The outline of the proposed research thesis is as follows:

- Chapter I — Introduction
  - Research Objectives
  - Statement of Research Problem
  - Summary
- Chapter II — Literature Review
  - Convolution and Superposition
  - Rate Normalization and Material Balance Deconvolution
  - Deconvolution
- Chapter III — Development of the New B-Spline Based Deconvolution Method
  - B-splines
  - Algorithm Development
  - Flow Rate Considerations
  - Decoupling the Constant-Rate Response and Its Logarithmic Derivative
  - Regularization
- Chapter IV — Validation
  - Input Data Generation for B-Spline Based Deconvolution
  - B-Spline Deconvolution Using Generated (Synthetic) Data
  - B-Spline Deconvolution under Presence of Errors in the Input Data

CHAPTER II

LITERATURE REVIEW — VARIABLE RATE TESTING

In this chapter we present an extensive survey of approaches regarding the solution of variable rate problems in the petroleum engineering literature.

As we begin our literature review, we will first categorize the various methods and references related to this subject. The categorization of literature for this work is given in the Table on page 15. We have gathered the methods in the following categories for reference:

- Superposition and Convolution
- Rate Normalization and Material Balance Deconvolution
- Deconvolution

2.1 Superposition and Convolution

In mathematical terms, convolution is defined as a mathematical operator which takes two functions *f* and *g* then produces a third function representing the amount of overlap between *f* and a reversed version of *g*. In other words convolution is defined as the integral of the product of the two functions after one is reversed and shifted[2]. Convolution of the functions $f(t)$ and $g(t)$ is defined as:

$$f(t) * g(t) = \int_0^t f(\tau)\, g(t-\tau) d\tau \quad \text{.....(2.1)}$$

In many engineering applications, the response of a *linear* system is the convolution of the input with the system's response to an impulse function. In addition convolution operation emerges whenever there is a linear system with superposition principle exists.

The right hand side of Eq. 2.1 can be approximated in discrete form over a finite interval as:

$$y(t) \approx \sum_{i=1}^{n} f(\tau_{i-1}) g(t-\tau_{i-1}) \Delta\tau \quad \text{.....(2.2)}$$

Where $y(t)$ is the response of the system — convolution of the functions $f(t)$ and $g(t)$. This leads us to the superposition principle which is defined as at a given time the total system response caused by two or more phenomena is equal to the summation of the results as if they have been resulted by each phenomenon independently.

Superposition principle[3] has particular importance in *Reservoir Engineering* (*especially in well test analysis*) since it is very useful in constructing reservoir response functions, representing various reservoir boundaries (by superposition in space) and determining variable rate reservoir response (by superposition

in time). The limitation of the superposition principle is that it is only valid for linear systems (governed by linear differential equations). When nonlinearities are present (*e.g.* gas flow) then superposition principle is not applicable. In those cases linearization (*i.e.* pseudopressure transform) has to be performed to apply superposition.

In petroleum engineering literature Duhamel's principle[4] states that the observed pressure drop is the convolution of the input rate function and the derivative of the constant-rate pressure response — at t=0 the system is assumed to be in equilibrium (*i.e.*, $p(r,t=0) = p_i$). For reference, the convolution integral is defined as:

$$\Delta p(t) = \int_0^t q(t-\tau) p'_u(\tau) d\tau \quad \text{.....(2.3)}$$

This can also be written in discrete form when a series of discrete changes in rate data are present, as:

$$\Delta p(t) = \sum_{i=1}^{n} (q_i - q_{i-1})(p_u(t - t_{i-1})) \text{ .....(2.4)}$$

Derivations of Equations 2.3 and 2.4 are provided in Appendix A. van Everdingen and Hurst[5] first initiated using Duhamel's principle in analysis of variable rate well-test data. They utilized Duhamel's principle to obtain dimensionless wellbore pressure-drop function response for a continuously (smoothly) varying flow rate. The underlying idea was to introduce a method to convolve/superimpose the constant rate pressure function response with a continuous (smooth) rate profile to produce the variable rate wellbore pressure-drop function response. Odeh and Jones[6] used the semilog approximation of the constant rate wellbore response function in combination with the rate profile to analyze variable rate pressure data. However, the issue related with this procedure is the wellbore response (constant rate solution) is assumed (*i.e.* semilog approximation). Methods of Soliman[7] and Stewart *et al.*[8] follow the similar procedure where in Soliman's method constant rate pressure function is given by the semilog approximation whereas in Stewart *et al.*'s method it is given by the exponential integral. Fetkovich and Vienot[9] presented the case of a well with a uniform flux vertical fracture. Agarwal[10] introduced a time axis correction for variable rates which is generally used for pressure buildup analysis. All of these methods are restricted because the theoretical foundation under these methods is based on assuming a particular model for the constant rate pressure function under the convolution integral.

2.2 Rate Normalization and Material Balance Deconvolution

Analysis of wellbore storage dominated pressure buildup responses was firstly introduced by Gladfelter *et al.*[11]. Rate normalization was also applied to drawdown tests by Winestock and Colpitts[12]. The objective

of rate normalization is to remove/correct the variable rate effects from the pressure data. Rate normalization can also be defined as an approximation to convolution integral[13] (see Raghavan).

$$\Delta p(t) \approx q(t)\, p_u(t) \quad \text{.....(2.5)}$$

Rate normalization is worth discussing because it presents substantial information on wellbore pressure drop response function with minimum attempt. In addition, rate normalization can remove the effects of wellbore storage when sandface rates are available. Thus, it is a very practical tool for analyzing wellbore storage distorted pressure drop response. Further attempts were made by Fetkovich and Vienot to variable rate gas and multiphase flow data confirming the applicability of rate normalization. Thompson[14] proposed explicit criteria for the use of rate normalization. However, Blasingame[15] performed numerical studies and concluded that a straight line — shifted from the one during radial flow period — could be observed during wellbore storage dominated flow which was resulted from a wrong estimate of skin factor. Furthermore, Raghavan described the some important situations where rate normalization should not be used — case of phase segregation and case of periodic or fluctuating rates.

Johnston[16] developed an extension of rate normalization method by defining a new x-axis plotting function which is called material balance time function.

$$t_{mb} = Q / q \quad \text{.....(2.6)}$$

where Q is the cumulative production and q is the flow rate. Plotting rate normalized pressure versus material balance time showed that material balance time function corrected the shift from the straight line obtained by rate normalization and therefore yielding a practical approach for analyzing wellbore storage distorted pressure data (correcting for variable rate effects). On the other hand, the concept of material balance time function — constant rate analog time function — can also be extended to production analysis as it was done in the work by McCray[17] where he noted that during boundary dominated flow the plot of rate normalized pressure versus constant rate analog time function should exhibit a straight line and the analysis procedure could be performed easily after obtaining the slope and intercept of the straight line. Additionally, plotting rate normalized pressure data against material balance time on logarithmic axes — *Log-log plot* — provides excellent diagnostics for production analysis, specifically for type curve matching (model based analysis).

Although the above methods are very practical to apply, they all have the major limitation that is they depend on the fact that the approximation is valid in Eq. 2.5 where in many cases it is not.

2.3 Deconvolution

The main goal of well test analysis is to identify/quantify the pressure drop response function of a well/reservoir system during an elapsed time t at constant/unit rate production. This pressure drop response may be referred as constant/unit rate pressure drop function or influence function[18] (Coats). The constant-rate drawdown pressure behavior of a well/reservoir system is the primary signature used to classify/establish the characteristic reservoir model. When varying rates are present during a production history, the pressure drop response function satisfies an integral equation which is given before as Eq. 2.3 (Duhamel's principle)

$$\Delta p(t) = \int_0^t q(t-\tau)\, p'_u(\tau)\, d\tau \quad \text{.....(2.3)}$$

In Equation 2.3, $q(t)$ is the flowrate function and $p_u'(t)$ is the derivative of the constant rate drawdown pressure (influence function) with respect to time. An alternative form of Eq. 2.3 (derived by integrating by parts and shown in Appendix A) can be written as below when $q(0) = 0$ and $p_u(0) = 0$.

$$\Delta p(t) = \int_0^t q'(\tau)\, p_u(t-\tau)\, d\tau \quad \text{.....(2.7)}$$

Unlike the previous methods which assume models for the constant rate pressure function under the convolution integral (convolution/superposition) or approximate convolution integral (rate normalization), in variable-rate deconvolution the objective is to find the constant rate pressure function with the given input functions — pressure drop response data function and flow rate data function which is essentially an inverse problem. Mathematically, we are attempting to solve a first-kind Volterra equation (Lamm).

The issue with deconvolution is that variable-rate deconvolution is mathematically ill-conditioned — several deconvolution methods have been emerged in petroleum engineering literature — very few deconvolution methods are in fact successful practically. The ill-conditioned nature of the deconvolution problem means that small changes in the input data cause large variations in the deconvolved constant-rate pressures. A comprehensive literature survey will be given in this section.

Before starting the literature survey we should state that the input signals — pressure drop response data, Δp and flow rate data, q — are known (measured) throughout a time span $(0,t)$ and flow rate is zero outside this duration and we are only (theoretically) able to recover the constant rate pressure function for this time span $(0,t)$ — no extrapolation is possible beyond t since the convolution integral (Eq. 2.3) is only defined between $(0,t)$.

In literature, methods regarding deconvolution are divided into two categories —time domain methods and spectral methods. Time domain methods require the solution of the convolution integral in time domain

This is performed by setting interpolation schemes (discretizing the time interval and selecting nodes and interpolate) for the functions under the convolution integral — flow rate data function (given) and constant rate drawdown pressure function (unknown and to be sought). Generally constant/stepwise and piecewise functions have been used for modeling purposes (*to our knowledge, no spline function has been used for modeling the unknown constant rate drawdown function up to now*). Interpolation scheme results in a linear system of equations (**Ax** = **b**) where **A** is called the sensitivity matrix. This linear structure is tridiagonal which can be solved directly — early methods[19-22] make use of solving the system explicitly. However, these methods are extremely unstable *i.e.* even minor errors in signals (pressure drop response data and flow rate data) amplify/accumulate in the solution process therefore ruining the result. In other words, there is a unique solution under the condition that input data (signals) are "ideal" *i.e.* containing *no errors* but generally (or always) this is not the case — the sensitivity matrix is ill-conditioned due to discretization of the convolution integral[1].

The stability issue of the variable-rate deconvolution has triggered the development of two basic concepts concerning how to manage instability. One concept is to incorporate an *a priori* knowledge regarding the properties of the deconvolved constant-rate response. The observations of Coats *et al.* on the strict monotonicity of the solution lead the authors impose sign constraints in the form of:

$$p_u(t) \geq 0, \quad p_u'(t) \geq 0, \quad p_u''(t) \leq 0 \qquad \text{.....(2.8)}$$

By imposing sign constraints, the number of unknown parameters in the solution are reduced — elements of vector **x** — and the linear system has turned into an overdetermined linear system of equations where the number of rows in the sensitivity matrix is relatively higher than the number of colums. The solution of an overdetermined system of equations is possible by minimizing the error term, $\| Ax - b \|_n$. If the norm, *n* of the error vector is 1 then the formulation of the solution is performed by *linear programming* which is the case of Coats *et al*. Otherwise, if the norm is equal to 2 then the formulation of the solution is performed by *least squares*. Kuchuk *et al*.[23] and Baygun *et al*.[24] further improved Coats' solution by minimizing the error using least squares. In particular, the formulation by Baygun *et al.* imposes a different set of constraints — autocorrelation constraint and derivative energy constraint — which tolerates error levels up to 2% in input data. In some respects imposing constraints is continued in the work given by von Schroeter *et al*.[25] when they incorporate non-negativity in the "encoding of the solution". As mentioned before in the examples given, this concept (non-negativity/monotonicity of the solution) requires non-standard numerical methods (linear programming, non-linear least-squares minimization).

The second concept regarding stability issue is to use a certain level of regularization[25,26] — where "regularization" is defined as the act/process of making a system regular or standard (smoothing or eliminating non-standard/irregular response features). Regularization can be performed indirectly by representing the desired solution using a restricted number of "elements" — or directly by *penalizing* the "non-smoothness" of the solution. In either case, the additional degree of freedom (the regularization parameter) has to be established — where this is facilitated by the discrepancy principle (effectively tuning the regularization parameter to a maximum value, while not causing intolerable deviation between the model and the observations).

In addition to these main features, individual deconvolution algorithms may have other distinctive features. From a numerical standpoint, recent deconvolution methods tend to use advanced techniques to solve the underlying system of linear equations (*e.g.*, Singular Value Decomposition, the equivalent concept of pseudoinverse, etc. (see ref. 27)).

Among all discussed methods, recent work by von Schroeter *et al*. exhibited major progress in variable-rate deconvolution problem under significant level of errors in pressure drop response and flow rate data. Their approach to the problem combined two concepts described above (non-negativity/monotonicity of the solution and regularization). They imposed the non-negativity constraint by appropriate encoding of the solution which causes the integral equation (Eq. 2.3) to be nonlinear. The resulting linear system is solved by total least squares formulation which provides nonlinear minimization. Additionally, regularization by curvature is utilized to implement smoothness of the solution. In the work by Levitan[26], some modifications were suggested such as applying deconvolution to each individual flow period for handling inconsistencies present in real well test data. Furthermore, Levitan *et al*.[28] also proposed critical considerations and recommendation on producing accurate deconvolution results.

Spectral methods — second category — make extensive use of transformations (*i.e.*, the Laplace transform, the Fourier transform, etc.). Several cases consider "numerical Laplace transformation of observed tabulated data" combined with numerical inversion[29-31]. As well as a group of methods which rely on the use of spline functions in various steps of the deconvolution algorithm — particularly for approximating data and then transforming into Laplace domain[32,33]. In addition, Cheng *et al*. [34] consider the application of the Fourier transformation to solve the deconvolution problem.

The basic idea of the spectral methods depends on the convolution theorem of spectral analysis which states that convolution product is equal to the product of the transforms.

$$\overline{\Delta p} = \bar{q} * \bar{p}_u' \quad \text{.....(2.9)}$$

Once the input functions are transformed into spectral domain, deconvolution operation is simply a division done in the spectral domain and then if the transform is invertible, the sought solution is found by inverting the operation — solving for constant rate pressure response function in Eq. 2.7. In addition, evaluation can also be done in the spectral domain as suggested by Bourgeois and Horne[30].

The common transformation in petroleum engineering literature is the Laplace transform and Stehfest's numerical algorithm[35] is utilized for transforming back into time domain. One of the main issues which Laplace transformation suffers from is basically Laplace transforms of functions are defined on the entire positive time axis which requires that pressure drop response must be in equilibrium *i.e.* value of $\Delta p(\infty)$ at the end of measurements (end of test). Having a value for equilibrium pressure drop response is not possible under economical conditions and various extrapolation methods[29,30] have been developed but none of them were successful enough to overcome this issue. The other issue regarding Laplace transformation is Laplace transformation of a function is possible if the function is continuous. Under the convolution integral, given flow rate data generally have some discontinuities making it extremely difficult for representing this data with a continuous function. The common approach is to use constant or piecewise functions for the rate data. However, Stehfest algorithm is not robust enough for inverse Laplace transformation when discontinuities are present in flow rate data. Instead of its attractiveness, spectral methods endure the problems discussed above but, using an appropriate method for estimating incomplete response data along with a robust numerical inversion algorithm may provide new developments in spectral based deconvolution algorithms.

In general terms, our method can easily be placed into existing categories described before and categorized in **Table 2.1**. Our approach combines the use of B-splines, numerical inversion of the Laplace transform is also used for constructing the one component of the solution — construction of the sensitivity matrix in the linear system of equations. In addition, we provide indirect (number of knots used in the selected B-spline and pseudoinverse, singular value decomposition) and direct (by imposing constraints on the logarithmic derivative of the reconstructed constant-rate response) regularization.

In depth our method is fundamentally different from the existing methods — spline functions are not used for fitting purposes to observed data. In fact, B-splines are used to represent the unknown response solution. We do not use the Laplace transformation of the observed data or we do not use the inverse Laplace transformation for obtaining the constant rate response. Therefore, our approach does not suffer from the limitations of the spectral transforms discussed before. In our method, we use the Laplace transformation for convolution of rate function and B-splines in Laplace domain and inverse Laplace transformation is restricted to the construction of the sensitivity matrix for the least squares problem.

We represent the derivative of the unknown constant-rate drawdown pressure response function as a weighted sum of B-splines. We use fixed knots which are distributed logarithmically. With respect to discrete flowrate function we use piecewise constant, piecewise linear, or any other proper representation for which the Laplace transform can easily be achieved. Further, we are able to split the production history into any number of segments where flowrate can be approximated in each segment. Taking the Laplace transform of the B-splines, we then apply the convolution theorem in the Laplace domain and we calculate the sensitivities of the observed pressure response with respect to the B-spline weights by numerical inversion of the Laplace transform.

Finally, additional constraints are introduced in the sensitivity matrix by direct regularization (by penalizing the non-smoothness of the logarithmic derivative of the reconstructed constant-rate response) and the resulting linear system of equations is solved by least-squares to yield the required B-spline weights/coefficients to generate the unit/constant rate response and well testing derivative functions in the real time domain.

Paradoxically, this new deconvolution approach is made possible by our ability to solve a certain class of convolution problems with any desired accuracy, in particular, by the availability of a robust numerical inversion procedure for the Laplace transform (*i.e.*, the Gaver-Wynn-Rho algorithm[36,37]).

Table 2.1 – Categorization of literature (variable rate testing) for this work.

Reference	Author	Method
Convolution/Superposition		
5	van Everdingen and Hurst	Convolution/Superposition
6	Odeh and Jones	Convolution/Superposition
7	Soliman	Convolution/Superposition
8	Stewart *et al*.	Convolution/Superposition
9	Fetkovich and Vienot	Convolution/Superposition
10	Agarwal	Convolution/Superposition
Rate Normalization/Material Balance Deconvolution		
9	Fetkovich and Vienot	Rate Normalization
11	Gladfelter *et al*.	Rate Normalization
12	Winestock and Colpitts	Rate Normalization
14	Thompson	Rate Normalization (Superposition)
15	Blasingame	Rate Normalization
16	Johnston	Material Balance Deconvolution
17	McCray	Material Balance Deconvolution
Deconvolution in Time Domain		
18	Coats *et al*.	Time Domain Deconvolution (Linear Programming)
19	Hutchinson and Sikora	Time Domain Deconvolution (Direct Solution)
20	Katz *et al*.	Time Domain Deconvolution (Direct Solution)
21	Jargon and van Poolen	Time Domain Deconvolution (Direct Solution)
22	Bostic and Agarwal	Time Domain Deconvolution (Direct Solution)
23	Kuchuk *et al*.	Time Domain Deconvolution (Least Squares Solution)
24	Baygun *et al*.	Time Domain Deconvolution (Least Squares Solution)
25	von Schroeter *et al*.	Time Domain Deconvolution (Total Least Squares Solution/Regularization)
26	Levitan	Time Domain Deconvolution (Total Least Squares Solution/Regularization)
Deconvolution in Spectral Domain		
29	Roumboutsos and Stewart	Laplace Domain Deconvolution
30	Bourgeois and Horne	Laplace Domain Deconvolution
31	Onur and Reynolds	Laplace Domain Deconvolution
32	Guillot and Horne	Laplace Domain Deconvolution
33	Mendes *et al*.	Laplace Domain Deconvolution
34	Cheng *et al*.	Fourier Domain Deconvolution

CHAPTER III

DEVELOPMENT OF THE NEW B-SPLINE BASED DECONVOLUTION METHOD

3.1 B-Splines

Spline functions are piecewise polynomial functions which are defined on subintervals connected by points called knots (t_i) and have the additional property of continuity (of the function and its derivatives)[27]. During early studies, splines were generally constructed by piecewise *polynomial* functions. Besides, it was shown that a spline function can effectively be represented using a linear combination of basis spline functions called B-splines[38]. B-splines are individually established by the knots and the order of the spline function. In this work we represent the unknown $p_u'(t)$ function — unknown signal — as a second order B-spline with logarithmically spaced knots.

Generally, spline approximation utilizes the n-th degree piecewise polynomials to preserve (n-1)th order derivatives at the data points. The advantages of spline approximation can be expressed as; splines are easy to compute, best in the sense of minimum mean square error criterion and totally local. During a spline approximation process, piecewise polynomial functions are employed to approximate the data between knots; however there exists a basis function which approximates the data same as piecewise polynomial functions. These "basis" functions are B-splines and they can also represent the data between knots and they are superior to piecewise polynomials since they are generally smooth and well-behaved rather than higher degree polynomials which can show oscillations. Furthermore, connecting polynomials in a piecewise fashion can reproduce discontinuities at knots (connecting points) whereas, B-splines are continuous everywhere. These reasons stated above make use of B-splines for a variety of applications very convenient and attractive[39-42] (de Boor, Schumaker, Ahlberg *et al*., Greville). On the other hand, B-spline approximation is not widely used for requiring computationally expensive matrix calculations such as direct matrix inversion. However, these problems can be overcome by using efficient techniques for the solution of linear system of equations which can be found in numerical methods literature[43,44].

It should be noted that B-spline functions have important features such as derivatives and integrals. Additional properties, support of B-splines, positivity of B-splines and partition of unity of B-splines as well as derivatives and integrals are covered in Appendix B in detail. Another important property of using B-splines for approximating unknown functions is that B-splines are very useful in noise reduction and data compression — by means of selecting knots. After stating the important facts above about B-splines,

we will start describing the development of the new B-spline based deconvolution method in the following section.

3.2 Algorithm Development

As mentioned before a spline function can successfully be represented by linear combination of B-spline functions. Once the knots (or continuity points) are set; generation of B-splines is easy because of their intrinsic recurrence relation. Distributing the knots logarithmically:

$$t_i = b^i, \quad b > 1 \quad i = 0, \pm 1, \pm 2, \ldots \quad (3.1)$$

With a suitable selected $b > 1$ *basis*, the B-spline of degree 0 is defined by:

$$B_i^0(t) = \begin{cases} 1 & t_i < t < t_{i+1} \\ 0 & otherwise \end{cases} \quad (3.2)$$

Higher degree B-splines are generated recursively

$$B_i^k(t) = \left[\frac{t - t_i}{t_{i+k} - t_i} \right] B_i^{k-1}(t) + \left[\frac{t_{i+k+1} - t}{t_{i+k+1} - t_{i+1}} \right] B_{i+1}^{k-1}(t) \quad (3.3)$$

where k = 1,2,…. — the order of the B-spline function. The "i-th" B-spline has a non-zero value (support) between t_i and t_{i+k+1} as it is illustrated in Appendix B.

Once B-splines are calculated, any k^{th} degree spline function can be represented as a linear combination in a finite interval divided into n intervals.

$$S^k(t) = \sum_{i=l}^{u} c_i B_i^k(t) \quad (3.4)$$

where the number of B-splines involved is u-l+1. For second order splines having support in an interval (t_{i1}, t_{i2}), we obtain l=i_1-2 (index of the first B-spline), u= i_2-1 (index of the last B-spline), and the number of B-splines involved is n=i_2-i_1+2 (by substituting l and u). By linearity, the Laplace transform of Eq. 3.4 is:

$$\overline{S}(s) = \sum_{i=l}^{u} c_i \overline{B}_i^k(s) \quad (3.5)$$

As we mentioned before, we will represent the derivative of unknown constant rate pressure response function, $p_u'(t)$, as a weighted sum of B-splines of degree 2, defined over logarithmically evenly-spaced knots:

$$P_u'(t) = \sum_{i=l}^{u} c_i B_i^2(t) \quad \text{.....(3.6)}$$

To reveal characteristic reservoir behavior, the number of knots should be on the order of at least 2–6 knots per log cycle (for typical kernels of interest (*i.e.*, input flowrate functions observed in reservoir engineering)). Therefore, we never use more knots, (but we may be forced to reduce the number of knots in cases where the data quality does not justify looking for sophisticated signatures.)

If we substitute Eq. 3.6 into the convolution integral, we have:

$$\Delta p(t) = \int_0^t \sum_{i=l}^{u} c_i B_i^2(\tau)\, q(t-\tau) d\tau \quad \text{.....(3.7)}$$

From this point forward we have two options — either solving the convolution equation in the real time domain or in the Laplace domain. In our work we choose to solve this equation in the Laplace domain. We denote the Laplace transform of function $f(t)$ by the operator L that acts on a function of time and creates a function of the Laplace variable s:

$$\bar{f}(s) = \mathrm{L}\left[f(t)\right][s] \quad \text{.....(3.8)}$$

For the inverse Laplace transformation we use the notation

$$f(t) = \mathrm{L}^{-1}\left[\bar{f}(s)\right][t] \quad \text{.....(3.9)}$$

When we cannot construct the function $f(t)$ analytically, the inversion can be still done numerically, that is we can calculate the value of $f(t)$ at any given t using an appropriate numerical inversion algorithm for the Laplace transform.

The Laplace transformation of Eq. (3.7) yields a simple multiplication given by

$$\Delta\bar{p}(s) = \sum_{i=l}^{u} c_i\, \bar{q}(s)\, \bar{B}_i^2(s) \quad \text{.....(3.10)}$$

If we have m drawdown observations collected in a vector $\Delta\tilde{\mathbf{p}}$ (pressure drop response data distorted by variable rate) that were observed at times ($\tilde{\mathbf{t}}_1, \tilde{\mathbf{t}}_2, \ldots \tilde{\mathbf{t}}_m$), then the problem can be written as a weighted over-determined system of linear equations:

$$\mathbf{W X c} = \mathbf{W}\,\Delta\tilde{\mathbf{p}} \quad \text{.....(3.11)}$$

Leading to the weighted linear least-squares problem:

$$\min_{c} (\Delta\tilde{\mathbf{p}} - \mathbf{X}\mathbf{c})^T \mathbf{W}^T \mathbf{W}(\Delta\tilde{\mathbf{p}} - \mathbf{X}\mathbf{c}) \quad (3.12)$$

where $\mathbf{X}$ is the m x n sensitivity matrix and $\mathbf{c}$ is the n-vector of unknown coefficients and $\mathbf{W}^T\mathbf{W}$ is the m x m diagonal weighting matrix. (In general, we select the weights as the measured pressure drawdowns assuming a constant level of relative errors in the drawdowns.) Naturally, we assume that $m >> n$ and the observations are distributed approximately evenly with respect to the logarithmically spaced knots. At this point we have to assure that the observed rates can be conveniently represented by a representative function for which the Laplace transform can easily be obtained.

We define the elements of the sensitivity matrix by (numerically) inverting

$$\mathbf{X}_{j,i} = \mathrm{L}^{-1}\left[\bar{q}(s)\bar{B}_i^2(s)\right]\left[\tilde{t}_j\right] \quad (3.13)$$

Eq. (3.7) becomes:

$$\Delta p_j = \mathrm{L}^{-1}\left[\bar{q}(s)\sum_{\mathrm{i}=1}^{u} c_i \bar{B}_i^2(s)\right] = \sum_{i=l}^{u} c_i \mathrm{L}^{-1}\left[\bar{q}(s)\bar{B}_i^2(s)\right]\left[\tilde{t}_j\right] \quad (3.14)$$

We note that calculating the elements of the sensitivity matrix is reduced to computing the convolution of the known rate with the B-splines. Construction of the sensitivity matrix requires

1. The Laplace transform of the second order B-splines (over even logarithmically-spaced knots);
2. A simple description of the rate that lends itself to an analytical (*i.e.*, functional) Laplace transformation;
3. An efficient numerical Laplace inversion algorithm that can provide results with any required accuracy and is tolerant to the fact that the B-splines are defined piecewise (in other words, the inverse Laplace transform (as a function of t) will contain "jump/discontinuity" features in its higher derivatives).

Once the sensitivity matrix ($\mathbf{X}$) has been constructed, the estimate of the unknown parameter vector ($\mathbf{c}$) is obtained from

$$\hat{\mathbf{c}} = \mathbf{X}^{+}\,\Delta\,\tilde{\mathbf{p}} \quad (3.15)$$

Since the sensitivity matrix, $\mathbf{X}$ is ill-conditioned and its inverse can not be taken, we use pseudoinverse — a generalization for the inverse of a non-square matrix — of matrix $\mathbf{X}$ for regularization (*converting an ill-*

conditioned problem to a well-conditioned problem) purposes. $\mathbf{X}^{+}$ ($\mathbf{X}^{+} = (\mathbf{X}^{T}\mathbf{X})^{-1}\mathbf{X}^{T}$) denotes the pseudoinverse of matrix **X**. (For simplicity, here we show the case where all the weights are unity.). We use a least-squares criterion to minimize error distortion by means of pseudoinverse. Naturally, we pay a penalty to make certain that the solution does not become unbounded, but we know that the input data has an uncertainty of definite extent, so it is rational to optimize using the least squares constraint. To create the pseudoinverse, small singular values are removed from the calculations (*i.e.* singular value decomposition) (in our computations the automatic cut-off selection of *Mathematica*[45] was employed). In Appendix C, we provide detailed information about the concepts of pseudoinverse and singular value decomposition.

Using the estimates of **c** coefficients obtained from this process, we reconstruct the constant-rate response as follows:

$$p_u(t) = \sum_{i=l}^{u} \hat{c}_i B^2_{i,int}(t) \quad \text{.....(3.16)}$$

And the logarithmic derivative of the constant-rate response (*i.e.* well testing derivative) is given as:

$$p_{u'}(t) = t\sum_{i=l}^{u} \hat{c}_i B^2_{i}(t) \quad \text{.....(3.17)}$$

where the integral of the second order B-spline, $B^2_{i,int}(t)$, is easily obtained analytically (*e.g.*, by *Mathematica*).

The method described above works for smoothly varying (continuous) rates. Whenever the flow rate (or its derivative) undergoes an abrupt change, the required condition for the successful numerical inversion of the required Laplace transform (in Eq. 3.13) is not satisfied — the function of which Laplace transform is taken has to be a *continuous* function. This is the case in most of the field applications where flow rate data usually have rapid changes (*e.g.* shut-in followed by a drawdown in pressure transient analysis or erratic flow rate data in long term production history). In these cases the computation of the sensitivity matrix has to be modified according to rate variations in order to satisfy safe numerical Laplace inversion. In the next section we are going to describe how modifications are done for the sensitivity matrix computation after briefly explaining the rate approximation for the smoothly changing rates.

3.3 Flow Rate Considerations

Rate approximation has a major role in deconvolution process (kernel of interest in convolution integral). In B-spline based deconvolution method; flow rate must be represented in functional form which can be

transformed into Laplace space. In well testing and production analysis, it is always engineer's decision to find a best approximation/fit to represent rate data. Constant piecewise, straight line fit, exponential or polynomial functions, *etc*. can all be used for representing rate data in a functional form.

In B-spline based deconvolution method, any type of rate function can be used to describe rate as long as it is transformed into Laplace space. For most cases where rate data are smoothly changing, linear combination of exponential terms is used to describe rate.

$$q_k(t) = 1 - Exp(-t / t_k) \quad \text{.....(3.18)}$$

To describe this process, first we divide the interval where we have rate measurements into n pieces. Then we will logarithmically distribute $n + 1$ t_k points — or we may call t_k as connection points (basically k is equal to n+1). We choose to distribute the points logarithmically since usually time span for measurements is extensive. When t_k points are determined, above equation is satisfied for each $q_k(t)$. If we call *ft* and *lt* as the first and last time points of measurements, determination of t_k points and q_k functions can be described as:

$$\begin{aligned} ift &= Log(ft) \\ ilt &= Log(lt) \\ r &= \frac{ilt - ift}{n} \\ t_k &= Exp(k) \\ q_k(t) &= 1 - Exp(-t / Exp(k)) \end{aligned} \quad \text{.....(3.19)}$$

where k starts at *ift* and ends at *ilt* with increments, r. As mentioned before, there will be n+1 t_k and $q_k(t)$ terms. However, approximation may fail at first and last points if the above procedure is used. To overcome this we add one exponential term to left and one exponential term to the right. It is seen that adding this additional terms improves the rate approximation. This procedure is described as:

$$\begin{aligned} ift &= Log(ft) \\ ilt &= Log(lt) \\ r &= \frac{ilt - ift}{n} \\ ist &= Log(ft) - r \\ ien &= Log(lt) + r \\ t_k &= Exp(k) \\ q_k(t) &= 1 - Exp(-t / Exp(k)) \end{aligned} \quad \text{.....(3.20)}$$

Now there are n+3 t_k and $q_k(t)$ terms. After determining $q_k(t)$ terms, we follow a least-squares (error minimization) procedure to find a best fit to discrete rate data. There are a_k coefficients (n+3) to be determined by least-squares. Finally rate function can be written as:

$$q(t) = \sum_{k=1}^{n+3} a_k q_k(t) \quad \text{.....(3.21)}$$

Laplace transform of Eq. 3.21 is given as:

$$\overline{q}(s) = \sum_{k=1}^{n+3} a_k \left(\frac{1}{s} - \frac{t_k}{1+t_k s} \right) \quad \text{.....(3.22)}$$

In the previous section we noted that in our algorithm rate data has to be approximated by functions which can be transformed into Laplace space. Typically well test and production data involve variable rate data which have sudden changes/discontinuities. Even in these cases, flow rate data can still be approximated with the procedure described above. However, the required condition for the successful numerical inversion of the required Laplace transform is not satisfied for the reasons discussed before. In particular, the inverse Laplace transformation when computing the elements of the sensitivity matrix fails at the discontinuities. Therefore, the success or failure of this approach depends primarily on the numerical Laplace transform inversion. For the previous three decades fixed precision computing has defined the status of numerical inversion[46,47] (see Davies and Martin, Narayanan and Beskos). Recently, several new algorithms were introduced using multi-precision methods[36,37].

In this work we use the publicly available GWR[48]. With this algorithm it is possible to invert a large class of Laplace transforms with essentially any desired accuracy. Since the algorithm relies on multi-precision computing, it can be realized only in software systems supporting variable precision methods for arithmetic and special functions.

Using the GWR algorithm can improve numerical Laplace inversion at the discontinuity points but, this requires that higher values of precision (at least 64 digits or over) have to be used for accuracy. However, on one hand we may still face with failure in inverse Laplace transformation at the discontinuities despite using very high precision (since in theory, the inverse Laplace transformation of piecewise functions is not defined, for reference inversion formula is given below[49]:

$$f(t) = \frac{1}{2\pi i} \int_{c-i\infty}^{c+i\infty} e^{ts} f(s)\, ds \quad \text{.....(3.23)}$$

And on the other hand, even if we get accurate results with using very high precision this takes enormous amount of computational time which makes it impossible to apply for practical purposes.

We overcome these issues by modifying our rate approximation by dividing the flow rate history into any number of segments and approximate the rate data within each segment. We can use any type of function for approximating rate within each segment as long as its Laplace transform exists. We note that in this case, sensitivity matrix, **X** is computed from two contributions. First, the effect of the continuous rate function is computed and second, the effect of the discontinuity must be taken into account. To account for the discontinuity we are going to define a new rate function $q_{jp}(t+t_{jp})$. Mathematically, $q_{jp}(t+t_{jp})$ is the same rate function, $q(t)$, which is t_{jp} (the time point where the discontinuity occurs) shifted on y axis. This procedure is analogous to superposition principle. We are going to present two example calculations to illustrate how the elements of **X** matrix are calculated when there are discontinuities in rate data. For illustration purposes, we are assuming a rate profile in **Fig. 3.1**.

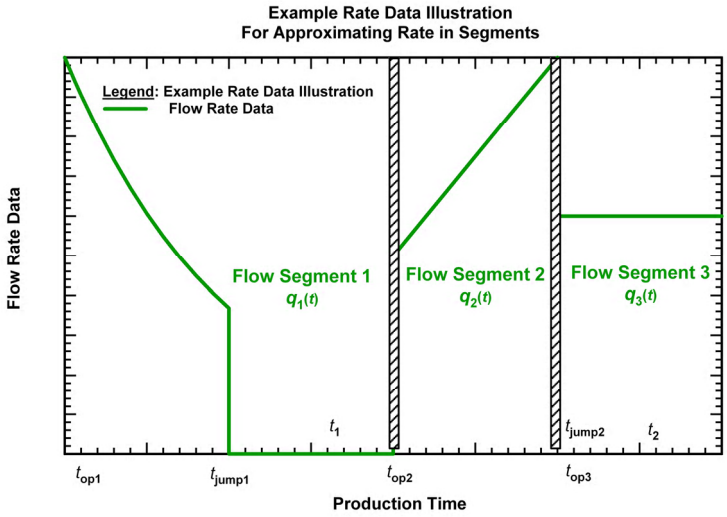

Figure 3.1 – Assumed rate profile for illustration purposes

For this rate profile, rate history is split into three segments and within each three segment, rate data is approximated by three different functions. Note that, shut-in part is included in the first segment and it can be seen as a continuation of the first rate function. However, in the first segment rate is approximated by using only the points before shut-in. The reason for including the shut-in part in the first segment is to ignore extra calculations since the value of the function is essentially zero. But, it is still possible to divide this rate history into four segments including the shut-in part as the second segment.

We are going to define the time points where jumps (discontinuities) are observed as $t_{jp,n}$ and time points where new rate function begin to operate as $t_{op,n}$. For n number of segments there are n t_{op} and (n-1) t_{jp}.

All in all, the underlying idea is to include the effects of the (previous) rates on matrix computation even if they are not present at the time of interest and to secure the safe numerical Laplace inversion process.

For our purposes, here we are going to compute the elements of matrix **X** at times t_1 and t_2. First, we begin with computing the element of sensitivity matrix **X** at time, t_1. We observe that a discontinuity is present at $t_{jp,1}$ (shut-in time). So, there will be two terms in the computation — the term supposing the rate function $q_1(t)$ continues to flow at time t_1 and the term which includes the effect of shut-in at $t_{jp,1}$. The value of the matrix element is the subtraction of the second term from the first term. This is shown as:

$$X_{j,i} = L^{-1}\left[\sum_{i=l}^{u} \bar{q}_1(s)\bar{B}_i^2(s)\right]\left[\tilde{t}_1 - t_{op,1}\right] - L^{-1}\left[\sum_{i=l}^{u} \bar{q}_{jp,1}(s)\bar{B}_i^2(s)\right]\left[\tilde{t}_1 - t_{jp,1}\right] \quad \text{.....(3.24)}$$

For the computation at time t_2, the effects of previous rates and discontinuities must be taken into account. Rates are described as $q_1(t\text{-}t_{op,1})$ ($t_{op,1} = 0$) (for the first segment), $q_2(t\text{-}t_{op,2})$ (for the second segment), $q_3(t\text{-}t_{op,3})$ (for the third segment) and for the discontinuities $q_{jp,1}(t\text{-}t_{op,1}+t_{jp,1})$, $q_{jp,2}(t\text{-}t_{op,2}+t_{jp,2})$, respectively. And the element of the sensitivity matrix, **X** at time t_2 will be:

$$L^{-1}\left[\sum_{i=l}^{u} \bar{q}_1(s)\bar{B}_i^2(s)\right]\left[\tilde{t}_2 - t_{op,1}\right] - L^{-1}\left[\sum_{i=l}^{u} \bar{q}_{jp,1}(s)\bar{B}_i^2(s)\right]\left[\tilde{t}_2 - t_{jp,1}\right] \text{(from the first segment)} \quad \text{.....(3.25)}$$

$$L^{-1}\left[\sum_{i=l}^{u} \bar{q}_2(s)\bar{B}_i^2(s)\right]\left[\tilde{t}_2 - t_{op,2}\right] - L^{-1}\left[\sum_{i=l}^{u} \bar{q}_{jp,2}(s)\bar{B}_i^2(s)\right]\left[\tilde{t}_2 - t_{jp,2}\right] \text{(from the second segment)} \quad \text{.....(3.26)}$$

$$L^{-1}\left[\sum_{i=l}^{u} \bar{q}_3(s)\bar{B}_i^2(s)\right]\left[\tilde{t}_2 - t_{op,3}\right] \text{ (from the third segment)} \quad \text{.....(3.27)}$$

Finally, $\mathbf{X_{j,i}}$ at t_2 is:

$$\begin{aligned} X_{j,i} = {} & L^{-1}\left[\sum_{i=l}^{u} \bar{q}_1(s)\bar{B}_i^2(s)\right]\left[\tilde{t}_2 - t_{op,1}\right] - L^{-1}\left[\sum_{i=l}^{u} \bar{q}_{jp,1}(s)\bar{B}_i^2(s)\right]\left[\tilde{t}_2 - t_{jp,1}\right] \\ & + L^{-1}\left[\sum_{i=l}^{u} \bar{q}_2(s)\bar{B}_i^2(s)\right]\left[\tilde{t}_2 - t_{op,2}\right] - L^{-1}\left[\sum_{i=l}^{u} \bar{q}_{jp,2}(s)\bar{B}_i^2(s)\right]\left[\tilde{t}_2 - t_{jp,2}\right] \\ & + L^{-1}\left[\sum_{i=l}^{u} \bar{q}_3(s)\bar{B}_i^2(s)\right]\left[\tilde{t}_2 - t_{op,3}\right] \end{aligned} \quad \text{.....(3.28)}$$

In our experiments we have found out that this procedure is very efficient to represent rate and honor rate data. However, computational time significantly increases as the number of segments increase.

3.4 Decoupling the constant-rate response and its logarithmic derivative

As we already mentioned, in general, the earliest part of the unknown $p_u(t)$ ($K(t)$) function is critical, especially if the observed variable-rate response contains a skin effect (but minimal (or no) wellbore storage effects). In such cases the $p_u(t)$ ($K(t)$) function contains a Dirac delta component. To reconcile this condition we add additional "anchor" B-splines to the left of the first observed time point. After considerable experimentation, we established that 4 (four) additional B-splines are sufficient for virtually any scenario.

These "anchor" B-splines do not affect the reconstructed $p_{ud}(t)$ function, that is the logarithmic derivative at the observation points, but do affect the reconstructed $p_u(t)$ constant-rate response at all observation points (*i.e.*, the integral of the $p_{ud}(t)$ function). In fact, these additional B-splines are a convenient vehicle to represent the Dirac delta component of the function $K(t)$.

3.5 Regularization

We found that using the concept of a pseudoinverse (a cut-off for small singular values) does not provide a sufficient regularization as the noise level in the data increases. Therefore, we require an additional regularization which makes sense in a physical context *and* ensures the relevance of the spline representation.

For the over-determined system (Eq. 3.11) to be solved by least squares, for each spline interval we must append the following two conditions:

$$\begin{aligned} \alpha \left[\left(t \sum_{i=l}^{u} c_i B_i^2(t) \right)_{t=t_k} - \left(t \sum_{i=l}^{u} c_i B_i^2(t) \right)_{t=t_{k+1/2}} \right] &= 0 \\ \alpha \left[\left(t \sum_{i=l}^{u} c_i B_i^2(t) \right)_{t=t_{k+1/2}} - \left(t \sum_{i=l}^{u} c_i B_i^2(t) \right)_{t=t_{k+1}} \right] &= 0 \end{aligned} \qquad \text{.....(3.29)}$$

In other words, we require that the value of the logarithmic derivative of the constant-rate response differ only "slightly" between the knot and the middle location between knots. When the value of the regularization parameter, $\alpha = 0$, there is no regularization. With generated data with practically no error, $\alpha = 0$ results in the required smooth solution for the constant-rate response and its logarithmic derivative. In the presence of random noise and/or other inconsistencies, a positive α is selected based on an informal interpretation of the discrepancy principle — *i.e.*, we increase the value of the regularization parameter

until the calculated (model) pressure difference begins to deviate from the observed pressure difference in a specific manner. The mean and standard deviation of the arithmetic difference of the computed and input pressure functions are also computed, but algorithmic rules (*e.g.,* L-curve method) for selecting α are not recommended — for reasons discussed by von Schroeter *et al.*[25]).

Applying the above conditions (Eq. 3.29), an additional system of equations can be defined as:

$$X_r \; c = 0 \qquad (3.30)$$

where $\mathbf{X}_r$ is (k x n) matrix — k is the number of points where $t\sum_{i=l}^{u} c_i B_i^2(t)$ is evaluated, it starts at first knot index (l) and it ends at the last knot index (u) and increases with half increment of the index (t_l, $t_{l+1/2}$,……,t_1 , $t_{1+1/2}$, t_2,……$t_{u-1/2}$, t_u). n is the number of unknown c coefficients in other words it is the number of B-splines. We solve $\mathbf{X}\,\mathbf{c} = \Delta\mathbf{p}$ and $\mathbf{X}_r\,\mathbf{c} = 0$ together.

$$\begin{aligned} (1-\alpha)\,X\,c &= (1-\alpha)\Delta\tilde{\mathbf{p}} \\ \alpha\,X_r\;c &= 0 \end{aligned} \qquad (3.31)$$

Finally, a new system of equations is obtained as

$$X^*\; c = \Delta\tilde{\mathbf{p}}^* \qquad (3.32)$$

$\mathbf{X}^*$ is obtained by joining (1-α) $\mathbf{X}$ and $\alpha\,\mathbf{X}_r$ and its dimensions are ((m+k) x n) and $\Delta\tilde{\mathbf{p}}^*$ is obtained by joining $(1-\alpha)\Delta\tilde{\mathbf{p}}$ and 0 (including k elements). Essentially, $\Delta\tilde{\mathbf{p}}^*$ will be a (m+k) column vector. The same procedure is followed (least squares solution by pseudoinverse) after performing these operations.

CHAPTER IV

VALIDATION OF THE METHOD

In this chapter we validate our new B-spline based deconvolution method by comparing the results obtained from a known reservoir model. Before going into further detail, we briefly summarize what is described in this chapter. First, we choose a reservoir model — which has an exact analytical solution — and generate the constant rate pressure drop response function with assumed reservoir and fluid properties given in **Table 4.1** for our purposes. The generated constant rate pressure drop response is going to be compared with the deconvolution results ultimately. After choosing the model and generating the exact solutions we then generate the variable rate pressure drop response using convolution theorem with our presumed rate function. We use the "generated" variable rate pressure drop data and our presumed rate data as inputs for deconvolution. Finally, deconvolved constant rate pressure drop data and exact results are compared to verify the methodology. Additionally, we corrupt both pressure and rate data with various levels of errors — ranging from 1% - 40% — and test if the new method is error tolerant. We use only one reservoir model in this chapter however various reservoir models are selected and variable rate pressure drop data are generated for each reservoir model with presumed rate data function for further validation of the deconvolution procedure in Appendix E. We emphasize various applications of deconvolution algorithm such as deconvolving individual flow periods. We also indicate the effects of regularization during deconvolving when input data are corrupted by errors.

4.1 Input Data Generation for B-Spline Based Deconvolution

As a base case, specifically the case of a reservoir model with a strong characteristic behavior, we selected a dual porosity reservoir with circular boundary ($\lambda = 1 \times 10^{-5}$, $\omega = 5 \times 10^{-2}$ and $r_{eD} = 1600$ — see **Table 4.1** for details). The dimensionless unit rate pressure response solution for a dual porosity reservoir with constant rate inner boundary and closed outer boundary is given in the Laplace domain as

$$\overline{P}_D = \frac{I_1(\sqrt{sf(s)}\, r_{eD})\, K_0(\sqrt{sf(s)}) + K_1(\sqrt{sf(s)}\, r_{eD})\, I_0(\sqrt{sf(s)})}{s\sqrt{sf(s)}\ [K_1(\sqrt{sf(s)})I_1(\sqrt{sf(s)}\, r_{eD}) - K_1(\sqrt{sf(s)}\, r_{eD})I_1(\sqrt{sf(s)})]} \quad \text{.....(4.1)}$$

Where $f(s)$ is defined as

$$\overline{f}(s) = \frac{\omega(1-\omega)s + \lambda}{(1-\omega)s + \lambda} \quad \text{.....(4.2)}$$

If wellbore storage and skin effects are to be incorporated into the solution then the constant rate pressure solution (Eq. 4.1) is expressed as:

$$\bar{P}_{wsD} = \frac{s\bar{P}_D + s_x}{s\,(1 + s\,C_D\,(s\bar{P}_D + s_x))} \qquad (4.3)$$

where s_x is the skin factor (dimensionless) and C_D is the dimensionless wellbore storage coefficient. The constant/unit rate pressure drawdown response function in real time domain — type curve solution — can be obtained by numerically inverting above equations by the numerical Laplace inversion algorithm (GWR) we described before. In the validation process we increase the complexity of the reservoir model step-by-step to assess, what (if any) influence the underlying reservoir model may have on the performance of our deconvolution procedure. We first consider a model without wellbore storage and skin effects (**Fig. 4.1**), we then incorporate a skin factor of 5 (**Fig. 4.2**), and finally we employ a dimensionless wellbore storage coefficient of 100 and skin factor of 5 (**Fig. 4.3**). The reservoir and fluid properties for the reservoir model is provided in **Table 4.1** below.

Table 4.1 – Reservoir and fluid properties for Validation Cases 1-4

Reservoir Properties:		
Wellbore radius, r_w	=	0.3 ft
Net Pay Thickness, h	=	30 ft
Formation permeability, k	=	3.333334 md
Total compressibility, c_t	=	5×10^{-6} 1/psi
Porosity, ϕ	=	0.15 (fraction)
Outer boundary radius, r_e	=	480 ft
Initial reservoir pressure, p_i	=	8000 psi
Dimensionless Wellbore storage coefficient, C_D	=	100
Skin factor, s_x	=	2 (dim.less)
Storativity ratio, ω	=	0.05 (dim.less)
Interporosity flow parameter, λ	=	1×10^{-5} (dim.less)
Fluid Properties:		
Fluid viscosity, μ	=	1 cp
Formation volume factor, B	=	1 RB/STB

We convolve the known constant/unit rate pressure solution with the flow history — which includes two variable rate production and two pressure buildup periods to generate the synthetic pressure histories required for the validation phase. In other words we distort/mask the constant rate pressure solution with a variable rate function. We note that in our process convolution is done in Laplace domain and synthetic pressure histories in real time domain are generated via inverse Laplace transformation. On the other hand, it is possible to generate the synthetic pressure histories using superposition theorem — if the

functional form of the solution is available in real time domain. Yet, it has to be emphasized that this process can be misleading because superposition involves the discretization of the convolution integral. If the rate profile is continuously (smoothly) changing then superimposing the constant rate pressure solution with discrete rate changes can result in erroneous generation of variable rate pressure drop response (*e.g.*, the generated pressure history may appear like stair step changes instead of continuously changing). As such, we strongly recommend that convolution should be done in Laplace domain — except for the case of constant rates — when there is a robust and efficient numerical Laplace inversion algorithm is available for inverting the solution back into time domain.

In our validation we use the following variable-rate profile:

$$q(t) = \begin{cases} 405.23 - 736.79\, e^{\frac{-t}{5}} + 368.39\, e^{\frac{-t}{20}} - 3.684\, t \ldots\ldots\ldots\ldots\ldots\ldots 0 < t \le 60\,\text{hr} \\ 0 \ldots\ldots\ldots\ldots\ldots\ldots\ldots\ldots\ldots\ldots\ldots\ldots\ldots\ldots\ldots\ldots\ldots\ldots 60 < t < 100\,\text{hr} \\ 300\, e^{\frac{(100-t)}{100}} \ldots\ldots\ldots\ldots\ldots\ldots\ldots\ldots\ldots\ldots\ldots\ldots 100 \le t \le 200\,\text{hr} \\ 0 \ldots\ldots\ldots\ldots\ldots\ldots\ldots\ldots\ldots\ldots\ldots\ldots\ldots\ldots\ldots\ldots\ldots\ldots 200 < t < 300\,\text{hr} \end{cases} \quad \ldots\ldots\ldots\ldots (4.4)$$

As we ultimately intend to process permanent (pressure) gauge data, this rate profile was selected to mimic typical pressure drawdown/buildup test sequences. The constant rate pressure drawdown response (type curve solutions) and variable rate pressure drop response data functions for three validation cases obtained by inverse Laplace transformation are presented below (**Figs. 4.1-4.3** and **Figs 4.4-4.6**, respectively).

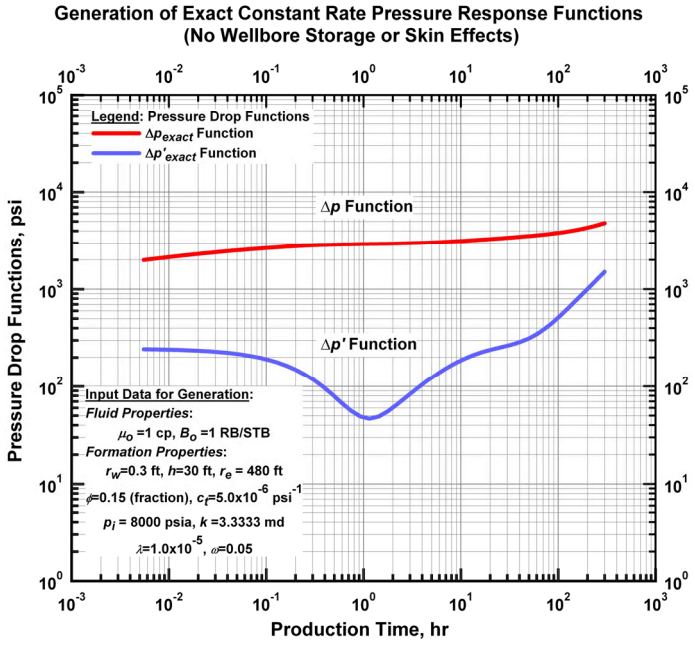

Figure 4.1 – Generation of the constant rate pressure response functions (exact solutions) of a dual porosity reservoir without wellbore storage or skin effects.

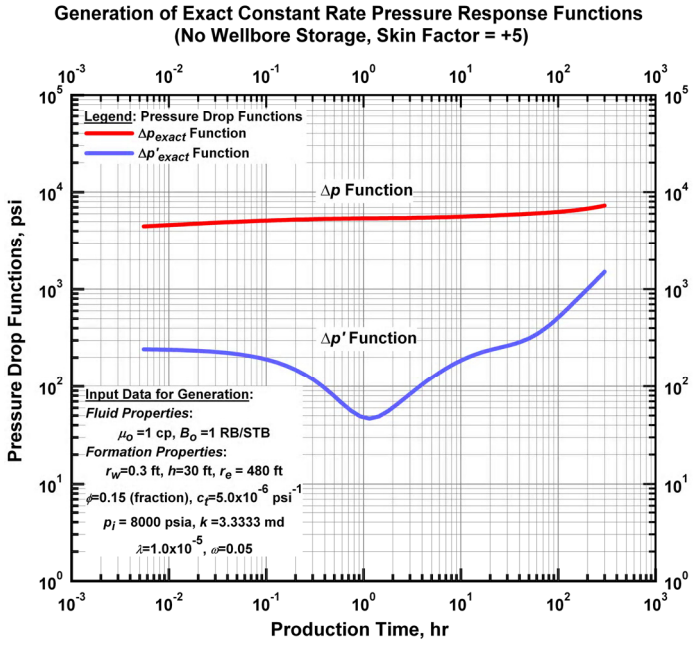

Figure 4.2 – Generation of the constant rate pressure response functions (exact solutions) of a dual porosity reservoir without wellbore storage and skin effect of +5.

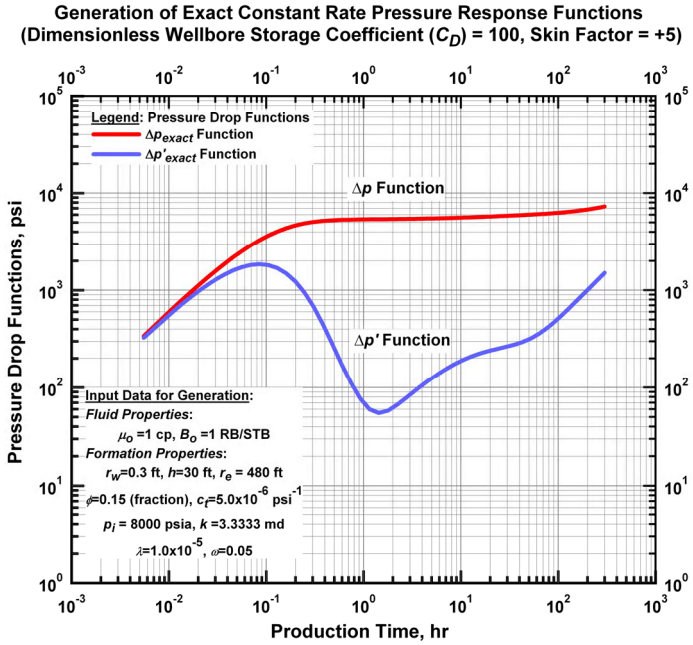

Figure 4.3 – Generation of the constant rate pressure response functions (exact solutions) of a dual porosity reservoir with wellbore storage and skin effects.

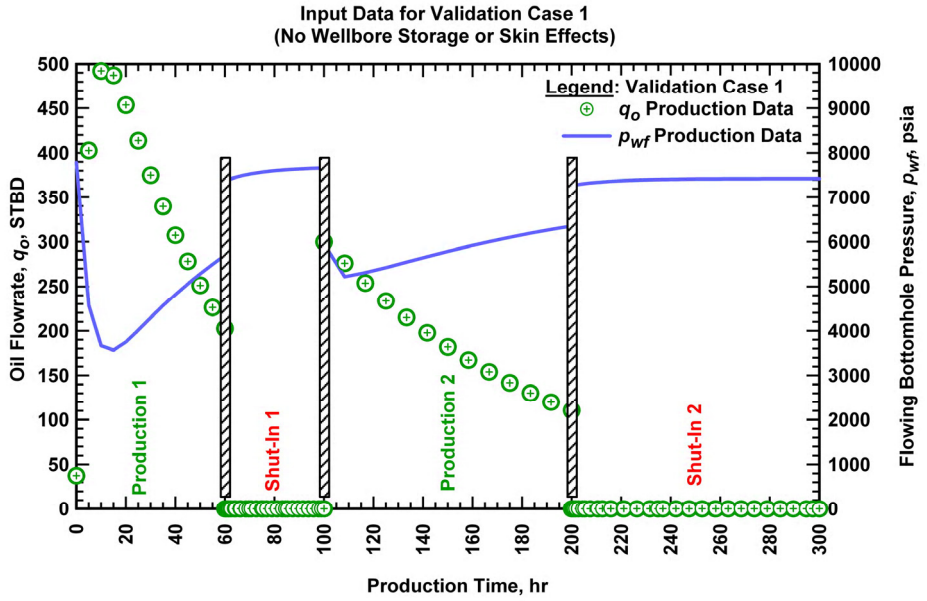

Figure 4.4 – Input data for Validation Case 1 (no wellbore storage effects, skin factor (s_x) = 0).

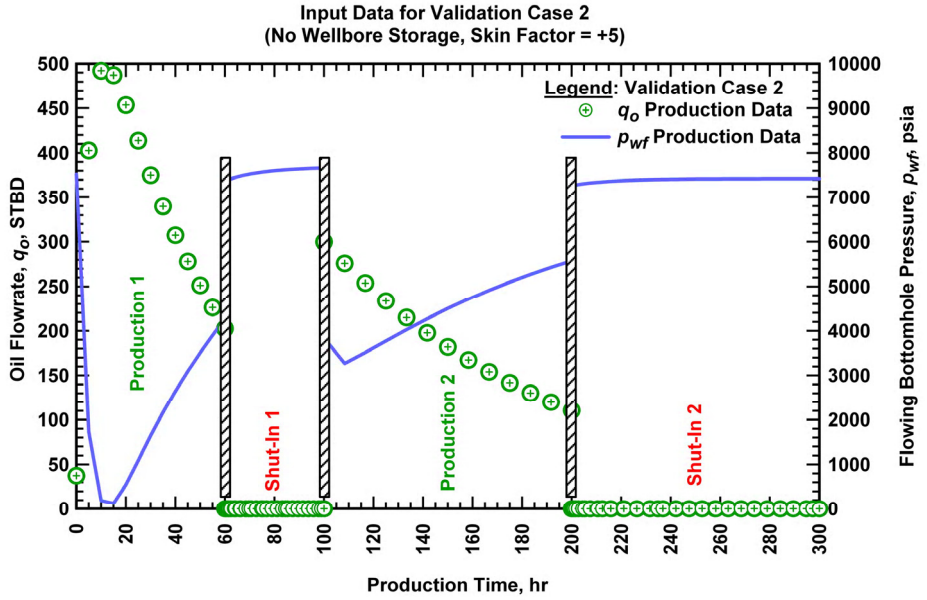

Figure 4.5 – Input data for Validation Case 2 (no wellbore storage effects, skin factor (s_x) = +5).

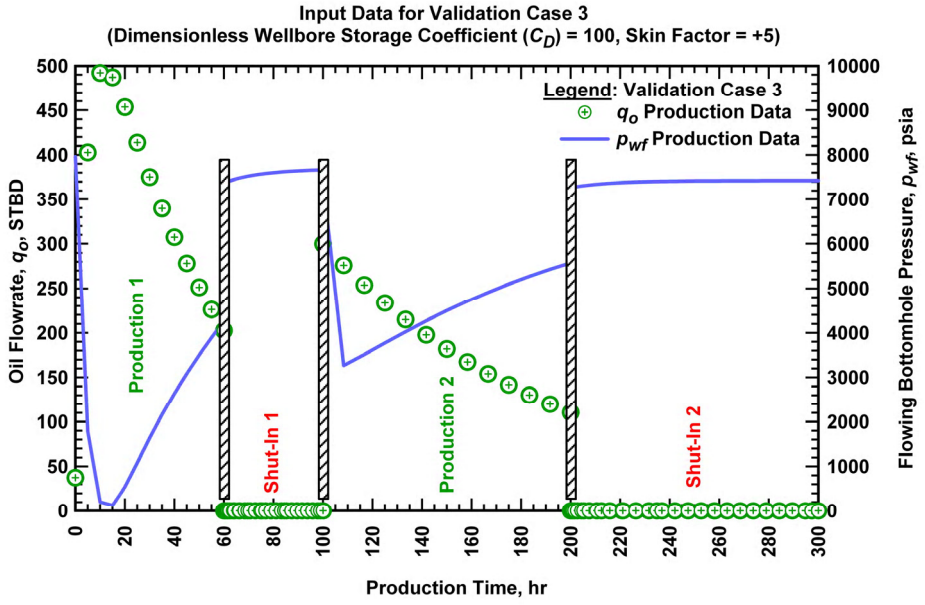

Figure 4.6 – Input data for Validation Case 3 (dimensionless wellbore storage coefficient (C_D) = 100, skin factor (s_x) = +5).

4.2 B-Spline Deconvolution Using Generated (Synthetic) Data

In this section we verify our new deconvolution method with using the data of three cases generated before (**Fig. 4.4 – Fig. 4.6**). We note that there are no errors associated with data and convolution and numerical Laplace inversion procedure is precise and robust enough to prevent incorrect pressures particularly at the rate discontinuities.

In the first example, we perform deconvolution with the input data shown in **Fig.4.4**. **Fig. 4.7** presents our deconvolution results for this case, and we note that when the deconvolution results are compared with the exact input response, our deconvolution methodology performs very well in this case. All of the characteristic features of a dual porosity reservoir model are present in the results — including the boundary dominated flow regime. In **Fig. 4.8** we present the deconvolution results for the case when a skin factor of 5 is included in the input pressure response — we note an additional increase in the unit rate drawdown pressure response (from the positive skin factor) and we see that the well testing derivative function remains essentially identically to the trends observed in **Fig. 4.4** (as would be expected). In **Fig. 4.9** we present the deconvolution results when wellbore storage and skin effects are incorporated into the base model. We note that the deconvolution shown in **Fig. 4.9** is performed using "surface" rates — which do not reflect wellbore storage conditions (although wellbore storage effects are (obviously) included in the observed pressure data).

Fig. 4.9 is of particular practical interest because we clearly must recognize that although deconvolution to remove wellbore storage effects is a worthwhile goal — in current practice, it is very unlikely that we would be able to obtain the downhole flowrate data at sufficiently accuracy such that we could "remove" wellbore storage effects. However, given a general variable-rate/variable pressure data sequence, we can use deconvolution to reconstruct the constant rate drawdown response which would include wellbore storage effects (as shown quite effectively in **Fig. 4.9**). By this way we can proceed and then match the deconvolved pressure response functions with an appropriate type curve solution.

From a theoretical perspective, we can perform deconvolution using *only* the pressure buildups (which typically contain higher quality data than drawdown periods (*i.e.*, less data noise)). And from a practical standpoint, in some cases only pressure buildup data are available for analysis (in addition to the production (flowrate) history). At this point we can not construct the entire pressure history from a limited portion of the available data (say from deconvolving only a single pressure buildup test in a larger production/shut-in test sequence).

However, we will illustrate that we can construct a reasonable portion of the entire pressure history from a single pressure buildup test. In **Fig. 4.10** we use only the final pressure buildup test data for deconvolution — in fact we only used the first 60 hours (of the available 100 hours) in this pressure buildup test. We note in **Fig. 4.10** that the entire "early portion" of the test sequence is effectively deconvolved — but we do not obtain the complete reservoir pressure signal because we truncated the deconvolution data set. In particular, we did complete re-construct the "late-time" boundary effects from the final pressure buildup test. For clarity, we present the "base data" for this deconvolution **Fig. 4.11** (*i.e.*, the first 60 hours of the final pressure buildup test in this sequence (see **Fig. 4.6** for orientation)).

In all these cases describe before we perform deconvolution using "ideal" data. We have not utilized regularization for the cases of ideal data. We can conclude that regularization is not needed for the cases where input data have no errors. Unfortunately, almost in every field case, pressure and flowrate data are contaminated by errors. Therefore, we are going to describe the application of regularization procedure to our B-spline based deconvolution method in the next chapter. In addition, we test the validity of the new deconvolution method under various levels of errors.

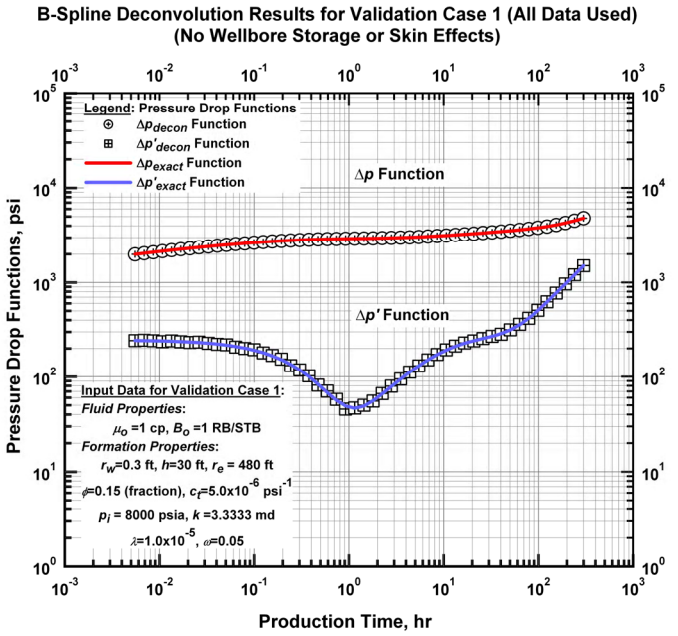

Figure 4.7 – Validation Case 1 — B-Spline deconvolution results for validation case 1 (all data used) (no wellbore storage or skin effects).

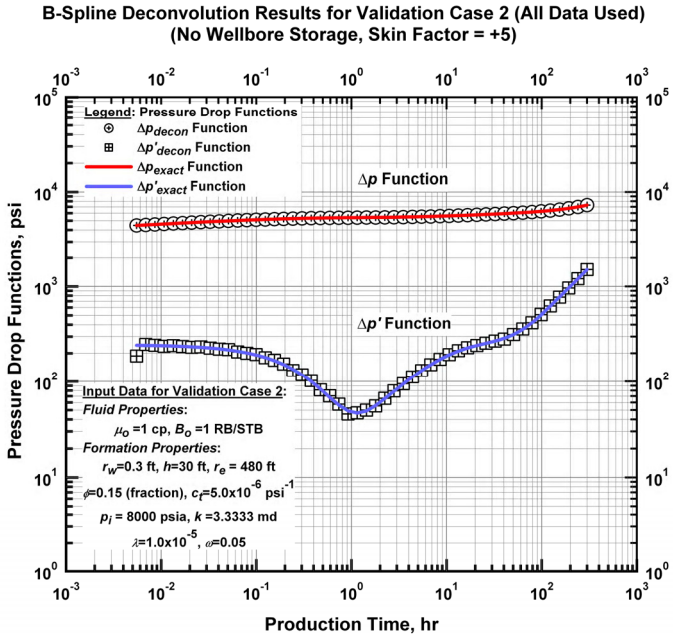

Figure 4.8 – Validation Case 2 — B-Spline deconvolution results for validation case 2 (all data used) (no wellbore storage, skin factor (s_x) = +5).

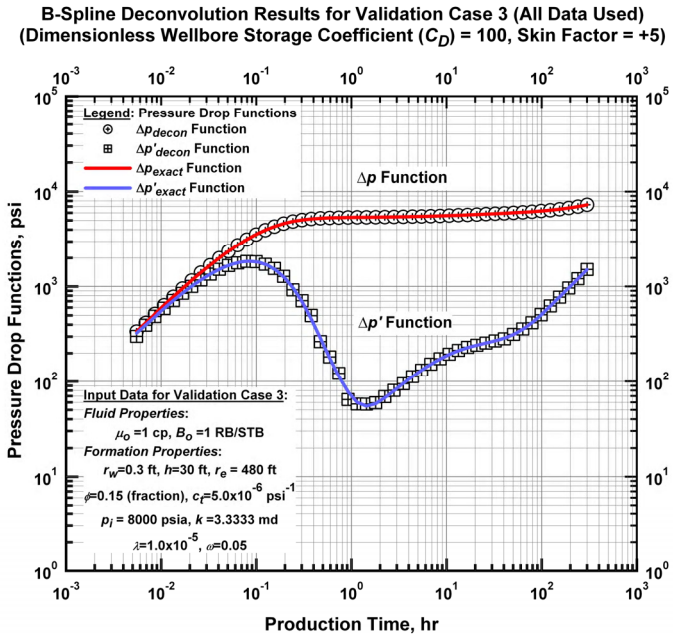

Figure 4.9 – Validation Case 3 — B-Spline deconvolution results for validation case 3 (all data used) (dimensionless wellbore storage coeffiecient (C_D) = 100, skin factor (s_x) = +5).

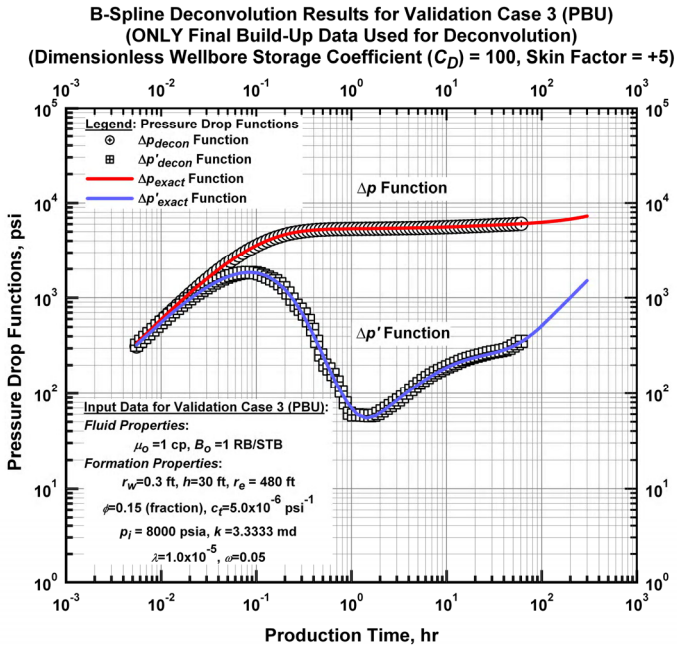

Figure 4.10 – Validation Case 3 — B-Spline deconvolution results for validation case 3 (ONLY final pressure buildup data are used for deconvolution) (dimensionless wellbore storage coeffiecient (C_D) = 100, skin factor (s_x) = +5).

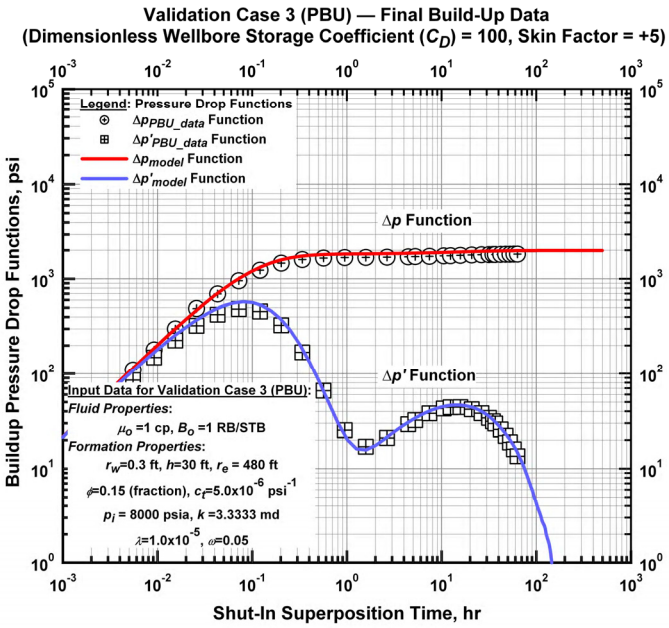

Figure 4.11 – Validation Case 3 — Illustration of first 60 hours of the final pressure buildup test sequence (data used for deconvolution in **Fig. 4.10**).

4.3 B-Spline Deconvolution under Presence of Errors in the Input Data

So far, we have validated our new method without error in the input data. However, almost in every field case, rate and pressure measurements contain errors. Broadly speaking noise in rate measurements is higher than the noise in pressure measurements in well test analysis. On the contrary, in production data analysis rate measurements are more accurate than pressure measurements. We provide five synthetic cases where we have added random and systematic data errors — random errors are ranged from 1 percent to 40 percent (we note that we have employed the same production history and reservoir model with wellbore storage and skin effects (base performance (no error) shown in **Figs. 4.6 and 4.9**)). In these examples, we have added various levels of random error to both the pressure and rate data, and we also seeded the data with a small systematic error in pressure — for error levels up to 10 percent. We can still perform deconvolution on these data, but in these cases, we must use regularization to address the combined effects of random and systematic errors in the data.

Fig. 4.12 describes the case (Validation case 4) where we have added 1 percent random error to both rate and pressure data. Decreasing the precision in the numerical Laplace inversion procedure employed in this work — GWR — results in systematic errors particularly at the discontinuities in production history. As expected, deconvolution performs very well in this case as seen in **Fig. 4.13**. The deconvolved results are essentially the same as the (input) ideal model responses.

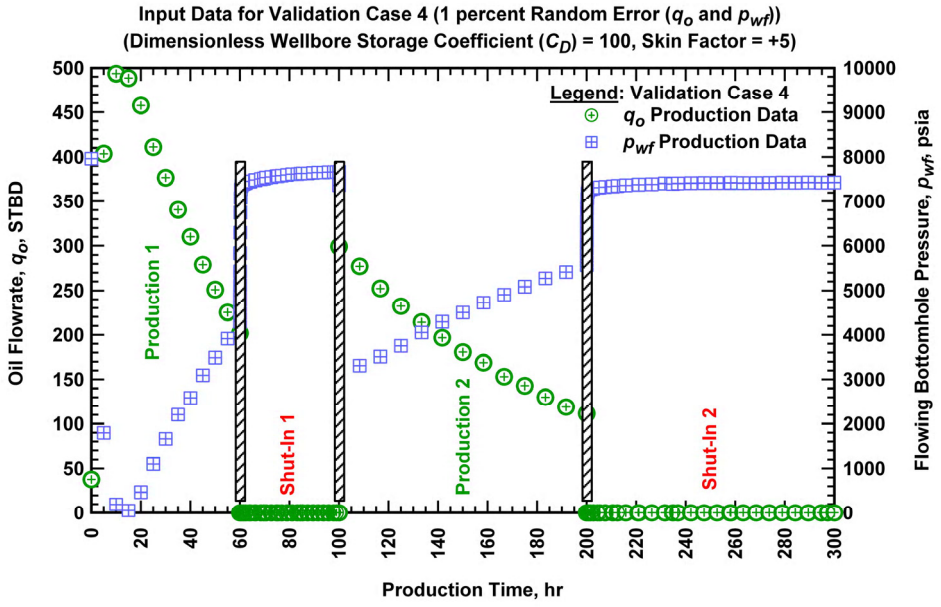

Figure 4.12– Input data for Validation Case 4 — with 1 percent random noise and systematic error (dimensionless wellbore storage coefficient (C_D) = 100, skin factor (s_x) = +5).

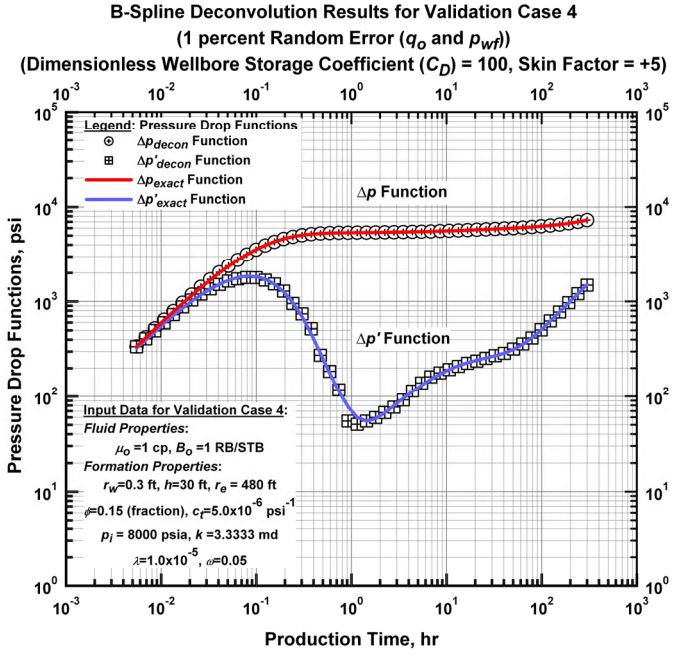

Figure 4.13– Validation Case 4 — Deconvolved pressure response (optimal regularization ($\alpha = 0.0001$)).

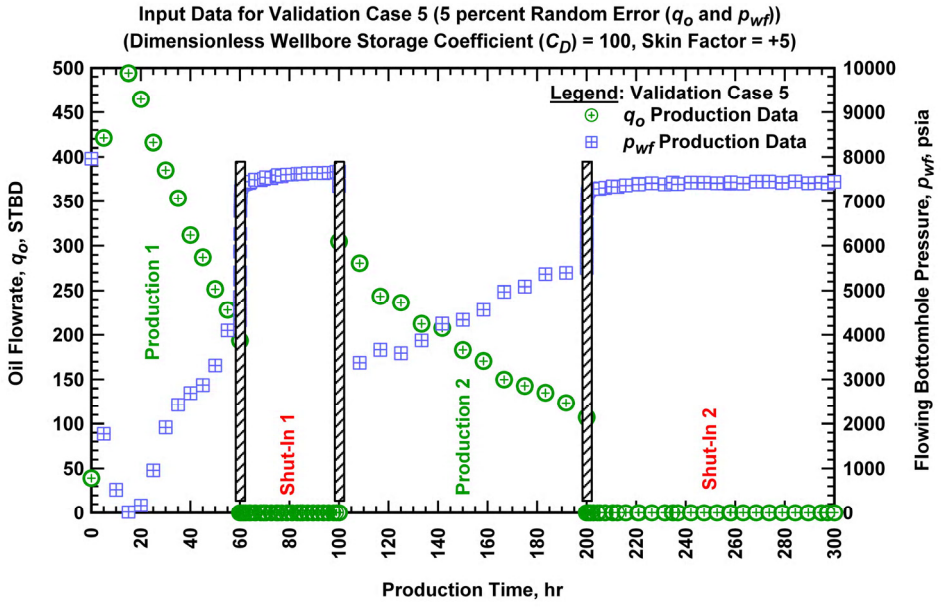

Figure 4.14– Input data for Validation Case 5 — with 5 percent random noise and systematic error (dimensionless wellbore storage coefficient (C_D) = 100, skin factor (s_x) = +5).

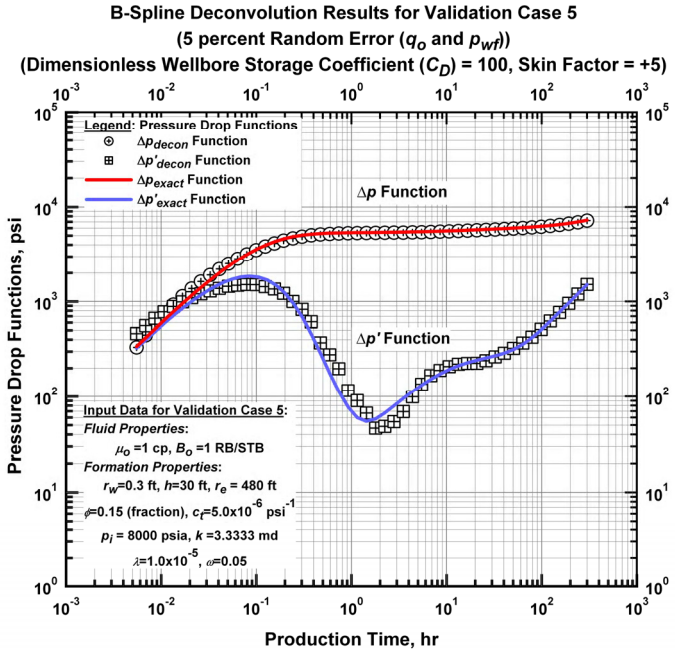

Figure 4.15– Validation Case 5 — Deconvolved pressure response (optimal regularization ($\alpha = 0.0005$)).

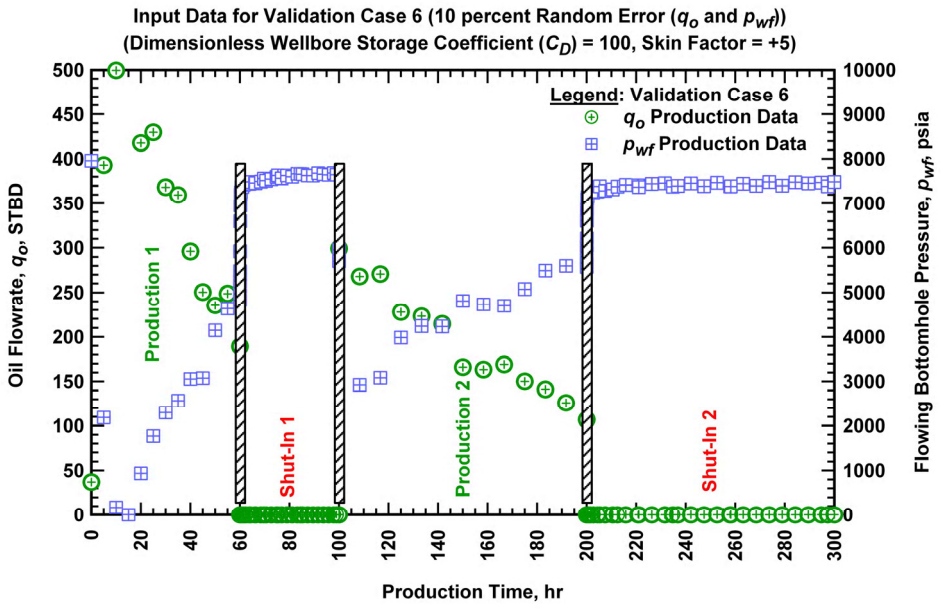

Figure 4.16– Input data for Validation Case 6 — with 10 percent random noise and systematic error (dimensionless wellbore storage coefficient (C_D) = 100, skin factor (s_x) = +5).

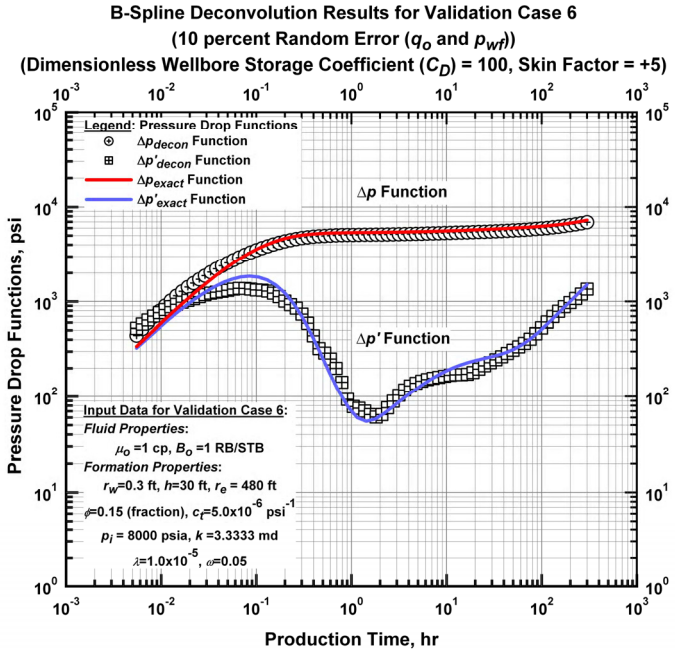

Figure 4.17– Validation Case 6 — Deconvolved pressure response (optimal regularization ($\alpha = 0.0007$)).

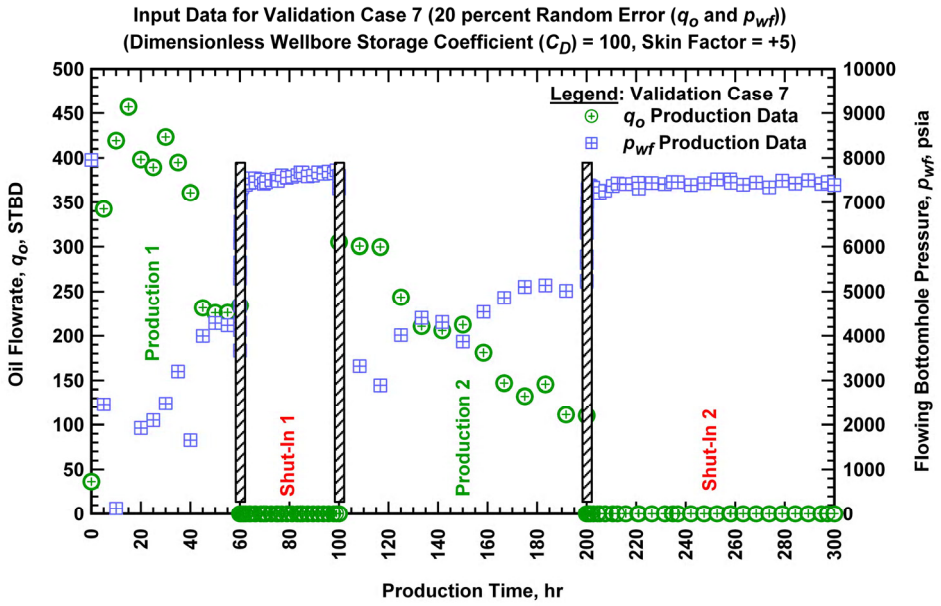

Figure 4.18– Input data for Validation Case 7 — with 20 percent random noise (dimensionless wellbore storage coefficient (C_D) = 100, skin factor (s_x) = +5).

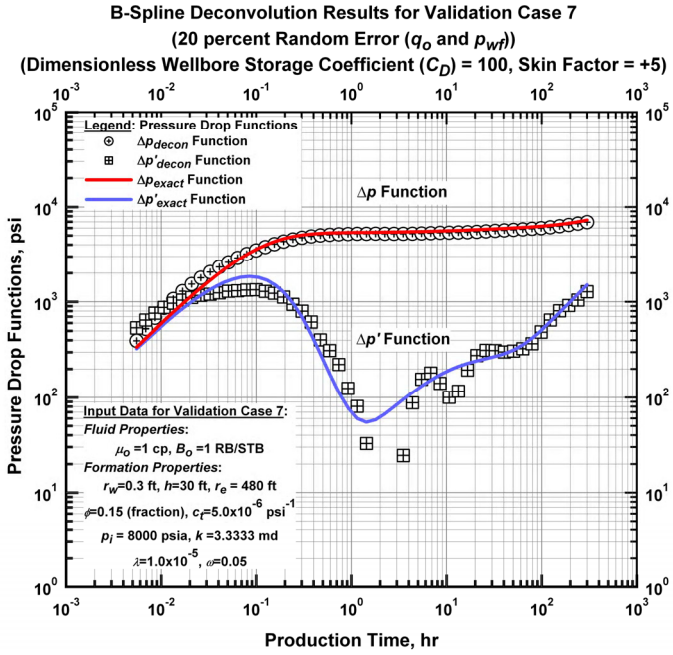

Figure 4.19– Validation Case 7 — Deconvolved pressure response (optimal regularization ($\alpha = 0.0008$)).

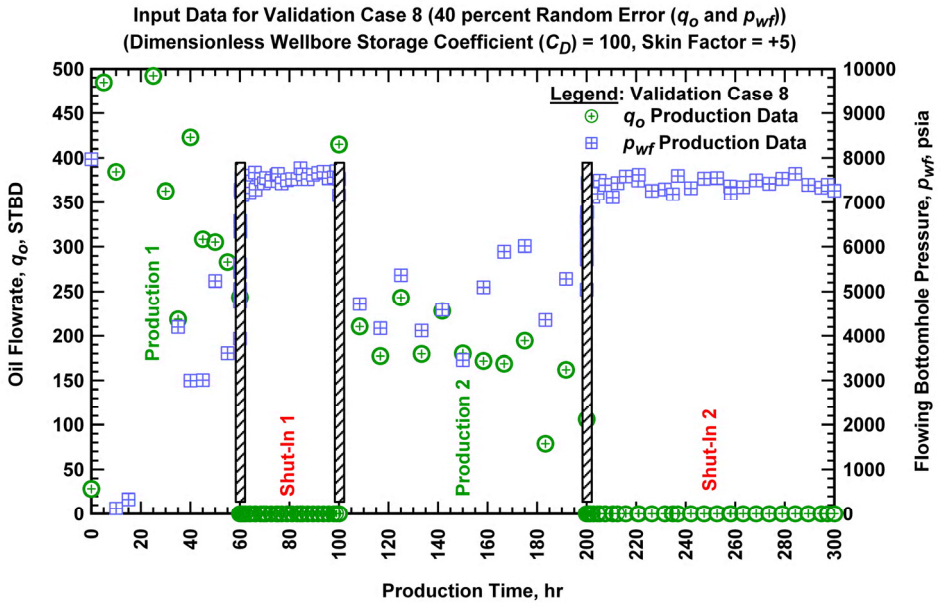

Figure 4.20– Input data for Validation Case 8 — with 40 percent random noise (dimensionless wellbore storage coefficient (C_D) = 100, skin factor (s_x) = +5).

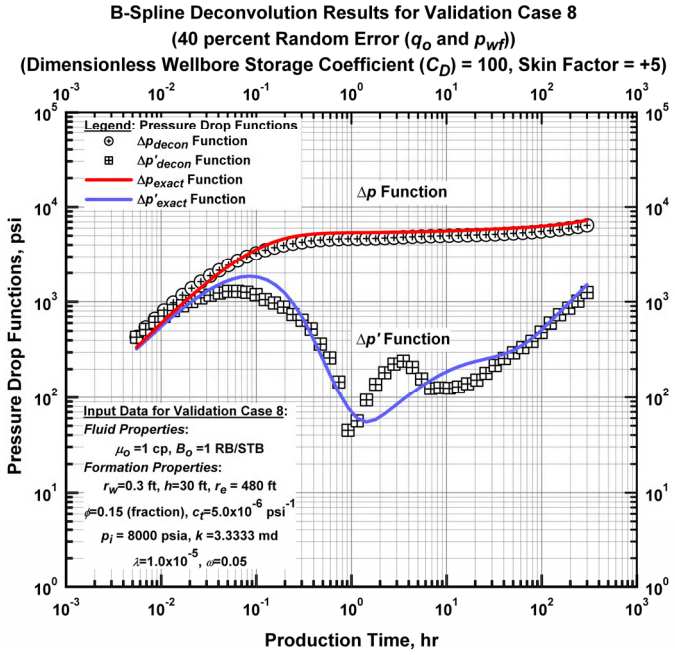

Figure 4.21– Validation Case 8 — Deconvolved pressure response (optimal regularization ($\alpha = 0.0011$)).

Fig. 4.14 presents the case (Validation case 5) of 5 percent random error in the input data. We note that in **Fig. 4.15** deconvolution reconstructs the characteristic features of the reservoir model for the entire test duration. Minor artifacts in the well testing derivative — particularly in transition flow region (dip feature) — are seen but in general deconvolved pressure functions are representative of the selected reservoir model. We have found the optimum deconvolution result by tuning the regularization parameter, α, which is found to be 0.0005 for 5 percent of error.

We subsequently increase the error level to 10 percent for case 6 (**Fig. 4.16**). Clearly, some artifacts caused by inconsistent data are seen (mostly in the well testing derivative). Thus, regularization has to be employed to overcome the effects of inconsistencies on deconvolution. With regularization, deconvolution recovers the characteristic features of the reservoir model for the whole test duration successfully (**Fig. 4.17**). As done in the previous cases before, the value of regularization parameter is picked by the discrepancy principle which will be illustrated later.

Fig. 4.18 and **Fig 4.20** presents the two cases (validation cases 7 and 8) where the error levels are relatively high. We recognize that the levels of errors — 20 and 40 percent — are not realistic at all. However, our purpose is to test the deconvolution algorithm under significant levels of errors and to identify how errors affect the deconvolved results. We previously mentioned that when errors are introduced, the first artifact occurs in the transition flow region in well testing derivative. Providing sufficient regularization this artifact can be eliminated to a considerable extent as illustrated before but when the error level is significantly higher (say 20 percent and above) then it is not possible to recover the well testing derivative function to a reasonable level as we expect. On the other hand, some part of the test duration can still be recovered by deconvolution — surprisingly boundary dominated flow region in well testing derivative function and major parts (particularly after wellbore storage dominated flow region) of the constant rate pressure function. **Figs. 4.19 and 4.21** illustrate the deconvolution results and confirm that the new B-spline based deconvolution method with regularization is tolerant to higher levels of errors. In the next section we are going to describe the effects of direct and indirect regularization.

4.4 Effect of Selecting the Optimum Value of Regularization Parameter on Deconvolution

Regularization can be described as smoothing the data which have errors associated with. One can easily fit error into data by using a low value of regularization parameter or the result can be over-smoothed by using a high value of regularization parameter. Therefore, the value of the regularization parameter has a profound effect the deconvolution solution for this case. **Figs**. **4.22, 4.23,** and **4.24** illustrate the discrepancy principle by which the regularization parameter, α is picked. Our base case for illustrating the effect of the value of regularization parameter is the case where we have 10 percent error in the input data.

We also present in **Fig. 4.25** the deconvolution results when no regularization is used and furthermore we show how over-smoothed results are deviated from the exact solution (**Fig. 4.26**).

When regularization is not used (**Fig. 4.22**) there is a random error between the observed response ($\Delta\tilde{\mathbf{p}}$) and its reconstructed value ($\mathbf{X}\hat{\mathbf{c}}$) — model response generated by B-splines. If a higher value of regularization parameter is used, over-smoothing is obvious from the one-sided deviations (**Fig. 4.24**). The optimum value of the regularization parameter (in this case α = 0.0007) is obtained as the largest value still not causing systematic discrepancy between observed and reconstructed responses (**Fig. 4.23**). If we proceed and reconstruct the constant rate pressure and well testing derivative function from the model response in **Fig. 4.22**, then obviously deconvolution does not seem accurate enough by any means (**Fig 4.26**) or if we reconstruct the deconvolved pressure functions with a higher value of α, then we lose all the information available by over-smoothing. In other words, deconvolved results are deviated from the exact solutions and the characteristic features of the reservoir model are eliminated.

4.5 Effect of Selecting the Base Value (*b*) for Logarithmic Knot Distribution on Deconvolution (Indirect Regularization)

In this section we demonstrate that for lower levels of noise, regularization procedure may not be needed (*i.e*. we are only going to rely on B-splines and least-squares for regularization purposes). As we have described in Chapter III, knots are distributed logarithmically once the base (*b*) is selected. The selection of *b* is arbitrary and *b* value essentially determines the number of knots. We recommend that to reveal characteristic reservoir behavior, the number of knots should be on the order of at least 2–6 knots per log cycle (for typical kernels of interest (*i.e.*, input flowrate functions observed in reservoir engineering)). Therefore, we never use more knots, (but we may be forced to reduce the number of knots in cases where the data quality does not justify looking for sophisticated signatures.).

We take three base cases where we have 1, 5, and 10 percent random error in the input data given in **Figs**. **4.12**, **4.14**, and **4.16**, respectively. We do not use the regularization process described before in these cases. But, we do change the value of *b* to recover the constant rate pressure and well testing derivatives to a considerable extent. For the first case (1 percent random error) it is seen that without regularization deconvolution reconstructs the entire test duration effectively (**Fig. 4.27**). Increasing the value of *b* (**Fig. 4.28)** causes some minor artifacts. For the second case, very interestingly, optimum value for *b* is shown. Starting with *b* = 1.9 we increase the value for *b* (**Figs. 4.29, 4.30 and 4.31**) and for *b* = 3.0 deconvolution results are comparable to exact solution as shown in **Fig. 4.30**. Also in this case it is seen that we can recover an important part of the test sequence without using regularization — instead by changing the value of *b*. Finally, for the third case (10 percent error) we use four values for *b* (**Figs. 4.32, 4.33, 4.34,** and **4.35)**.and *b* = 3.5 seems to give a reasonable result comparable to exact solution. An important part of

the constant rate pressure function can be recovered without regularization. However, deconvolved well testing derivative function exhibits artifacts and regularization is required for this case (for reference compare **Fig. 4.17** and **Fig. 4.34**).

We conclude from these experiments that for lower level of errors, finding the optimum value of b or in other words, optimum number of knots (or knot locations) can provide sufficient regularization. We prefer to call this process *indirect regularization*. In our method we find the optimum value of b the hard way (*i.e.* trying several values and comparing the results) which takes a considerable amount of computational since b is selected before numerical Laplace inversion (sensitivity matrix construction). Future efforts can be focused on developing an algorithm for finding the optimum number and location of knots. Our final comments in this section will be combining indirect and direct regularization eliminates the noise efficiently and in our work we recommend using these two approaches together rather than focusing on one.

4.6 Considerations before Deconvolution and Discussion

In the deconvolution process the initial pressure is required to create the observed pressure response ($\Delta\tilde{\mathbf{p}}$). As it is pointed by Levitan *et al.*, an accurate estimate of the initial pressure is a critical element of deconvolution. We also confirm this statement with our experiments — in particular, using a significantly erroneous estimate of initial reservoir pressure will cause a systematic error in the deconvolved, equivalent constant-rate pressure response. For example, using an initial pressure larger than the actual initial pressure will result in an apparent pseudosteady-state flow regime at the end of the deconvolved test sequence or production data set. Thus, we note that that an apparent pseudosteady-state flow regime is a possible artifact of using an incorrect estimate of the initial reservoir pressure.

It is worth noting that input data should be treated very carefully before deconvolution. First, an accurate estimate of initial pressure should be available. Pressure and rate data should be analyzed very carefully to reveal inconsistencies. If we reveal any inconsistency regarding test history, we choose not to use inconsistent data. We either choose to apply deconvolution to individual flow periods — or if the rate data is reliable, then we can use all the rate data and consistent pressure (disregarding inconsistent data) data to construct constant rate pressure and well testing derivative functions for the entire test duration. We will discuss this issue in Appendix D. Also, consistent rate data should be honored at almost every given measurement by splitting the flow history into segments. We note that these issues are very critical prior to deconvolution and accurate results can be obtained if these issues are taken into consideration.

From our validation experiments we can conclude that very accurate (essentially exact) results can be obtained using any major event in the test sequence (*i.e.*, a production test, a shut-in, or the complete

history). We also note that when the input data have errors or inconsistencies, we require some form of regularization to provide meaningful resolution of these corrupted data. As a comment, we believe that our deconvolution approach can address relatively high levels of noise and other data inconsistencies — further proof of this hypothesis is found in our field examples given later in this work.

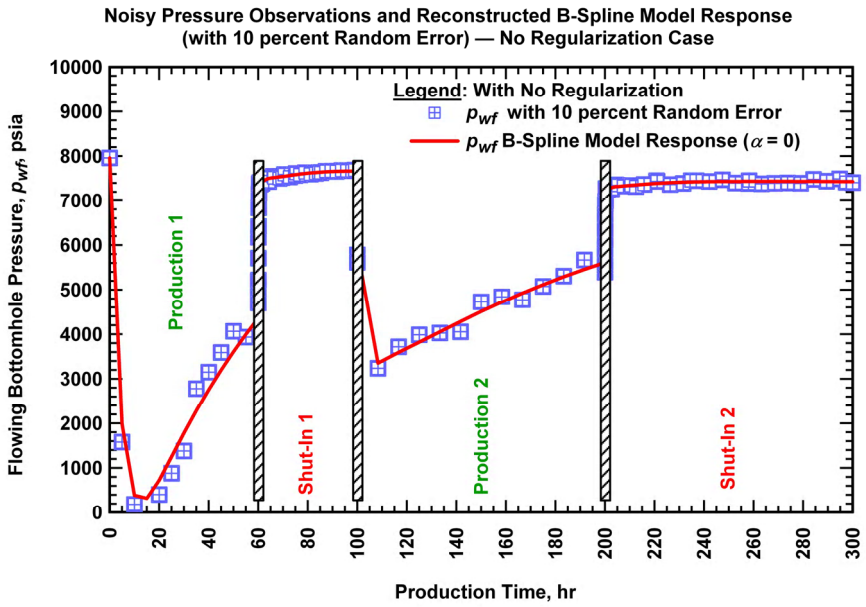

Figure 4.22 – Effect of regularization parameter (Validation Case 6) — Noisy pressure observations and the B-spline p_{wf} model response (no regularization).

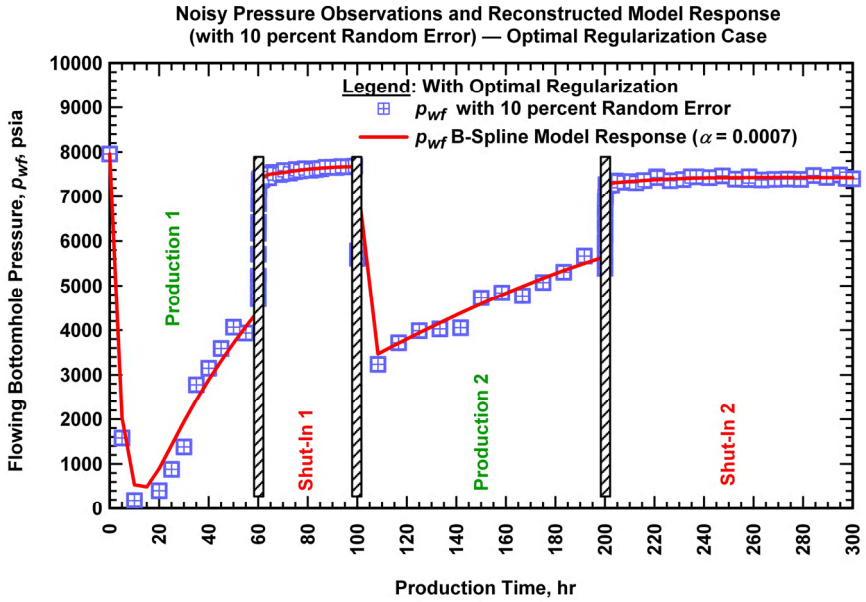

Figure 4.23– Effect of regularization parameter (Validation Case 6) — Noisy pressure observations and the B-spline p_{wf} model response (optimal regularization (α = 0.0007)).

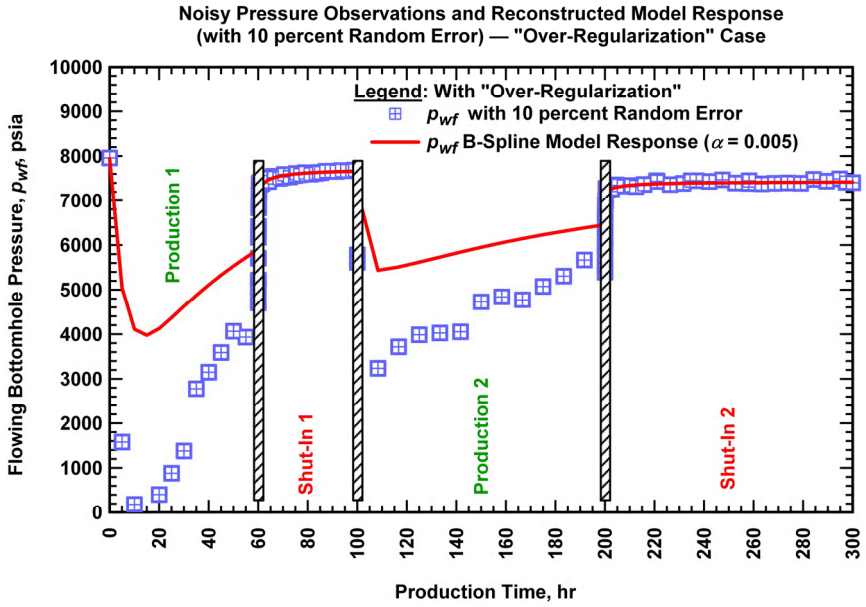

Figure 4.24– Effect of regularization parameter (Validation Case 6) — Noisy pressure observations and the B-spline p_{wf} model response ("over-regularization" case (α = 0.005)).

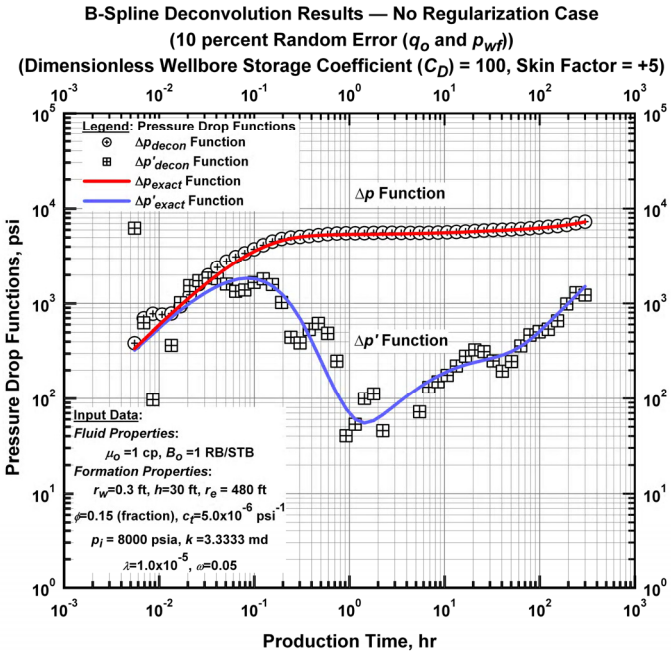

Figure 4.25– Effect of regularization parameter (Validation Case 6) — Deconvolved pressure response (no-regularization).

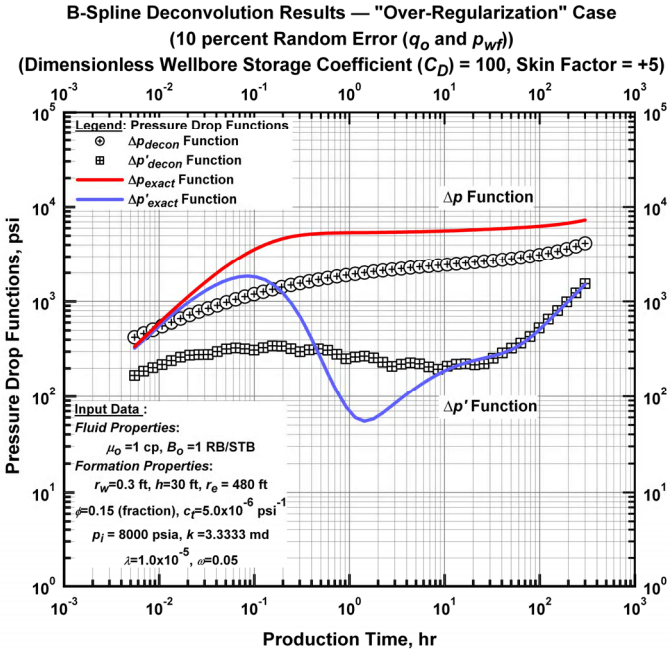

Figure 4.26– Effect of regularization parameter (Validation Case 6) — Deconvolved pressure response ("over-regularization" case ($\alpha = 0.005$)).

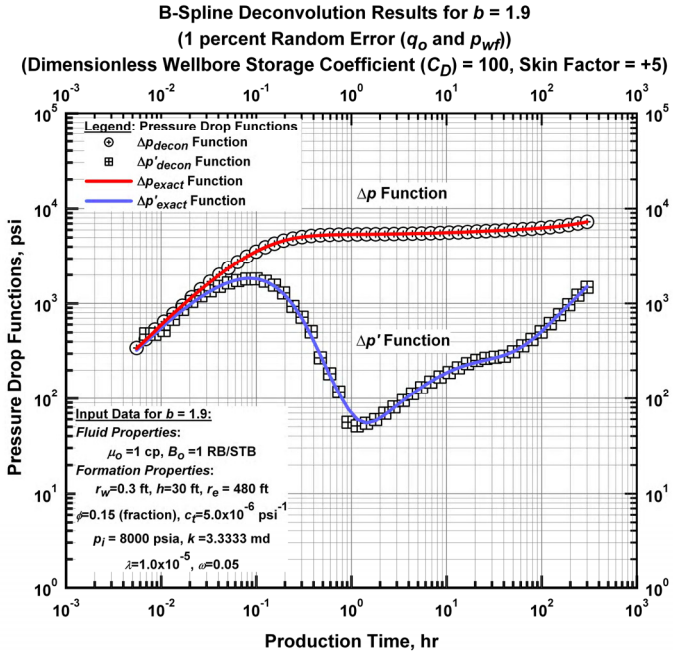

Figure 4.27– Effect of logarithmic knot distribution (b value) on deconvolution results (Validation Case 4) — Deconvolved pressure response (b = 1.9)

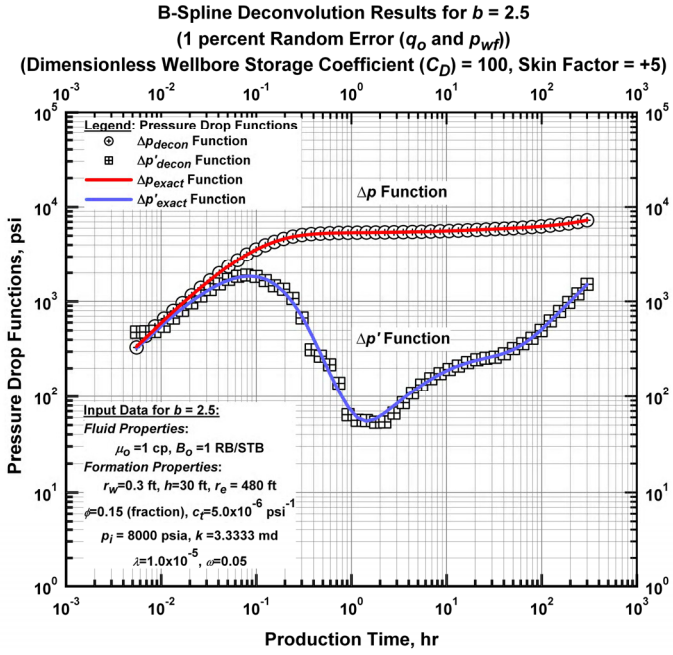

Figure 4.28– Effect of logarithmic knot distribution (b value) on deconvolution results (Validation Case 4) — Deconvolved pressure response (b = 2.5).

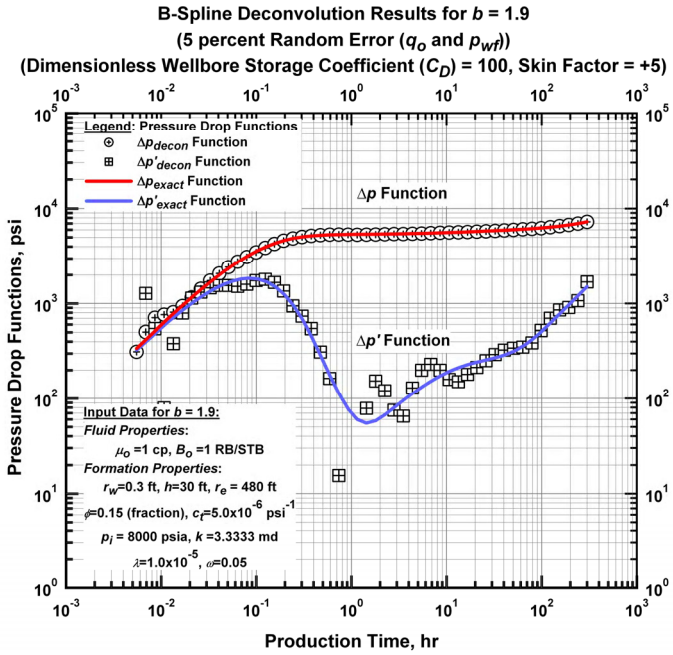

Figure 4.29– Effect of logarithmic knot distribution (b value) on deconvolution results (Validation Case 5) — Deconvolved pressure response (b = 1.9).

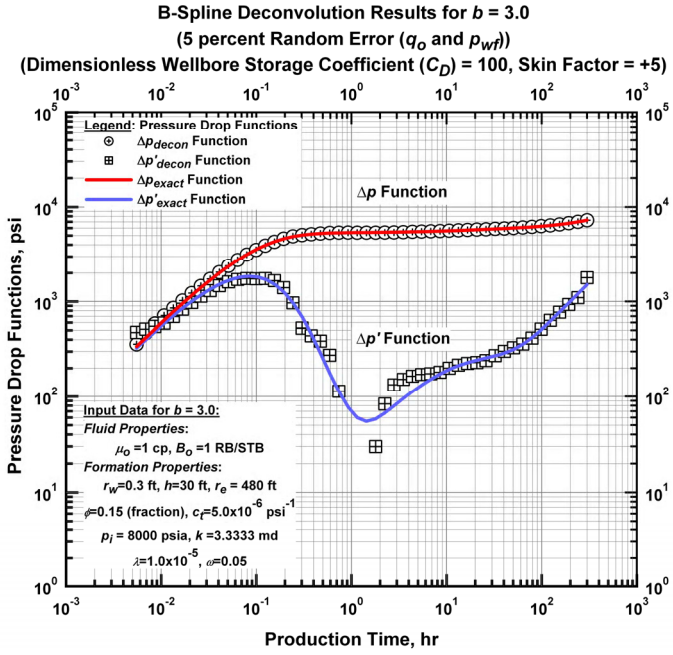

Figure 4.30– Effect of logarithmic knot distribution (b value) on deconvolution results (Validation Case 5) — Deconvolved pressure response (b = 3.0).

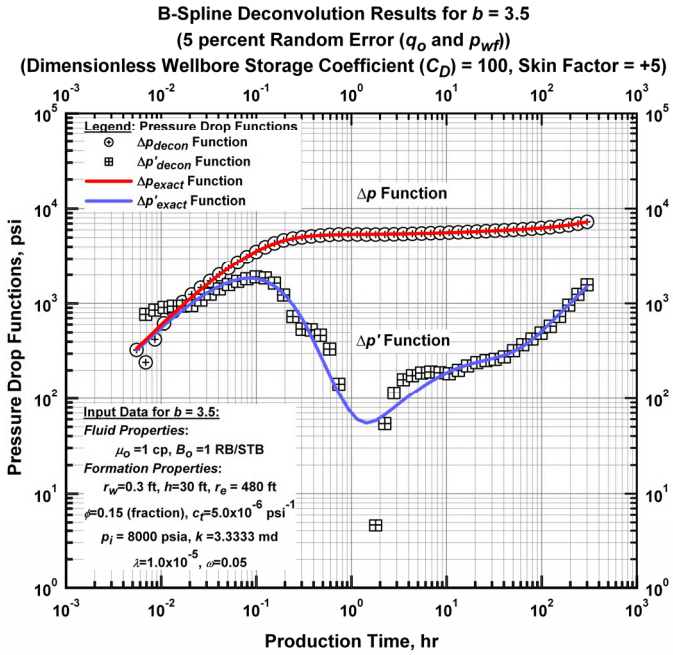

Figure 4.31 – Effect of logarithmic knot distribution (b value) on deconvolution results (Validation Case 5) — Deconvolved pressure response (b = 3.5).

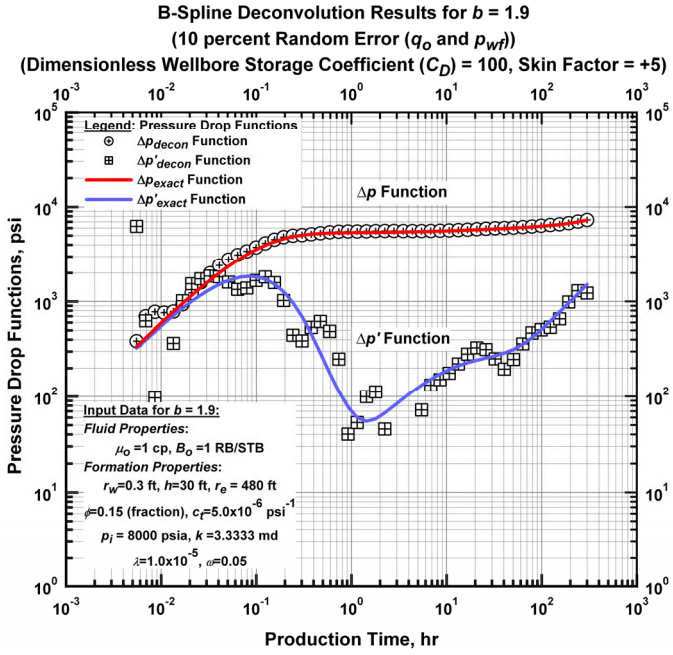

Figure 4.32 – Effect of logarithmic knot distribution (b value) on deconvolution results (Validation Case 6) — Deconvolved pressure response (b = 1.9).

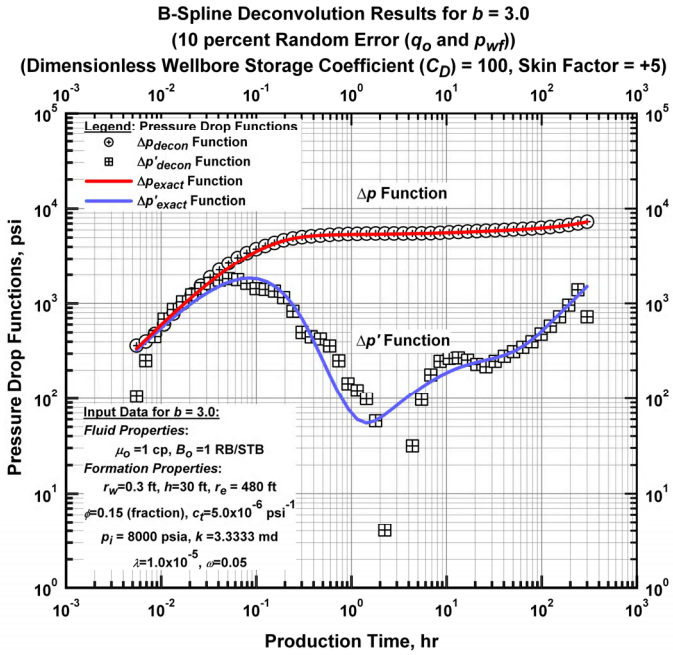

Figure 4.33– Effect of logarithmic knot distribution (b value) on deconvolution results (Validation Case 6) — Deconvolved pressure response (b = 3.0).

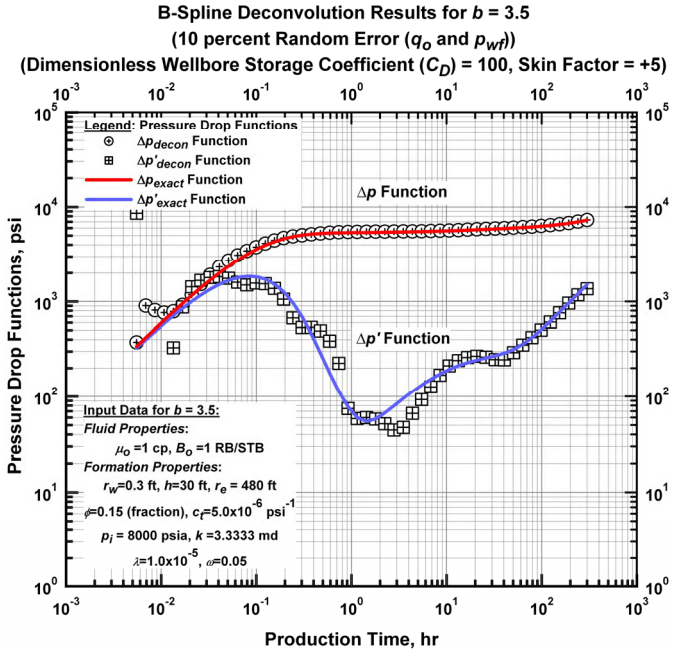

Figure 4.34– Effect of logarithmic knot distribution (b value) on deconvolution results (Validation Case 6) — Deconvolved pressure response (b = 3.5).

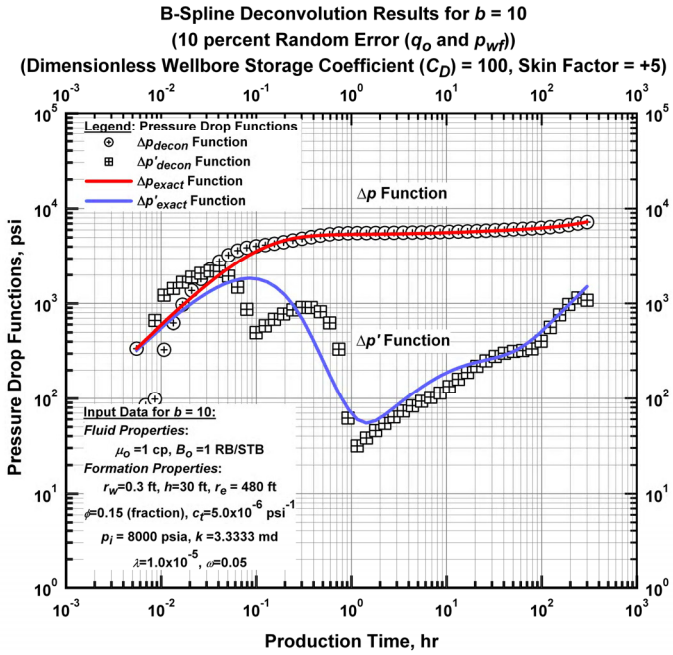

Figure 4.35– Effect of logarithmic knot distribution (*b* value) on deconvolution results (Validation Case 6) — Deconvolved pressure response (*b* = 10).

CHAPTER V

APPLICATION OF THE METHOD TO FIELD EXAMPLES

Having verified our new technique, we can now apply the same procedure to field data. We note that our technique is not limited to a specific event (*e.g.* eliminating wellbore storage). In fact, we are able to apply our new deconvolution method to several classes of field applications. For convenience, we classify our field examples into four groups:

- Wellbore storage distorted pressure data.
- Well test data including multiple flow sequences.
- Permanent downhole gauge data (several flow sequences).
- Long-term production data (rates and pressures).

These examples illustrate the use of B-spline deconvolution for analyzing various events (production/shut-in sequences), and should be considered typical of cases that could be encountered in field operations.

5.1 B-Spline Deconvolution of Pressure Transient Data Distorted by Wellbore Storage

The most straightforward application of deconvolution is to deconvolve pressure buildup data in order to eliminate the effects of wellbore storage. Earlier deconvolution efforts were mostly concentrated on removing the effects of wellbore storage. There are several methods available — described in Chapter II — for analyzing distorted pressure transient data. These methods require the knowledge of sandface rates for deconvolution as our method requires also. The main goal of removing wellbore storage effects is to obtain knowledge of permeability and skin factor in a shorter time.

We analyze the case which was published by Fetkovich *et al*.[9] on an oil well which was hydraulically fractured at initial completion. The early time pressure response is distorted by wellbore storage effects, but sandface rates are available (**Fig. 5.1**). One can refer to SPE 12179 (ref. 9) for additional information for this well and analysis done by Fetkovich *et al*. Using this input we perform deconvolution, the results of which are shown in **Fig. 5.2**.

We compare the deconvolved response along with reservoir model responses (simulation) for consistency. **Fig. 5.2** presents the distorted pressure data, the deconvolved constant-rate pressure drawdown and its logarithmic derivative, as well as model matches for the deconvolved response. We used two models to match the deconvolved pressure response — the uniform flux fracture (Fetkovich *et. al*. used this model in their analysis, as a comment it was the only available model for a hydraulically fractured well at that time) and the finite conductivity vertical fracture model. Our deconvolution results compare extremely well with these model responses and serves as confirmation of previous interpretations.

In this case we have used deconvolution to eliminate wellbore storage effects, and we suggest that this case serves to verify our contention that our method is sufficiently accurate for use in eliminating wellbore storage effects (when sandface rates are available).

5.2 B-Spline Deconvolution Applied to Conventional Well Test Analysis

The application of deconvolution to conventional well test analysis where production history has usually more than one flow periods seems to be new. The traditional approach is to take an individual flow period which is usually buildup and analyze the flow period in isolation. A particular model is assumed and non-linear regression is performed to estimate reservoir properties. This approach is limited to maximum elapsed time during the individual flow period which is usually quite shorter than test duration therefore, information obtained is inadequate.

Estimating the constant rate pressure drawdown response from production history which has multiple flow periods is a variable rate problem which can be solved by deconvolution. By this way we can avoid using assumptions for the reservoir model, as well as information during entire test duration is used for deconvolution. However, when the linearity of the equation under the convolution integral is not satisfied due to inconsistencies in the input data, then we can choose to apply deconvolution for an individual flow period where data seems consistent but the deconvolution estimates can be insufficient for the reasons stated above. In this section we are going to describe two cases where we first perform deconvolution for entire test duration and next we deconvolution is performed for an individual flow period.

In **Fig**. **5.3** we present the rate and pressure data obtained during the four-point test of a gas well, which was followed by an extended shut-in. In this case the pressure buildup data seem to be of sufficient duration for a conventional pressure buildup (or PBU) analysis — therefore we could simply proceed and analyze the individual PBU portion of this data. However, our intention is not to replace PBU analysis by deconvolution, but rather, to implement our deconvolution algorithm as an option for well test analysis. We choose to analyze all the available data including the production periods. We perform deconvolution and present the results in **Fig. 5.4**, together with model matches of the deconvolved pressure drawdown.

Since the flowing fluid is gas we must perform the pseudo-pressure transform to adhere to theoretical considerations — linearity of integral equation — (we note that pseudotime should also be considered, but to be theoretically rigorous, pseudotime requires the average reservoir pressure history (which is never available in practice) and may not be needed during transient flow period. The deconvolved pressure response suggests that a complex channel type reservoir geometry is possible.

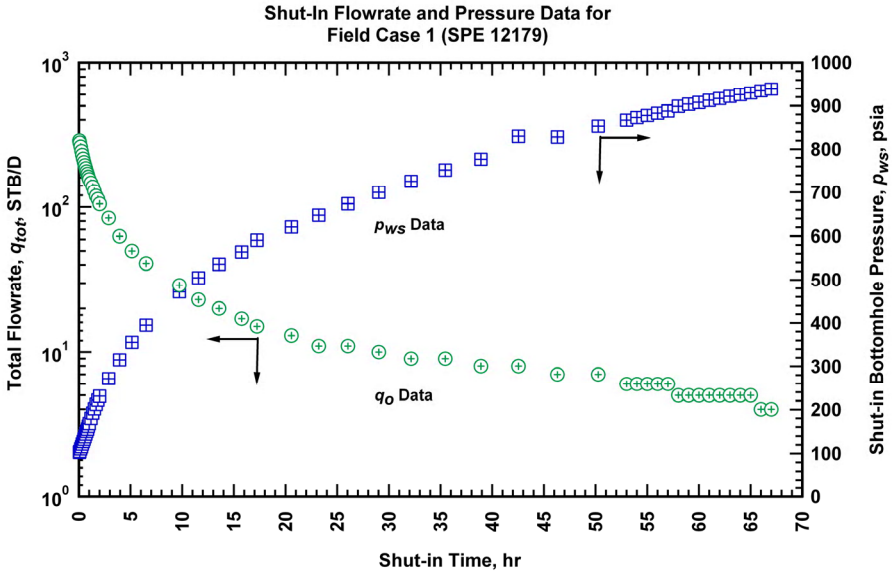

Figure 5.1 – Field Case 1 — Shut-in flowrate and pressure data for pumping oil well (SPE 12179 (ref. 9))).

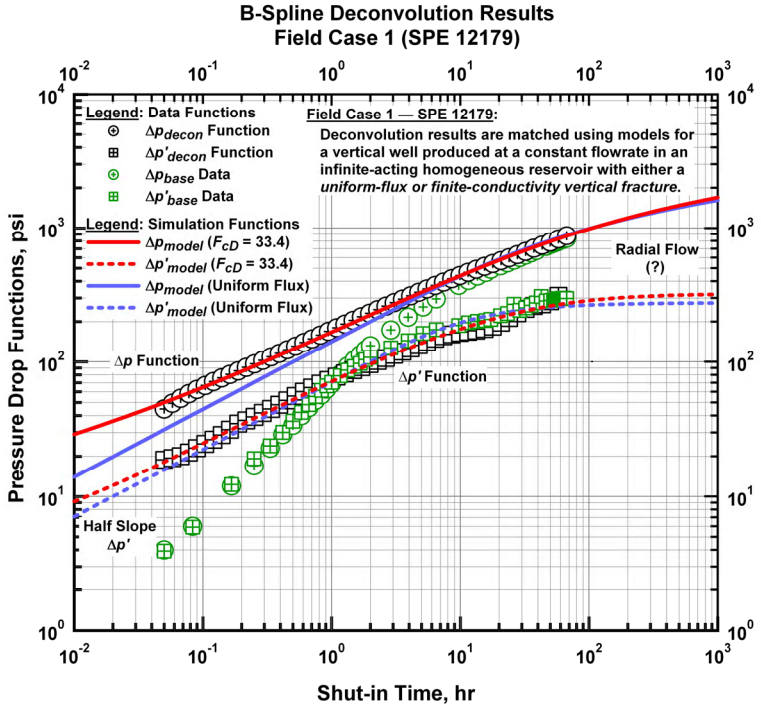

Figure 5.2 – Field Case 1 — Wellbore storage distorted pressure response, deconvolved response and model match (Data from SPE 12179 (ref. 9)).

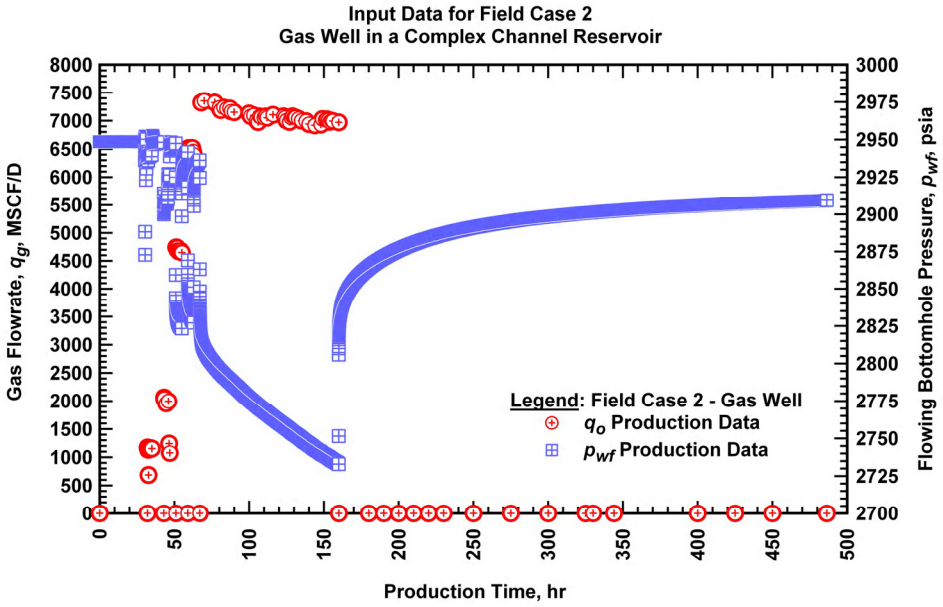

Figure 5.3 – Field Case 2 — Moderate pressure gas well in a complex reservoir.

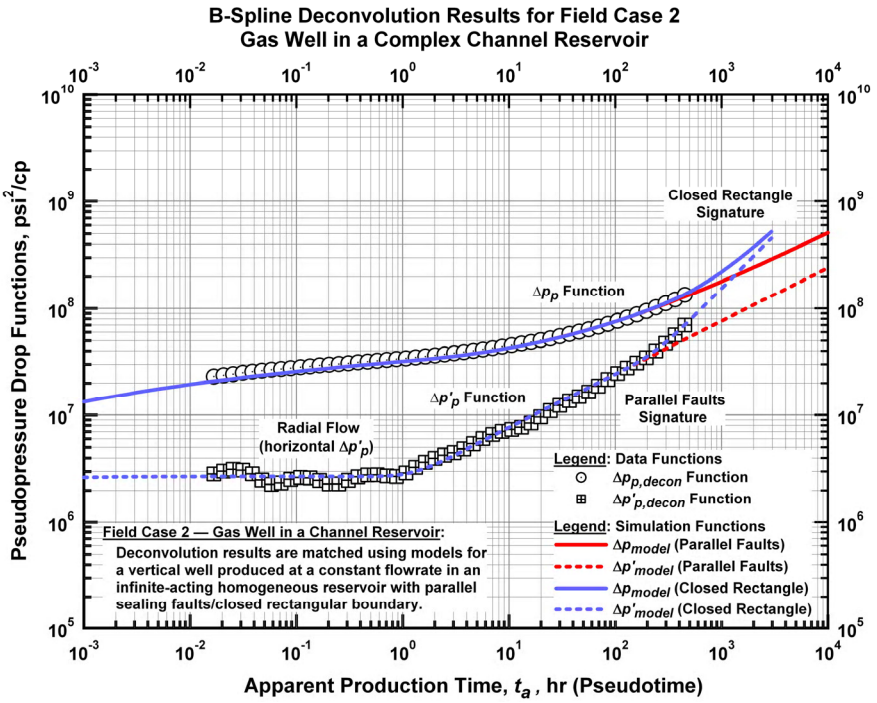

Figure 5.4 – Field Case 2 — Deconvolved response and model match (entire history used in this deconvolution).

Therefore, we proceed and match the deconvolved response with two models to verify this possibility. The models considered include a well in a homogeneous reservoir bounded by parallel faults and a well in a homogeneous reservoir with closed rectangular boundaries. The results of our model matches validate the complexity of the reservoir. We do observe the familiar "half-slope" trend of the pressure and pressure derivative functions on the log-log plot, which indicates a channel type reservoir geometry. On the other hand, we also note that the signature of a closed reservoir is evident in the pseudopressure drop and pseudopressure drop derivative functions at late times.

In this application we have used deconvolution to extract information from a larger time interval than just the pressure buildup test sequence. Analysis of the entire testing sequence using deconvolution may reveal reservoir characteristics not "seen" by a single event in the sequence. Therefore, we recommend analyzing the entire test sequence but we must be very careful when dealing with apparent inconsistencies. As we mentioned before if we rely on rate data, we can choose not to use the inconsistent pressure data instead we can pick the pressure data from the consistent part of the measurements in conjunction with entire rate data as long as it is honored sufficiently. In this case we divide the flow history into four segments and approximate the rate data with a function within each segment where it is evident that it is not possible to approximate the entire rate data in one segment.

In our next example we analyze only a selected flow period during a well test sequence as shown for the selected oil well in **Fig. 5.5**. This test sequence includes 170 hours of data where we have a 50 hour constant-rate production (at 200 STB/D) followed by a shut-in for 16 hours, then production resumes at a constant rate of 160 STB/D for 24 hours and is then shut-in for 80 hours.

Inconsistencies are observed — in particular, we suspect that in the first production period the given rate is not correct (we note fluctuations in the drawdown pressure profile). We have two options in this case — first we can deconvolve the entire sequence, but we have to use a high value of regularization parameter to overcome the effects of inconsistencies — we believe that rate data is not correct for this reason we can not disregard any pressure data. Or we can focus on the final buildup period, but taking the preceding flow history into account and analyze the final buildup individually. We choose the second option.

The deconvolved pressure response and a model match are shown in **Fig. 5.6**. The deconvolved well-testing pressure derivative function suggests that the well has a finite conductivity vertical fracture that this portion of the reservoir is bounded by parallel faults. We confirm this supposed reservoir model by matching the deconvolved pressures with just such a model. This example verifies that we can perform deconvolution based on a selected flow period.

5.3 B-Spline Deconvolution Applied to Permanent Downhole Gauge Data

In this section we apply our deconvolution technique to permanent downhole gauge data. Our example is taken from an oil well equipped with a permanent downhole measurement system which is used to provide continuous (downhole) pressure and rate data. In this case a tremendous amount of data is available for a very short time — 10 hours (as shown in **Fig. 5.7**). We recognize that this is an extreme case but we are going to show that we can reveal some characteristic features of the reservoir using our deconvolution technique. On the other hand, pressure buildup analysis or other traditional type analysis is not a realistic option because the buildups are very short and, in addition, other phenomena (most likely temperature change and/or phase resegregation) cause non-intuitive behavior (*e.g.*, between 2-4 hours the well is shut-in but the observed pressure is decreasing).

We use piecewise linear approximation to rates resulting in a higher number of segments and we do not use the pressure data which has inconsistencies. In addition, we associate weights to some observations which we depend on more (since we are using weighted least squares we can associate weights anytime). Furthermore, huge amount of pressure data are reduced by linear interpolation sampled at selected points.

Fig. **5.8** presents the results of deconvolution for this case. The apparent oscillations in deconvolved pressure derivative function indicate that the data are somewhat inconsistent — but we can proceed and match the deconvolved pressure with simple models (well in an infinite acting homogenoeuos reservoir with wellbore storage and skin / well in a homogenoeuos reservoir with single sealing fault (with wellbore storage and skin)). Using analytic simulation, we reproduce the pressure response relative to the observed rate history for the entire test sequence as shown in **Fig. 5.9**. The pressures generated by the model fail to honor observed data at some points (especially in the intervals where we already revealed inconsistencies) — but, these simulations do honor the observed pressures at later times, in agreement with our expectations.

This example demonstrates that deconvolution is a viable option for analyzing permanent downhole gauge data. Once again it is confirmed that upon successful manipulation of the input data, deconvolution can recover a considerable part of characteristic features of the reservoir even though very limited amount of information available such as 10 hours of data available in this case.

5.4 B-Spline Deconvolution Applied to Production Data Analysis

Our deconvolution technique is not limited to analyzing well tests — we can also apply this methodology to analyze and interpret traditional (long-term) production data. Production data is regarded as a "low frequency" and "low resolution" type of data. Because of these reasons, rigorous variable rate/pressure analysis of production data is rarely attempted. Our objective is to "convert" the entire production sequence (including poor quality data) into an equivalent constant flow-rate pressure response. We corroborate our results with material balance deconvolution which includes plotting $\Delta p/q$ (rate normalized pressure/pseudopressure) versus material balance time/pseudotime, and comparing our deconvolution results and the material balance deconvolution results with a reservoir model established from the deconvolved data.

Our first example considers a tight gas reservoir (Pratikno *et al.*[50]). The data are of good (to excellent) quality, and we note the effect of shut-ins and daily production fluctuations (**Fig. 5.10**). We note that in our rate approximation we honor all rate data including the buildup part instead of using an exponential function for the rate decline. There a variety of ways to analyze this data set — buildup part can be analyzed in isolation to obtain reservoir properties (permeability, skin factor and reservoir model) but the preceding variable flow history prevents accurate results. On the other hand, conventional production data analysis methods such as decline curve analysis, type curve analysis can be applied to get reservoir properties and reserves estimates. All of these methods perform well under some assumptions and data manipulation.

Our deconvolution method is not an alternative to these methods. Instead, we recommend using deconvolution as an additional analysis technique. In general terms, we are attempting to obtain the constant rate pressure response from a production history including variable flow rates. Therefore, we do not need to classify our method as a pressure transient data analysis method or a production data analysis method. In other words, we can apply our deconvolution method to any type of data set.

In **Fig. 5.11** we present the deconvolved responses (our method and material balance time) compared with an appropriate reservoir model (well with a finite conductivity vertical fracture in a bounded reservoir), and we note good agreement. We have tried several other reservoir models but we obtain the best match with the finite conductivity vertical fracture model. We note some anomalies in the well testing pressure derivative function at early times caused presumably by inconsistencies in the data (or simply a sparcity of data at early time). Also, there does exist a slight difference in our interpretation of the data and model for the early portion of the analysis. Finally, it is seen from the derivative trend that boundary dominated flow is in transition to full development.

The second example is also a gas field case (Palacio *et. al.*[51].). The daily production data are quite erratic (**Fig. 5.12**) due to liquid loading, in spite of these features, the B-spline deconvolution method performs reasonably well (*i.e.*, the data deconvolution data functions appear to be reasonable and well-behaved (see **Fig. 5.13**)). In **Fig. 5.13** we again compare our deconvolution results with traditional production analysis based on material balance time deconvolution.

Artifacts caused by inconsistencies are seen at early times in the well testing pressure derivative function (again (we believe) due to sparse/erratic data). The late time well testing pressure derivative function trend confirms that boundary-dominated flow regime has been reached. The solution for a homogeneous reservoir with closed circular boundary matches all of the deconvolved pressure response functions reasonably well (except for earlier times), which also confirms our analysis.

Our final example is an oil field case (East Asia Oil Well). Data quality seems excellent except for the earlier times (**Fig 5.14**). We also suspect in this case that early time data is sparse and not accurate. The results of B-spline deconvolution and material balance deconvolution show excellent agreement. Deconvolution results suggest that this can be a high-productivity reservoir with high permeability. Taking this into account, once again we compare our deconvolution results with an appropriately chosen reservoir model which is a homogenous reservoir with closed circular boundary. The selected reservoir model matches all of the deconvolved pressure response functions considerably well except for the earlier time (**Fig 5.15**). We believe that due to sparcity of early time data, in each case we have minor issues with deconvolution results. We note that the data we have is "low quality" type of data which include average rates/pressures instead of continuous measurements. Thus, it is anticipated to have such artifacts in results. Given more accurate continuous/permanent measurements, we expect that deconvolution results will improve especially for the earlier part of the data. As a comment, implementation of continuous/permanent measurements will eliminate the need for separate analysis (*i.e.* pressure transient or production data).

All in all, we believe that B-spline deconvolution can be successfully applied to production data (regularly measured flowrate and pressure data). Processing "low quality" production data with deconvolution can provide additional insight into reservoir performance based analysis.

It is worth noting that numerous other field cases of long-term flowrate and (surface) pressure data have been successfully analyzed/interpreted using the proposed B-spline deconvolution technique. In fact, we believe that B-spline deconvolution may be more utilized for the analysis of production data, compared to its potential use for well test data. This hypothesis arise from the fact that while often poor quality, production data are generally available

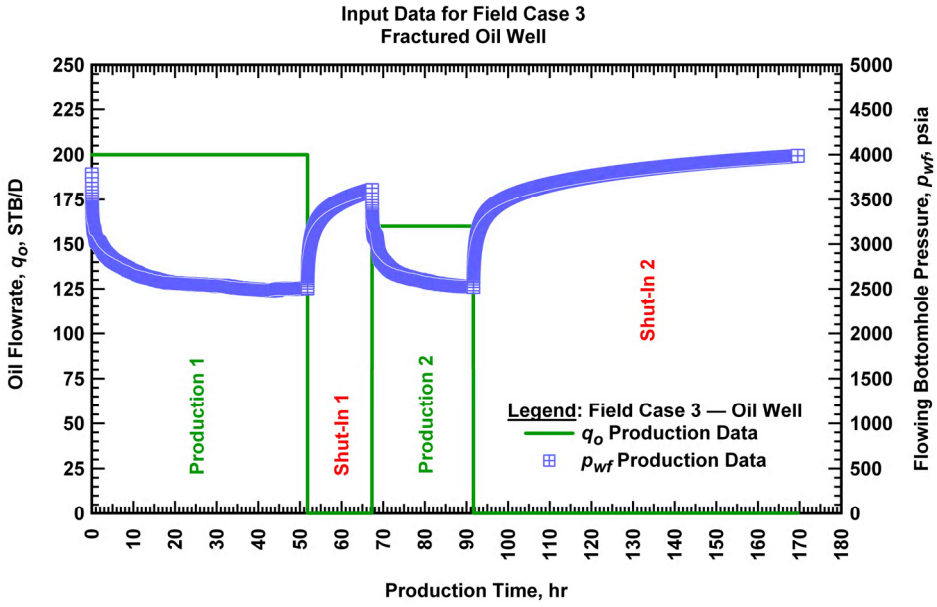

Figure 5.5 – Field Case 3 — Input data for fractured oil well.

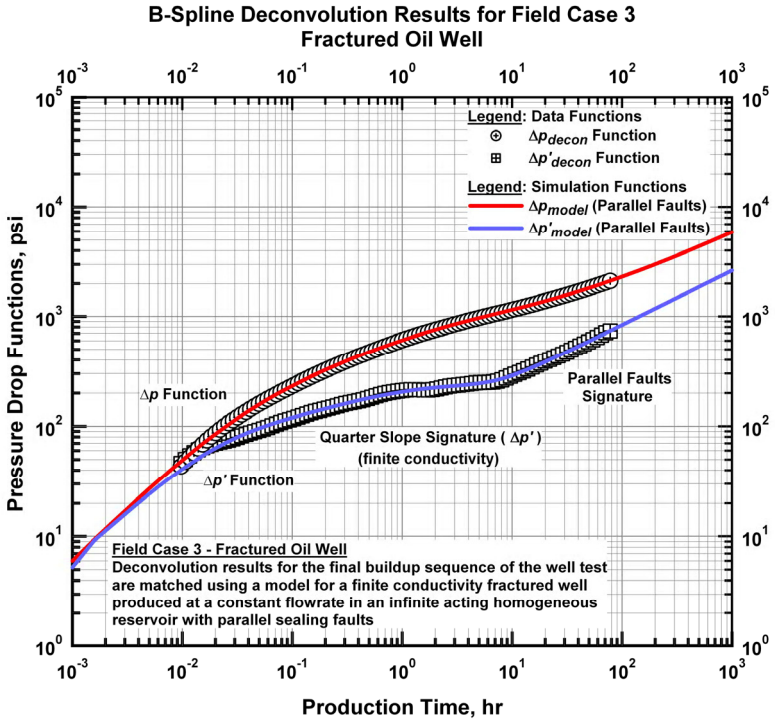

Figure 5.6 – Field Case 3 — Deconvolved response and model match (ONLY final PBU data used in this deconvolution).

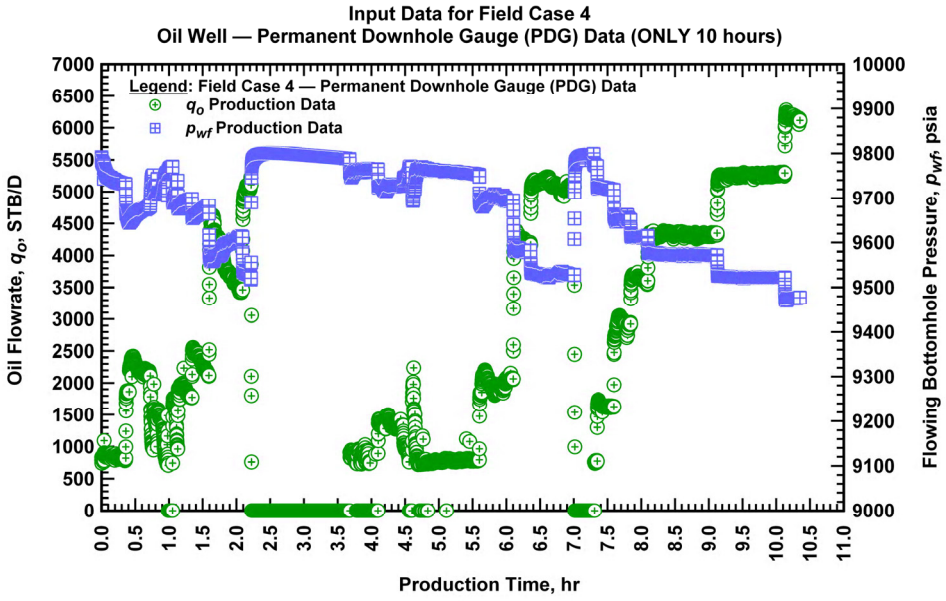

Figure 5.7 – Field Case 4 — Permanent downhole gauge data for 10 hours.

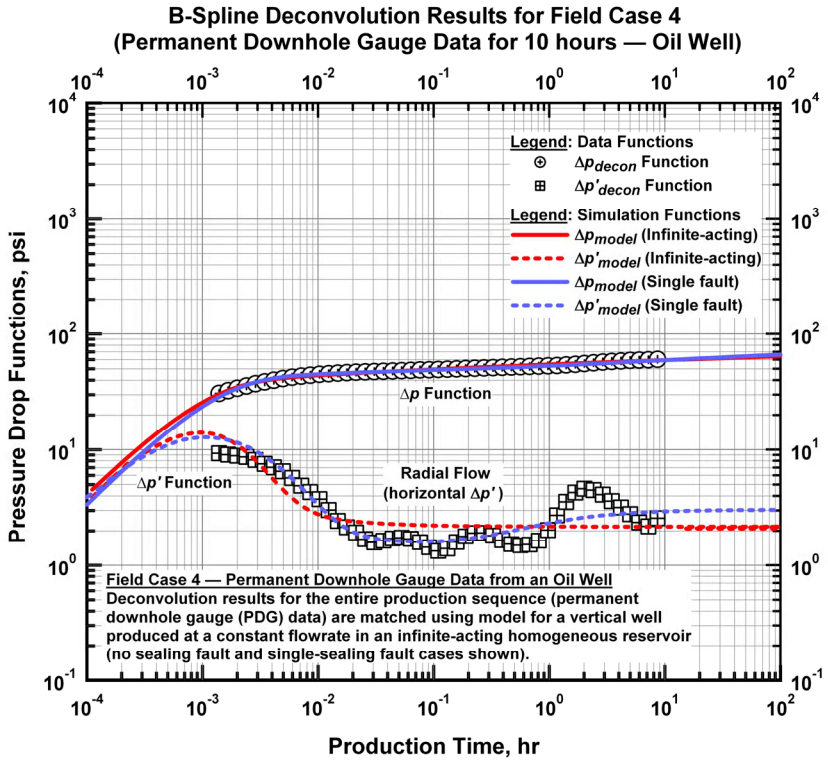

Figure 5.8 – Field Case 4 — Deconvolved response and model match (entire data sequence used).

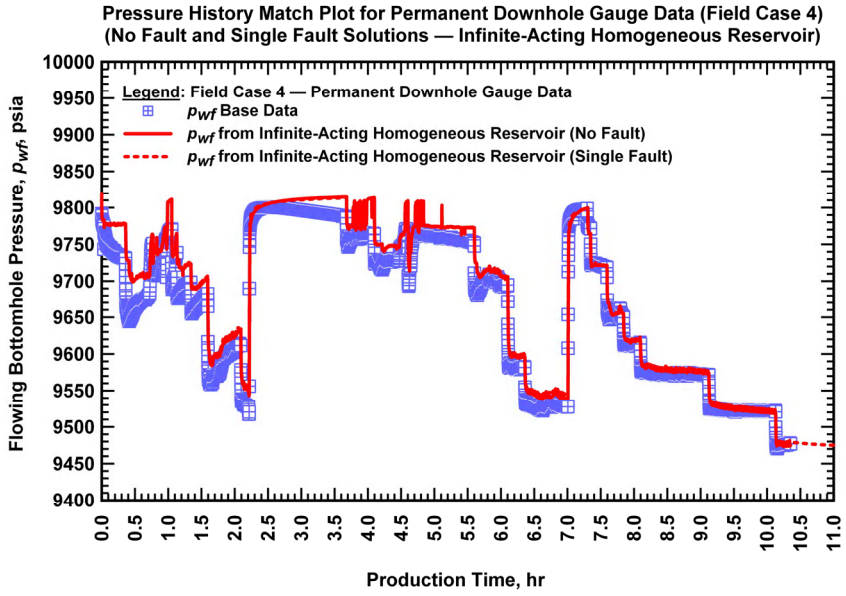

Figure 5.9 – Pressure history match using the models shown in Fig. 5.8.

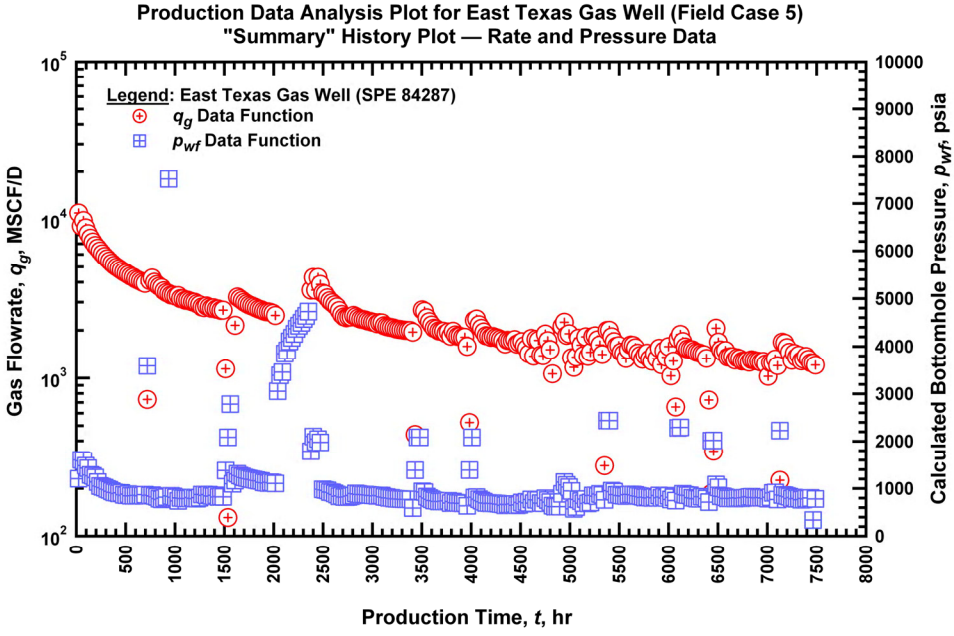

Figure 5.10– Field Case 5 — Production data history plot for East Texas Gas Well.

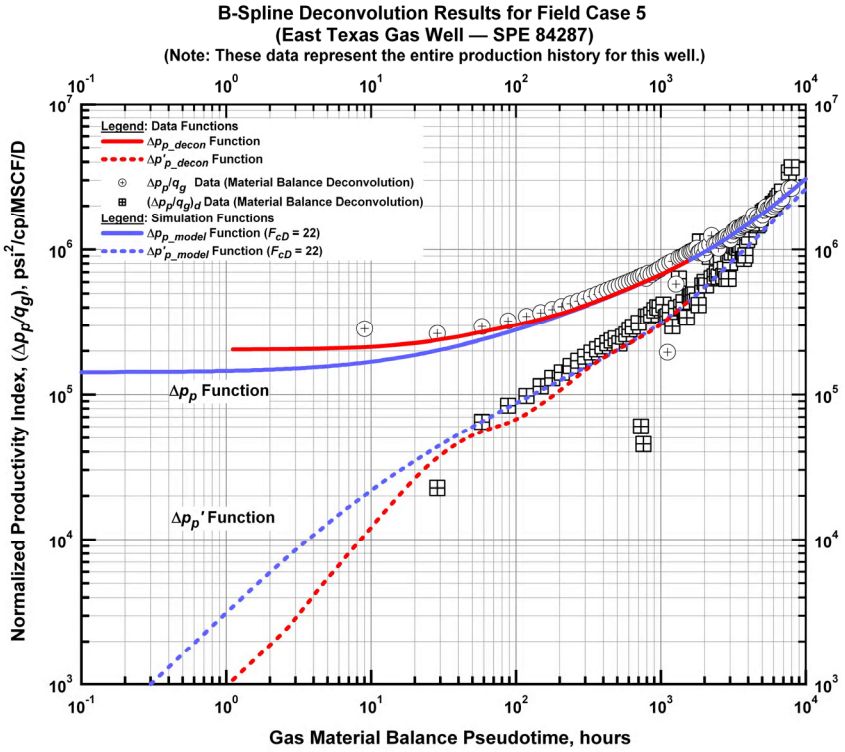

Figure 5.11– Field Case 5 — Deconvolution response functions, model match and material balance time normalized data.

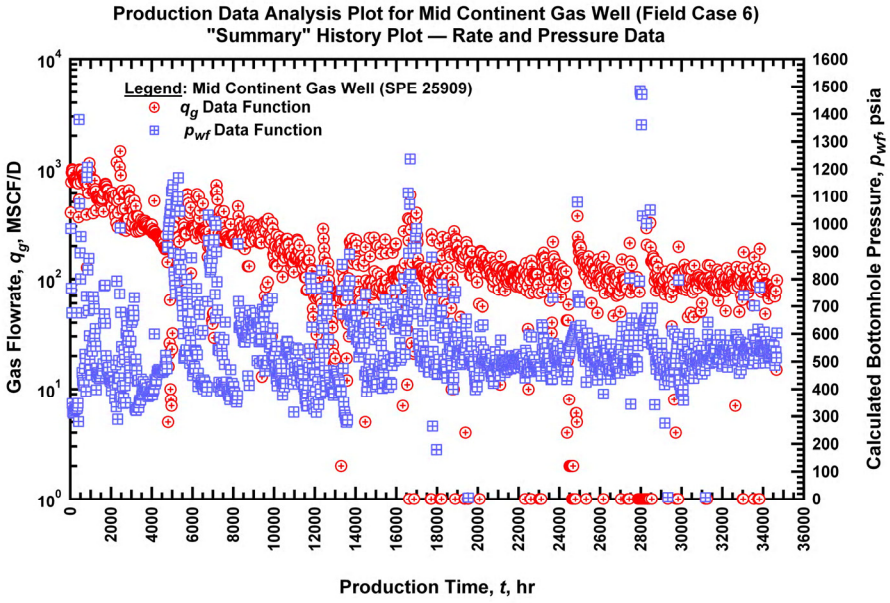

Figure 5.12– Field Case 6 — Production data history plot for Mid Continent Gas Well.

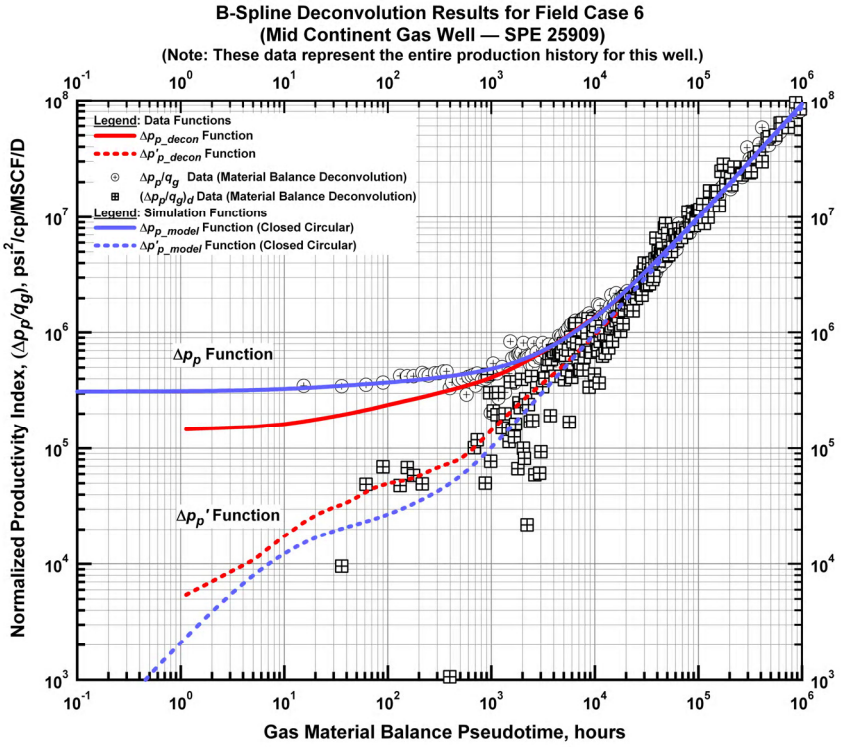

Figure 5.13– Field Case 6 — Deconvolution response functions, model match and material balance time normalized data.

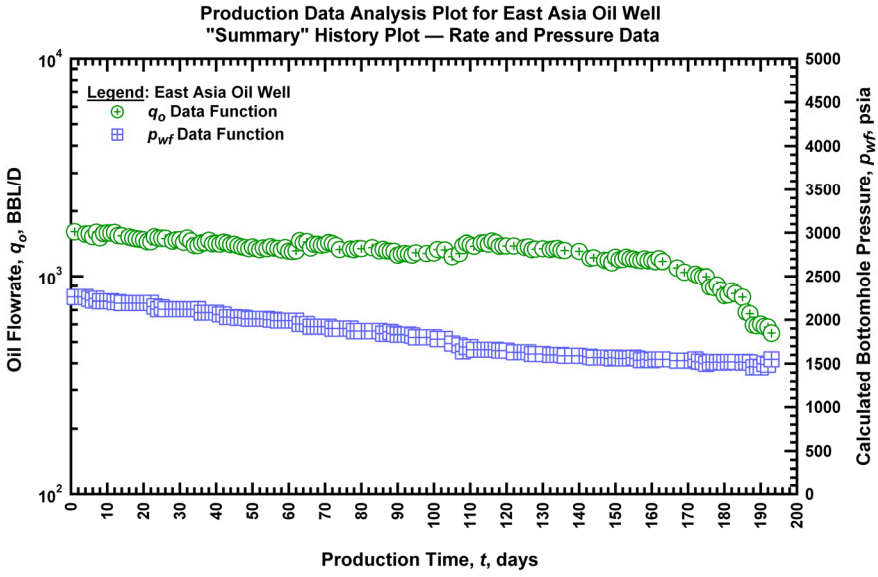

Figure 5.14– Field Case 7 — Production data history plot for East Asia Oil Well.

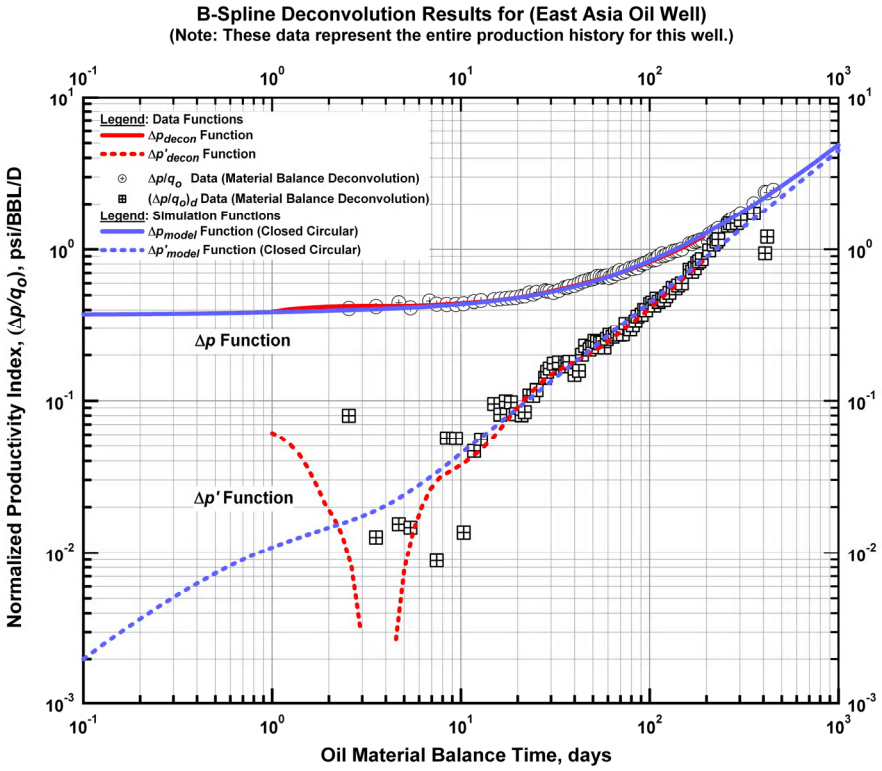

Figure 5.15– Field Case 7 — Deconvolution response functions, model match and material balance time normalized data.

CHAPTER VI

SUMMARY, CONCLUSIONS, AND RECOMMENDATIONS FOR FUTURE WORK

6.1 Summary

We believe that the developed deconvolution technique in this work is an important addition to existing well test/production data analysis methods where few deconvolution methods are practically applicable.

We use B-splines for representing the derivative of unknown unit-rate drawdown pressure and numerical inversion of the Laplace transform is utilized in our formulation. When significant errors and inconsistencies are present in the data functions, the direct and indirect regularization methods (*i.e.*, mathematical "uniformity" processes) are used. We provide examples of under and over-regularization, and we discuss procedures for ensuring proper regularization.

We validate our method with synthetic examples generated with and without errors. We then show that our deconvolution method using a variety of field cases — including traditional well tests, permanent downhole gauge data as well as production data.

6.2 Conclusions

The following conclusions are made based on the results obtained from this work

1. Methodology: A unique deconvolution technique is achieved due to semi-logarithmic B-spline representation of the unknown impulse response and to the high reliability of the numerical Laplace transform inversion technique used, the elements of the coefficient matrix are computed accurately. The sensitivity matrix is used in conjunction with a least-squares criterion (in the real domain) to minimize error distortion, which yields the required B-spline coefficients to construct the unit-rate response and the well testing derivative functions. For the deconvolution of data in practice, we have implemented a physically sound regularization scheme into our proposed deconvolution method. Regularization might be seen as an "add-on" to the proposed algorithm, but in a practical sense (*i.e.*, for field applications), our proposed deconvolution scheme is likely to perform poorly without the use of regularization methods. We have developed a computer module in *Mathematica* for performing the computational efforts required in this work.

2. Validation: We have validated our technique against selected reservoir models by generating the exact unit rate drawdown and its derivative functions analytically and comparing with the results from our technique. Further, we add random error to both generated input data as a mechanism to test the robustness of the proposed technique. The new technique can recover the unit rate drawdown

pressure response and its derivative to a practical extent when higher magnitudes of errors are present in both the rate and pressure observations. We demonstrate the use of direct and indirect regularization and we provide examples of indirect regularization (*i.e*. knot selection) as well as under and over-regularization. From this validation effort, we can conclude that our new method is error tolerant — sufficiently so for applications in the petroleum industry.

3. Application: We have successfully demonstrated the used of B-spline deconvolution for the analysis of a wide range of field data — traditional variable-rate/ pressure problems, such as wellbore storage distortion, long-term production data, permanent downhole (pressure) gauge data, and well tests having multiple flow sequences. Finally, our work suggests that the new deconvolution method is *innovative and robust* and has broad applicability in variable rate/pressure problems — and can be implemented in typical well test and production data analysis applications.

6.3 Recommendations for Future Work

The following recommendations are made to extend this research.

1. Methodology: Continue efforts using regularization for "noisy" data and develop an algorithm for automated knot selection.
2. Rate Deconvolution: By rate deconvolution (variable pressure deconvolution instead of variable rate deconvolution) constant pressure rate response function can be obtained for production data analysis. Our future efforts will include establishing a stable rate deconvolution algorithm.
3. Wellbore Storage: For pressure transient data analysis, incorporation of wellbore storage flowrate model will be sought when there is no sandface flowrate information available (*i.e.*, we may try to implement a wellbore storage rate model).
4. Computational Purposes: Use alternatives for B-splines for decreasing computational time.

NOMENCLATURE

Variables:

a_k = ...Coefficient of rate approximation function

b = ... Base of logarithmically evenly distributed knots

B = ... Formation volume factor, RB/STB (or CF/SCF)

$B_i^k(t)$ = ... k-th degree B-spline starting at b^i

$B_{i,int}^k(t)$ = ...Integral of the k-th degree B-spline

$\boldsymbol{c}$ = ... Vector of unknown coefficients

c_t = ...Total system compressibility, 1/psi

C_D = ... Dimensionless wellbore storage coefficient

F_c = ... Fracture conductivity, md-ft

G_p = ... Cumulative gas production, MSCF (or BSCF)

h = ... Pay thickness, ft

k = ...Permeability, md

k_z/k_r = ...Ratio of vertical to radial permeability

$K(t)$ = ... Impulse response (= p_{ud} / t)

L_w = ...Horizontal well length, ft

$p(t)$ = ...Pressure, psi

p_u = ... Constant (unit) rate pressure response, psi

p_{ud} = ... Well-testing (log) derivative of p_u, psi

p_i = ...Initial reservoir pressure, psi

$q(t)$ = ... Rate, STB/D or MSCF/D

r_e = ...Reservoir outer boundary radius, ft

r_w = ... Wellbore radius, ft

r_{eD} = ... Outer reservoir boundary radius, dimensionless

s = ... Laplace transform variable

s_x = ... Skin factor

$S(t)$ = ...Spline function

t = ...Flowing time, hr

t_i = ...Knot for index (b^i), i

t_j = ...*j-th* time information data

t_{sh} = ... Shut-in time, hr

$\mathbf{U}$ = Orthogonal matrix

$\mathbf{V}$ = Orthogonal matrix

$\mathbf{W}$ = Weighting matrix

$\mathbf{X}$ = Sensitivity matrix

x_f = Fracture half length, ft

$\mathbf{X}_r$ = Regularization matrix

z_w = Distance to the bottom of formation, ft

Greek Symbols:

α = Regularization parameter

Δp = Drawdown (with respect to p_i)

ϕ = Porosity, fraction

μ = Viscosity, cp

ε = Small positive time

τ = Dummy variable

σ = Singular values

ω = Storativity parameter

λ = Interporosity flow parameter

Subscript:

i = Index for i-th B-spline

j = Time information data index

u = Last observation index

l = First observation index

k = Index for the rate approximation function

jp = Jump point (discontinuity)

op = Operating time

sh = Shut-in

int = Integral

Superscript:

k = Degree of B-spline

$\hat{}$ = Estimated (from least squares)

$\sim$ = Observed

$\bar{}$ = Laplace transform

$^{+}$ = ... Pseudoinverse

^{T} = ... Transpose of matrix

Special Functions:

$I_0(x)$ = ...Modified Bessel function of the first kind, zero order

$I_1(x)$ = ... Modified Bessel function of the first kind, first order

$K_0(x)$ = ... Modified Bessel function of the second kind, zero order

$K_1(x)$ = ...Modified Bessel function of the second kind, first order

REFERENCES

1. Lamm, P. K.:"A Survey of Regularization Methods for First-Kind Volterra Equations," *Surveys on Solution Methods for Inverse Problems*," D. Colton, H. W. Engl, A. Louis, J. R. McLaughlin, W. Rundell, (eds), Springer, Vienna, New York, (2000) 53-82.
2. Churchill, R.V.: *Operational Mathematics*, McGraw-Hill, New York, (1972).
3. Horne, R.N.: *Modern Well Test Analysis*, Petroway Inc., Palo Alto, (2002).
4. Duhamel, J.M.C.:"Mémoire sur la méthode générale relative au mouvement de la chaleur dans les corps solides plongés dans les milieux dont la température varie avec le temps," *J. de Ec. Polyt*. (Paris) **14** (1833) 20-77.
5. van Everdingen, A.F. and Hurst, W.: "Application of the Laplace Transformation to Flow Problems in Reservoirs," *Trans,* AIME (1949) **186**, 305-324.
6. Odeh, A.S. and Jones, L.G.: "Pressure Drawdown Analysis, Variable-Rate Case," *JPT* (Aug 1965) 960-964; *Trans*., AIME **234**.
7. Soliman, M.Y.: "New Technique for Analysis of Variable Rate or Slug Test," paper SPE 10083 presented at the 1981 SPE Annual Technical Convention and Exhibition, San Antonio, TX, 5-7 October.
8. Stewart, G., Wittmann, M.J., Meunier, D.: "Afterflow Measurement and Deconvolution in Well Test Analysis," paper SPE 12174 presented at the 1983 Annual Technical Conference and Exhibition, San Francisco, CA, 5-8 October.
9. Fetkovich, M.J. and Vienot, M.E.: "Rate Normalization of Buildup Pressure By Using Afterflow Data," *JPT*. (December 1984), 2211-2224.
10. Agarwal, R.G.: "A New Method to Account for Producing Time Effects When Drawdown Type Curves Are Used to Analyze Pressure Buildup and Other Test Data," paper SPE 9289 presented at the 1980 SPE Annual Technical Convention and Exhibition, Dallas, TX, 21-24 September.
11. Gladfelter, R.E., Tracy, G.W., and Wilsey, L.E.: "Selecting Wells Which Will Respond to Production-Stimulation Treatment," *Drill. and Prod. Prac*., API (1955), 117-129.
12. Winestock, A.G. and Colpitts, G.P.: "Advances in Estimating Gas Well Deliverability," *JCPT* (July-Sept. 1965) 111-119.
13. Raghavan, R.: *Well Test Analysis*, Prentice-Hall, Upper Saddle River, NJ (1993).

14. Thompson, L.: "Analysis of Variable Rate Pressure Data Using Duhamel's Principle," PhD Dissertation, University of Tulsa, Tulsa, OK (1985).

15. Blasingame, T.A.: "Variable Rate Analysis: Transient and Pseudosteady State Methods of Interpretation and Application," M.S. Thesis, Texas A&M University, College Station, TX (1986).

16. Johnston, J.L., Lee, W.J.: "Interpreting Short-Term Buildup Tests From Low-Productivity Gas Wells Using Deconvolution," paper SPE 21503 presented at the 1991 Gas Technology Symposium, Houston, TX, 22-24 January.

17. McCray, T.L.: "Reservoir Analysis Using Production Decline Data and Adjusted Time," M.S. Thesis, Texas A&M University, College Station, TX (1990).

18. Coats, K.H., Rapoport, L.A., McCord, J.R., Drews, W.P.: "Determination of Aquifer Influence Functions From Field Data," *JPT*. (December 1964) 1417-1424.

19. Hutchinson, T.S. and Sikora, V.J.: "A Generalized Water-Drive Analysis," *Trans*., AIME (1959) **216**, 169.

20. Katz, D.L., Tek, M.R., and Jones, S.C.: "A Generalized Model for Predicting the Performance of Gas Reservoirs Subject to Water Drive," paper SPE 428 presented at the 1962 SPE Annual Meeting, Los Angeles, CA, 7-10 October.

21. Jargon, J.R. and van Poolen, H.K.: "Unit Response Function From Varying-Rate Data," *JPT* (August 1965) **965**; *Trans*., AIME, 234.

22. Bostic, J.N., Agarwal, R.G., and Carter, R.D.: "Combined Analysis of Postfracturing Performance and Pressure Buildup Data for Evaluating an MHF Gas Well," *JPT* (October 1980) 1711.

23. Kucuk, F.J. and Ayestaran, L.: "Analysis of Simultaneously Measured Pressure and Sandface Flow Rate in Transient Well Testing," *JPT* (February 1985), 323.

24. Baygun, B., Kuchuk, F.J., and Arikan, O.: "Deconvolution Under Normalized Autocorrelation Constraints," *SPEJ* (September 1997), 246.

25. von Schroeter, T., Hollaender, F., and Gringarten, A.C.: "Deconvolution of Well-Test Data as a Nonlinear Total Least-Squares Problem," *SPE Journal* 2004, **9**, No. 4, 375-390

26. Levitan, M.M.: "Practical Application of Pressure-Rate Deconvolution to Analysis of Real Well Tests," paper SPE 84290 presented at the 2003 Annual Technical Conference and Exhibition, Denver, CO, 5-8 October.

27. Cheney, E. W. and Kincaid, D. R.: *Numerical Mathematics and Computing*, Brooks Cole, Pacific Grove, CA (2003).

28. Levitan, M.M., Crawford, G.E., Hardwick, A.: "Practical Considerations for Pressure-Rate Deconvolution of Well Test Data," paper SPE 90680 presented at the 2004 Annual Technical Conference and Exhibition, Houston, TX, 26-29 September.

29. Roumboutsos, A., and Stewart, G.: "A Direct Deconvolution or Convolution Algorithm for Well Test Analysis," paper SPE 18157 presented at the 1988 Annual Technical Conference and Exhibition, Houston, TX, 2-5 October.

30. Bourgeois, M.J., and Horne, R.N.: "Well Test Model Recognition with Laplace Space," *SPEFE* (March 1993) 17.

31. Onur, M., and Reynolds, A.C.: "Well Testing Applications of Numerical Laplace Transformation of Sampled-Data," *SPE Reservoir Evaluation & Engineering* 1998. **1**, No. 3, 268-277.

32. Roumboutsos, A., and Stewart, G.: "A Direct Deconvolution or Convolution Algorithm for Well Test Analysis," paper SPE 18157 presented at the 1988 Annual Technical Conference and Exhibition, Houston, TX, 2-5 October.

33. Mendes, L.C.C., Tygel, M., and Correa, A.C.F.: "A Deconvolution Algorithm for Analysis of Variable-Rate Well Test Pressure Data," paper SPE 19815 presented at the 1989 Annual Technical Conference and Exhibition, San Antonio, TX, 8-11 October.

34. Cheng, Y., Lee, W. J., and McVay, D. A.: "A Deconvolution Technique Using Fast-Fourier Transforms," paper SPE 84471 presented at the 2003 Annual Technical Conference and Exhibition, Denver, CO, 5-8 October.

35. Stehfest, H.: "Algorithm 368: Numerical Inversion of Laplace Transforms," *Comm. Assoc. Computing Machinery* (1970) **13**, 47.

36. Valkó, P.P., and Abate, J. "Comparison of Sequence Accelerators for the Gaver Method of Numerical Laplace Transform Inversion" *Computers and Mathematics with Application* 2004 **48** 629-636.

37. Abate, J., and Valkó, P.P.: "Multi-precision Laplace Transform Inversion" *International Journal for Numerical Methods in Engineering*, 2004 **60**, 979–993.

38. Schoenberg, I.J.: "On Spline Functions," *Inequalities*, O. Shisha, (Ed.) Academic Press, New York, (1967), 255-291.

39. de Boor, C.: *A Practical Guide to Splines*, Springer, New York, (1978).

40. Schumaker, L.L.: *Spline Functions*: *Basic Theory*, Wiley, New York, (1981).

41. Ahlberg, J.H., Nilson, E.N., and G.E., Walsh, J.L.: *The Theory of Splines and their Applications*, Academic Press, New York, (1967).

42. Greville, T.N.E.: *Introduction to Spline Functions. In Theory and Application of Spline Functions*, Academic Press, New York, (1969).

43. Golub, G.H., and van Loan, C.F.: *Matrix Computations*, Johns Hopkins University Press, Baltimore, (1996).

44. Bjorck, Å.: *Numerical Methods for Least Squares Problems*, Society for Industrial and Applied Mathematics (SIAM), Philadelphia, (1996).

45. *Mathematica* (software) Ver. 5.1, Wolfram Research, Champaign-Urbana, IL (2005).

46. Davies, B., and Martin, B.: "Numerical Inversion of the Laplace Transform: A Survey and Comparison of Methods," *J. of Computational Physics*, 1979, **33** 1 -32.

47. Narayanan, G.V., and Beskos, D.E.: "Numerical Operational Methods for Time-Dependent Linear Problems," *International Journal for Numerical Methods in Engineering,* 1982, **18** 1829 - 1854.

48. *Mathematica* Information Center, http//library.wolfram.com/database/MathSource/4738/

49. Abramovitz, M., and Stegun, I.A.: *Handbook of Mathematical Functions*, Dover, New York, (1972).

50. Pratikno, H., Rushing, J.A., and Blasingame, T.A.: "Decline Curve Analysis Using Type Curves: Fractured Wells," paper SPE 84287 presented at the 2003 Annual SPE Technical Conference and Exhibition, Denver, CO, 05-08 October.

51. Palacio, J.C. and Blasingame, T.A.: "Decline Curve Analysis Using Type Curves — Analysis of Gas Well Production Data," paper SPE 25909 presented at the 1993 Joint Rocky Mountain Regional/Low Permeability Reservoirs Symposium, Denver, CO, 26-28 April.

APPENDIX A

DERIVATION OF THE CONVOLUTION INTEGRAL EQUATION

In this appendix we are going to derive the continuous form of the equation for the pressure drop response function under variable rate effects. If a series of discrete changes are present in rate data acting over a particular interval, wellbore pressure profile is affected by these rate changes. And the total pressure change is the sum of previous pressure drops. This total pressure drop is given as (superposition principle):

$$\Delta p(t) = p_i - p_{wf,n} = (p_i - p_{wf,1}) + (p_{wf,1} - p_{wf,2}) + (p_{wf,2} - p_{wf,3}) + \ldots\ldots\ldots\ldots\ldots\ldots + (p_{wf,n-1} - p_{wf,n}) \quad \text{.....(A-1)}$$

Pressure drop over a particular interval $(p_{wf,j-1} - p_{wf,j})$ is equal to the pressure drop for a unit rate $p_u(t\text{-}t_{j-1})$ multiplied by the rate difference over the interval $(q_j - q_{j-1})$.

$$(p_{wf,j-1} - p_{wf,j}) = (q_j - q_{j-1}) p_u(t - t_{j-1}) \quad \text{.....(A-2)}$$

If we combine Eqs. A-1 and A-2, then we have

$$(p_i - p_{wf,n}) = \sum_{j=1}^{n} (q_j - q_{j-1}) p_u(t - t_{j-1}) \quad \text{.....(A-3)}$$

Where $p_u(t\text{-}t_{j-1})$ is the unit/constant rate pressure solution. We develop a continuous or integral form of the equation by defining $\tau = t_{j-1}$ and $\Delta\tau = t_j - t_{j-1}$ and multiplying the summation term by $\Delta\tau/\Delta\tau$ which gives

$$(p_i - p_{wf,n}) = \sum_{j=1}^{n} \frac{\Delta q}{\Delta \tau} p_u(t - \tau) \Delta\tau \quad \text{.....(A-4)}$$

Taking the limit as $\Delta\tau \rightarrow 0$, we have

$$(p_i - p_{wf,n}) = \lim_{\Delta\tau \to 0} \sum_{j=1}^{n} \frac{\Delta q}{\Delta \tau} p_u(t - \tau) \Delta\tau \quad \text{.....(A-5)}$$

or

$$p_i - p_{wf}(t) = \int_0^t q'(\tau) p_u(t - \tau) d\tau \quad \text{.....(A-6)}$$

This equation is equal to the equation below.

$$p_i - p_{wf}(t) = \int_0^t q(\tau) p_u'(t-\tau) d\tau \quad \text{.....(A-7)}$$

To prove this we are going to use integration by parts. Integration by parts is defined as

$$\int u\, dv = uv - \int v du \quad \text{.....(A-8)}$$

In our case (Eq. A-6), $u = p_u(t-\tau)$ and $dv = q'(\tau)d\tau$. Consequently, $du = - p'_u(t-\tau)\, d\tau$ and $v = q(\tau)$. This gives

$$p_i - p_{wf}(t) = (q(0) p_u(t) - q(t) p_u(0)) + \int_0^t q(\tau) p_u'(t-\tau) d\tau \quad \text{.....(A-9)}$$

Since $q(0) = 0$ and $p_u(0) = 0$, the above equation will reduce to

$$p_i - p_{wf}(t) = \int_0^t q(\tau) p_u'(t-\tau) d\tau \quad \text{.....(A-10)}$$

APPENDIX B

PROPERTIES OF B-SPLINES AND LAPLACE TRANSFORM OF B-SPLINES

In this appendix we are going to define the important properties of B-splines. First, we start with the support of B-splines. Support of the B-splines is defined as the non-zero value of the *k*-th order $B_i^k(t)$. The *k*-th order $B_i^k(t)$ has a support between the interval (t_i, t_{i+k+1}). If *t* is in the interval (t_i, t_{i+k+1}), then $B_i^k(t)>0$ for all values of *t*.

If the degree if the B-spline, *k*, is greater equal than 1 (one), then we have the property of "partition of unity" for B-splines which is defined as:

$$\sum_{i=-\infty}^{\infty} B_i^k(t) = 1 \quad \text{.....(B-1)}$$

The derivatives of B-spline functions exist and can be calculated as[27] (for higher orders than first-order B-splines):

$$\frac{d}{dt} B_i^k(t) = \left(\frac{k}{t_{i+k} - t_i}\right) B_i^{k-1}(t) - \left(\frac{k}{t_{i+k+1} - t_{i+1}}\right) B_{i+1}^{k-1}(t) \quad \text{.....(B-2)}$$

If $df(t)/dt$ is the derivative of function, $f(t)$ with respect to *t*, then this derivative function can also be written in terms of linear combination of B-splines:

$$\frac{df(t)}{dt} \approx \sum_{i=l}^{u} c_i \frac{d}{dt} B_i^k(t) \quad \text{.....(B-3)}$$

Integrals of B-spline functions are calculated by the given formula below[27]:

$$B_{int}^k(t) = \int_{-\infty}^{t} B_i^k(x)dx = \left(\frac{t_{i+k-1}}{k+1}\right) \sum_{j=i}^{\infty} B_j^{k+1}(t) \quad \text{.....(B-4)}$$

Similarly, integral of the function, $f(t)$ can be written as:

$$\int_0^t f(x)dx \approx \sum_{i=l}^{u} c_i B_{int}^k(t) \quad \text{.....(B-5)}$$

The zero-th zero order B-spline (defined over logarithmically spaced knots with basis $b > 1$) is given by Eq. B.6, where $\theta(x)$ denotes the Heaviside function. In addition we provide the zero-th first and second order B-splines in Eqs. B.7 and B.8. The Laplace transform of the zero-th quadratic B-spline can be written in a compact form (Eq. B.9). In **Figs. B.1, B.2,** and **B.3** we show two B-splines (of orders 0,1,and, 2, basis $b = 2$ and indices 0 and 1) — we note that the zero-th index B-spline is non-zero only in the interval (1,8) for quadratic B-splines (similarly first index quadratic B-spline is non-zero only in the interval (2,16)). An interesting property is that the Heaviside function can be represented as the sum of all B-splines with indices from negative to positive infinity (this is the "partition of unity" property which was mentioned before).

$$B_0^0(t) = \theta(t-1) - \theta(t-b) \quad \text{.....(B-6)}$$

$$B_0^1(t) = \frac{b(t-1)\theta(t-1) + (b+1)(b-t)\theta(t-b) + (t-b^2)\theta(t-b^2)}{(b-1)b} \quad \text{.....(B-7)}$$

$$B_0^2(t) = \frac{b^3(t-1)^2\theta(t-1) + (b^2+b+1)(-b(b-t)^2\theta(t-b) + (b^2-t)^2\theta(t-b^2))}{(b-1)^2 b^3(1+b)} - \frac{(b^3-t)^2\theta(t-b^3)}{(b-1)^2 b^3(1+b)} \quad \text{.....(B-8)}$$

$$\bar{B}_0^2(s) = \frac{2e^{(-1-b-b^2-b^3)s}(b^3 e^{b(1+b+b^2)s} + (1+b+b^2)e^{b(1+b+b^2)s}}{(b-1)^2 b^2(b+1)s^2} - \frac{2e^{(-1-b-b^2-b^3)s}(e^{(1+b+b^2)s} + b(1+b+b^2)e^{(1+b+b^2)s}}{(b-1)^2 b^2(b+1)s^2} \quad \text{.....(B-9)}$$

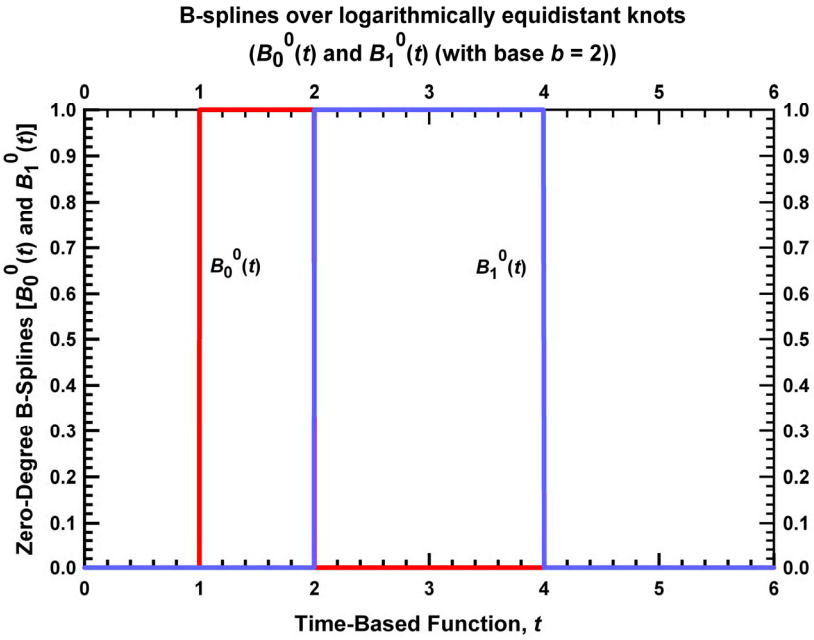

Figure B.1 – B-splines over logarithmically equidistant knots, $B_0^0(t)$ and $B_1^0(t)$ (with base $b = 2$).

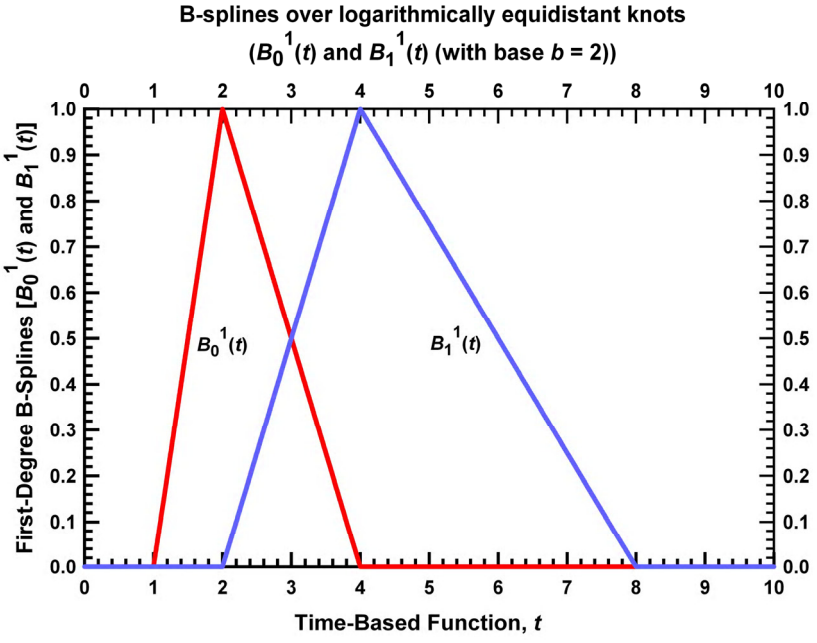

Figure B.2 – B-splines over logarithmically equidistant knots, $B_0^1(t)$ and $B_1^1(t)$ (with base $b = 2$).

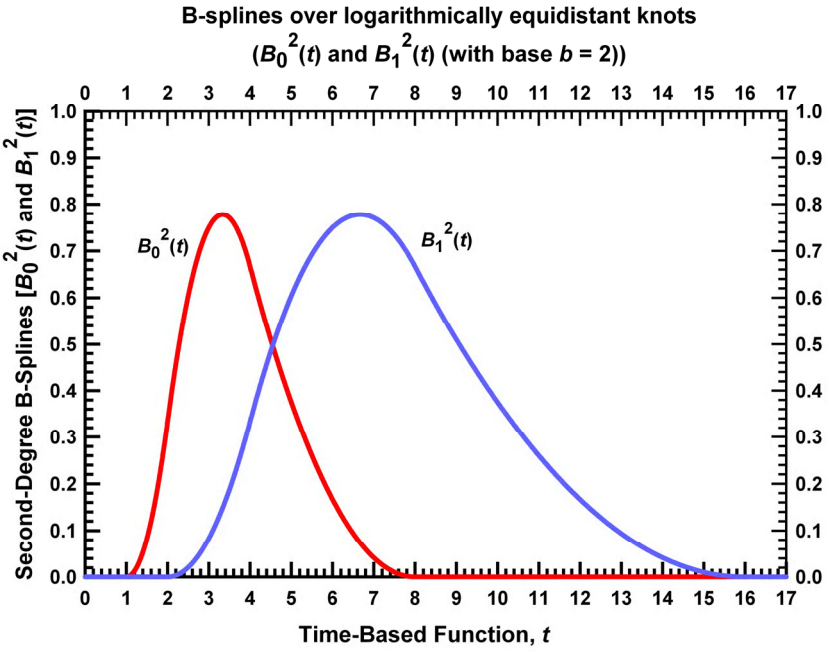

Figure B.3 – B-splines over logarithmically equidistant knots, $B_0^2(t)$ and $B_1^2(t)$ (with base $b = 2$).

APPENDIX C

PSEUDOINVERSE AND REGULARIZATION

If we have a set of linear system of equations given below,

$$\mathbf{A}\mathbf{x} = \mathbf{b} \quad \text{..... (C.1)}$$

Where **A** is (*m* x *n*) matrix and **b** is a column vector of length *n* and **x** is the *n* length column vector of unknown coefficients. Transpose of a matrix is a matrix produced by turning rows into columns, transpose of matrix **A** is $\mathbf{A}^T$ where $\mathbf{A}^T$ has dimensions (*n* x *m*). Inverse of matrix **A** exists if matrix **A** is a square matrix (*i.e.* $m = n$) and it has full rank. If we suppose matrix **A** is invertible then the solution of Eq. C.1 is given as

$$\begin{aligned} (\mathbf{A}^T\mathbf{A})\,\mathbf{x} &= \mathbf{A}^T\mathbf{b} \\ \mathbf{x} &= (\mathbf{A}^T\mathbf{A})^{-1}\mathbf{A}^T\mathbf{b} \end{aligned} \quad \text{..... (C.2)}$$

In this case **x** is the unique solution of this linear system of equations. If ($m > n$) and matrix **A** is not invertible, we can either have an over-determined ($m>n$) or under-determined ($n>m$) system and it is inconsistent. In addition, matrix **A** can be an ill-conditioned matrix. Under these circumstances the system of equations (Eq. C.1) can be solved by means of *Least-Squares* which is minimizing the error between the two column vectors **Ax** and **b**. It is based on a linear model for the system. Column vector **x** contains variables in the model and column vector **b** contains the experimental measurements. In most cases, *e.g.* $m>n$ (more rows than columns) **Ax** does not exactly equal **b**, (*i.e.* **b** does not lie in the column space of **A**). The system of equations is inconsistent (*i.e.* more than one solutions). The objective of least-squares is to find a *regular* solution vector **x'** that solves the system with minimum error. The solution for least-squares is given as:

$$\mathbf{x}' = (\mathbf{A}^T\mathbf{A})^{-1}\mathbf{A}^T\mathbf{b} \quad \text{..... (C.3)}$$

Since matrix **A** is not invertible (due to conditions described above), a generalization for the inverse of matrix **A** is used. This is called the *pseudoinverse* of a matrix. In other words, pseudoinverse provides a least squares solution (*best* solution/approximation) to a system of linear equations. Pseudoinverse exists for all matrices whose entries are real or complex numbers.

When **A** is rank (rank of the matrix is the number of independent number of rows or columns) deficient (or has more columns than rows), small changes (perturbations) in vector **b** will yield very different solution vectors, **x**. This is called an ill-conditioned problem. Converting an ill-conditioned problem into well-conditioned problem is called regularization and in this case pseudoinverse provides regularization (*i.e.* gives more stable solution) in the sense of least-squares.

Pseudoinverse of matrix **A** is given as:

$$\mathbf{A}^{+} = (\mathbf{A}^{T}\mathbf{A})^{-1}\mathbf{A}^{T} \quad \text{(C.4)}$$

and the solution by pseudoinverse is:

$$\mathbf{x}^{+} = \mathbf{A}^{+}\mathbf{b} \quad \text{(C.5)}$$

In simple terms, $\mathbf{x}^{+}$ is the optimal solution of the linear system of equations which is ill-conditioned and matrix $\mathbf{A}^{+}$ which gives $\mathbf{x}^{+}$ is called the pseudoinverse of matrix **A**. Pseudoinverse of a matrix can be calculated by *singular value decomposition*. Before proceeding to singular value decomposition, we are going to define the solution of the system (Eq. C.1) when weights are used. This case is known as weighted least squares and different weights can be associated when some observations are more accurate than others. The weighted linear system of equations can be written as:

$$\mathbf{W}\mathbf{A}\mathbf{x} = \mathbf{W}\mathbf{b} \quad \text{(C.6)}$$

where W is a *diagonal matrix* with the weighting factors on the diagonal. The solution is going to be:

$$\begin{aligned} &(\mathbf{WA})^{T}(\mathbf{WA})\mathbf{x} = (\mathbf{WA})^{T}\mathbf{W}\mathbf{b} \\ &\mathbf{x} = ((\mathbf{WA})^{T}(\mathbf{WA}))^{-1}(\mathbf{WA})^{T}\mathbf{W}\mathbf{b} \end{aligned} \quad \text{(C.7)}$$

As mentioned before we can compute the pseudoinverse of a matrix by singular value decomposition. Singular value decomposition of matrix **A** is:

$$\mathbf{A} = \mathbf{U}\mathbf{S}\mathbf{V}^{T} \quad \text{(C.8)}$$

where **U** is (m x m) orthogonal matrix whose columns are eigenvectors of ($\mathbf{AA}^{T}$). Similarly, **V** is (n x n) orthogonal matrix whose columns are eigenvectors of ($\mathbf{A}^{T}\mathbf{A}$). Matrix **S** (m x n) is a diagonal matrix (same size as **A**) and its entries are called sigma, $\sigma_1,\sigma_2,.....,\sigma_r$ are the square roots of the nonzero eigenvalues of ($\mathbf{AA}^{T}$) and ($\mathbf{A}^{T}\mathbf{A}$). σ are called the *singular values* of **A** and they fill the first r (r is the rank of matrix A) places on the main diagonal of **S**. After calculating the singular value decomposition of **A** then the pseudoinverse of matrix is defined as

$$\mathbf{A}^{+} = \mathbf{V}\mathbf{S}^{+}\mathbf{U}^{T} \quad \text{(C.9)}$$

The reciprocals of singular values $1/\sigma_1,1/\sigma_2,.....,1/\sigma_r$ are on the diagonals of $\mathbf{S}^{+}$ (n x m). The optimum solution to, $\mathbf{Ax} = \mathbf{b}$ is then $\mathbf{x}^{+} = \mathbf{VS}^{+}\mathbf{U}^{T}\mathbf{b}$.

In B-spline based deconvolution algorithm we have *m* drawdown observations collected in a vector $\Delta\tilde{\mathbf{p}}$ that were observed at times ($\tilde{\mathbf{t}}_1, \tilde{\mathbf{t}}_2, \ldots \tilde{\mathbf{t}}_m$) and then the problem can be written as an over-determined system of linear equations:

$$\mathbf{W}\,\mathbf{X}\,\mathbf{c} = \mathbf{W}\,\Delta\tilde{\mathbf{p}} \quad \text{..... (C.10)}$$

Where **X** is the *m* x *n* sensitivity matrix and **c** is the *n*-vector of unknown coefficients and **W** is the *m* x *m* diagonal weighting matrix. Least squares solution for this system is written as

$$\mathbf{c}^{+} = ((\mathbf{WX})^{T}(\mathbf{WX}))^{-1}(\mathbf{WX})^{T}\,\mathbf{W}\,\Delta\tilde{\mathbf{p}} \quad \text{..... (C.11)}$$

For simplicity if we take **W** as unity, then the least square formulation and the solution by pseudoinverse is given respectively:

$$\begin{pmatrix} x_{j,i} & x_{j,i+1} & \cdots & x_{j,i+n} \\ \vdots & \cdots & x_{j+1,i+n-1} & \vdots \\ \vdots & \cdots & \cdots & \vdots \\ \vdots & \cdots & \cdots & \vdots \\ \vdots & \cdots & \cdots & \vdots \\ \vdots & \cdots & \cdots & \vdots \\ \vdots & \cdots & x_{j+m-2,i+n-1} & \vdots \\ \vdots & x_{j+m-1,i+1} & \cdots & \vdots \\ x_{j+m,i} & \cdots & \cdots & x_{j+m,i+n} \end{pmatrix} \begin{pmatrix} c_i \\ c_{i+1} \\ \vdots \\ c_{i+n} \end{pmatrix} = \begin{pmatrix} \Delta p_{w\,j} \\ \Delta p_{w\,j+1} \\ \vdots \\ \vdots \\ \vdots \\ \vdots \\ \vdots \\ \Delta p_{w\,j+m} \end{pmatrix} \quad \text{..... (C.12)}$$

$$\mathbf{c}^{+} = \mathbf{X}^{+}\,\Delta\tilde{\mathbf{p}} \quad \text{..... (C.13)}$$

Where $x_{j,i}$ are the elements of the sensitivity matrix and $\mathbf{X}^{+}$ is the pseudoinverse of the sensitivity matrix **X** and is calculated by singular value decomposition.

Solving for **c** by pseudoinverse in the above equation does not provide sufficient regularization as the noise level increases in the data. Therefore, we need additional regularization which makes sense in a physical context and ensures the relevance of the spline representation. For the over-determined system (Eq. C.10) to be solved by least squares, for each spline interval we must append the following two conditions:

$$\alpha \left[\left(t \sum_{i=l}^{u} c_i B_i^2(t) \right)_{t=t_k} - \left(t \sum_{i=l}^{u} c_i B_i^2(t) \right)_{t=t_{k+1/2}} \right] = 0$$

$$\alpha \left[\left(t \sum_{i=l}^{u} c_i B_i^2(t) \right)_{t=t_{k+1/2}} - \left(t \sum_{i=l}^{u} c_i B_i^2(t) \right)_{t=t_{k+1}} \right] = 0$$

..... (C.14)

In other words, we require that the value of the logarithmic derivative of the constant-rate response differ only "slightly" between the knot and the middle location between knots. When α = 0, there is no regularization, and with generated data with practically no error, α = 0 results in the required smooth solution for the constant-rate response and its logarithmic derivative. In the presence of random noise and/or other inconsistencies, a positive α is selected based on an informal interpretation of the discrepancy principle — *i.e.*, we increase the value of the regularization parameter until the calculated (model) pressure difference begins to deviate from the observed pressure difference in a specific manner.

If we take the above conditions, an additional system of equations can be defined as:

$$\mathbf{X}_r \ \mathbf{c} = 0 \quad \text{..... (C.15)}$$

$$\begin{pmatrix} t_j(B_i^2(t_j) - B_i^2(t_{j+1/2})) & \cdots & \cdots & t_j(B_{i+n}^2(t_j) - B_{i+n}^2(t_{j+1/2})) \\ \vdots & \cdots & \cdots & \vdots \\ \vdots & \cdots & \cdots & \vdots \\ \vdots & \cdots & \cdots & \vdots \\ \vdots & \cdots & \cdots & \vdots \\ \vdots & \cdots & \cdots & \vdots \\ \vdots & \cdots & \cdots & \vdots \\ \vdots & \cdots & \cdots & \vdots \\ t_{j+k}(B_i^2(t_{j+k}) - B_i^2(t_{j+k+1/2})) & \cdots & \cdots & t_{j+k}(B_{i+n}^2(t_{j+k}) - B_{i+n}^2(t_{j+k+1/2})) \end{pmatrix} \begin{pmatrix} c_i \\ c_{i+1} \\ \vdots \\ c_{i+n} \end{pmatrix} = \begin{pmatrix} 0 \\ 0 \\ \vdots \\ \vdots \\ \vdots \\ \vdots \\ \vdots \\ 0 \end{pmatrix}$$

..... (C.16)

where $\mathbf{X}_r$ is (k x n) matrix — k is the number of points where logarithmic derivative of the constant-rate response (spline formulation in Eq. C.14) is evaluated, it starts at first knot index (l) and it ends at the last knot index (u) and increases with ½ increment of the index (t_l, $t_{l+1/2}$, ……t_1,$t_{1+1/2}$,t_2, ……$t_{u-1/2}$,t_u). n is the number of unknown c coefficients in other words it is the

number of B-splines. We solve $\mathbf{X}\,\mathbf{c} = \Delta\mathbf{p}$ and $\mathbf{X}_r\,\mathbf{c} = 0$ together:

$$\begin{matrix}(1-\alpha)\,\mathbf{X}\,\mathbf{c} = (1-\alpha)\Delta\tilde{\mathbf{p}} \\ \alpha\,\mathbf{X}_r\,\mathbf{c} = 0\end{matrix} \quad \text{..... (C.17)}$$

Finally, a new system of equations is obtained as

$$\mathbf{X}^*\,\mathbf{c} = \Delta\tilde{\mathbf{p}}^* \quad \text{..... (C.18)}$$

$\mathbf{X}^*$ is obtained by joining (1-α) $\mathbf{X}$ and $\alpha\,\mathbf{X}_r$ and its dimensions are ((m+k) x n) and $\Delta\tilde{\mathbf{p}}^*$ is obtained by joining $(1-\alpha)\Delta\tilde{\mathbf{p}}$ and 0 (including k elements). Basically $\Delta\tilde{\mathbf{p}}^*$ will be a (m+k) column vector. The same procedure is followed (least squares solution by pseudoinverse) after performing these operations. In another point of view we are adding k additional degrees of freedom to solve the system with additional regularization.

APPENDIX D

TEST OF NEW DECONVOLUTION METHOD FOR ONLY PRESSURE BUILDUP DATA

In this appendix we will address the issues when there are significant differences between the durations of drawdown and buildup tests. For our purposes we have generated 2 (two) synthetic cases where we select a simple homogeneous reservoir model with wellbore storage effects for simplicity. The properties for the base reservoir model are provided in **Table D.1**:

Table D.1 – Reservoir and fluid properties for Cases D1-D4

Reservoir Properties:		
Wellbore radius, r_w	=	0.3 ft
Net pay thickness, h	=	30 ft
Formation permeability, k	=	3.333334 md
Total compressibility, c_t	=	1×10^{-5} 1/psi
Porosity, ϕ	=	0.15 (fraction)
Outer boundary radius, r_e	=	480 ft
Initial reservoir pressure, p_i	=	4800 psi
Wellbore storage coefficient, C	=	0.001 RB/psi
Skin factor, s_x	=	0 (dim.less)
Fluid Properties:		
Fluid viscosity, μ	=	1 cp
Formation volume factor, B	=	1 RB/STB
Production Parameters:		
Production rate 1, q_1	=	50 STB/D
Production rate 2, q_2	=	25 STB/D

In the first case, a constant rate production of 50 STB/D is held for 5 hours and is followed by 500 hours shut-in. We specifically set the duration of the buildup to be one hundred times larger than the duration of the drawdown in order to establish the difference between deconvolution and conventional pressure buildup analysis when the durations of production sequences are not consistent.

We recognize that this is an extreme test of the algorithm — *i.e.*, to use only pressure buildup data (plus the production history) to yield the equivalent constant rate drawdown response by deconvolution. However, in practice, the primary utility of our algorithm is likely to be the resolution of pressure buildup data. While obvious, it is worth restating that an accurate production history is absolutely critical for deconvolution. **Fig. D.1** presents the input data for deconvolution and pressure buildup analysis.

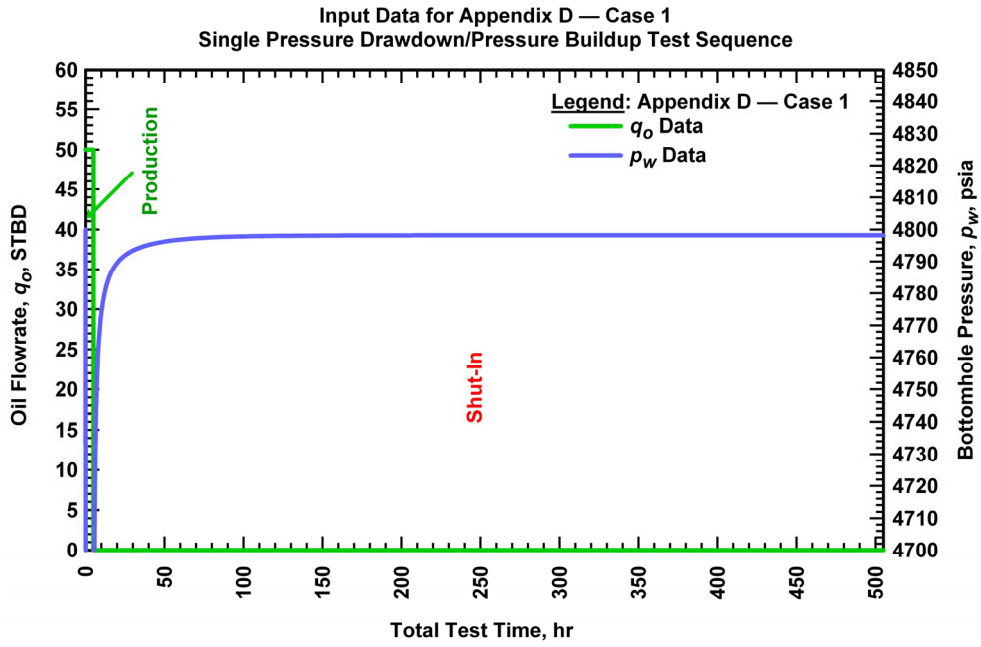

Figure D.1 – Appendix B Case 1: Input data for the first case where the duration of the buildup is hundred times larger than the duration of drawdown.

In **Fig. D.2** we immediately note artifacts in the very late-time pressure derivative of the pressure buildup case, where these artifacts are caused by fact that the reservoir pressure has completely built-up to the limiting value of the average reservoir pressure.

However, our deconvolution method is not affected by this behavior. Using only the pressure buildup data for this case, we perform deconvolution and we then construct the constant rate pressure drawdown response for the entire history. We present the results of the deconvolution as well as the conventional pressure buildup data functions in **Fig. D.2** and we compared these data functions to the correct model responses for each case.

As shown in **Fig. D.3**, for our second case, we add another production and shut-in period to the well test sequence. The duration ratio between both drawdown and build-up sequences is preserved (shut-in duration is hundred times larger than the duration of the drawdown). In this case we use ONLY the data from the final pressure buildup for the deconvolution process. As noted previously, we can construct the constant rate pressure drawdown response for the duration of the buildup using deconvolution. As a caveat, we note that all deconvolution methods require direct knowledge of the initial reservoir pressure (this condition (obviously) also applies to the process of convolution).

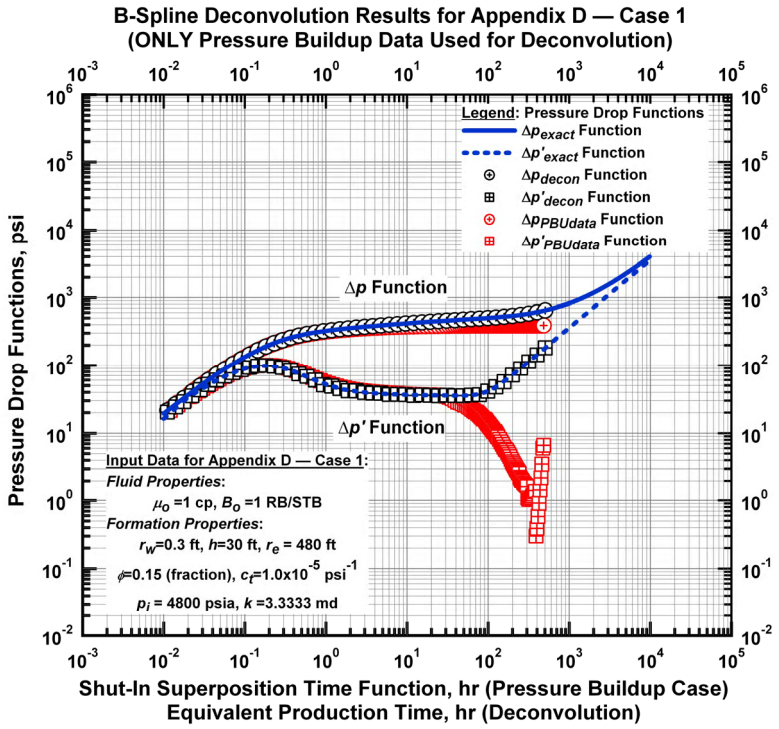

Figure D.2 – Appendix D Case 1: B-Spline deconvolution results for the first case with conventional pressure buildup analysis and exact results (ONLY pressure buildup data are used for deconvolution).

In our work, we require a reference pressure — where this pressure can be the initial reservoir pressure or any (single) pressure taken during production. As a practical point, we suggest that any reference pressure (other than initial reservoir pressure) be taken as early as possible during production.

As such, we use the data from the second (final) pressure buildup and a reference pressure taken a short time into the initial production period as input for deconvolution in this case. The results for this case are presented in **Fig. D.4**.

It is worth noting that using only a single (early production) pressure data point for reference and the pressure buildup data from the second (final) pressure buildup test, we can recover the equivalent constant rate pressure drawdown response for the entire well test sequence using deconvolution.

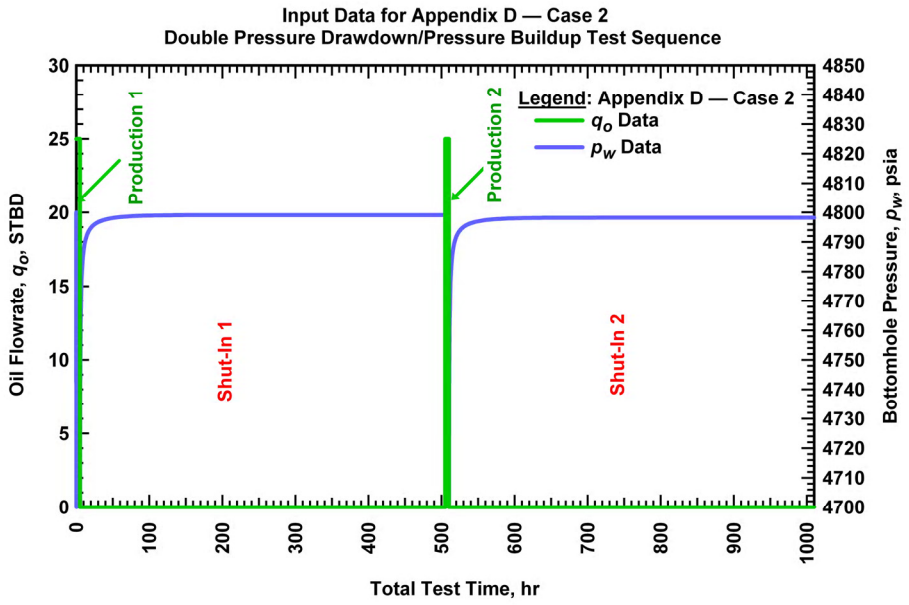

Figure D.3 – Appendix D Case 2: Input data for the second case where the durations of the buildups are hundred times larger than the durations of drawdowns.

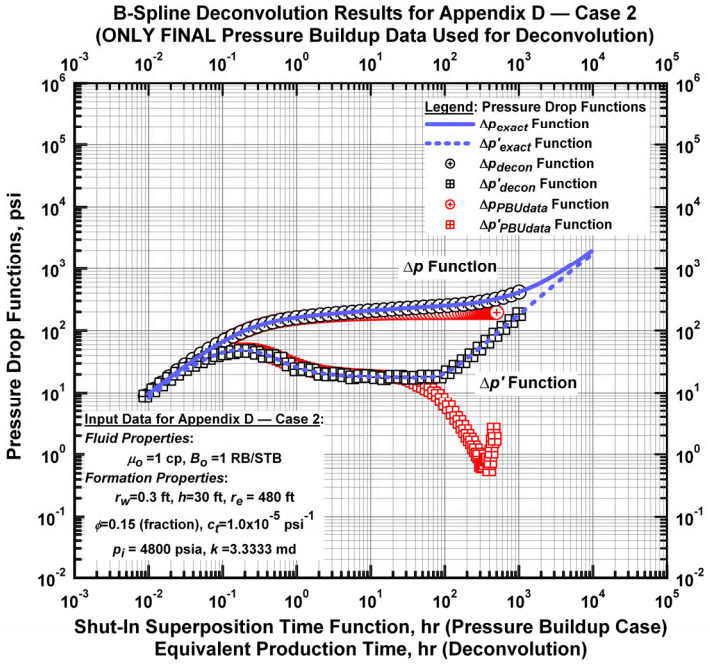

Figure D.4 – Appendix D Case 2: B-Spline deconvolution results for the second case with conventional pressure buildup analysis and exact results (ONLY data from the final pressure buildup are used for deconvolution).

APPENDIX E

VALIDATION OF THE B-SPLINE BASED DECONVOLUTION METHOD USING ADDITIONAL RESERVOIR MODELS

In this appendix, we are going to validate our new B-spline based deconvolution method with additional validation examples. For our purposes we use 4 (four) reservoir models starting from the basic case increasing the complexity in each case. The properties of each reservoir model are given in **Tables E.1 – E.4**. In each case, we presume a production history which contains 2 pressure drawdown sequences (with constant rates) followed by pressure buildup sequences. We perform deconvolution for entire test sequence and generate the constant rate pressure drawdown and well testing derivative functions. Finally, we compare the deconvolved pressure responses with the exact/analytical model solutions.

We note that our deconvolution method performs very well in all these cases as expected. We can conclude from these experiments that no matter how complex the reservoir model is, with deconvolution we can always find the exact solution for the entire time span of data as long as the data is consistent (*i.e.* the linearity of the convolution integral has to be preserved).

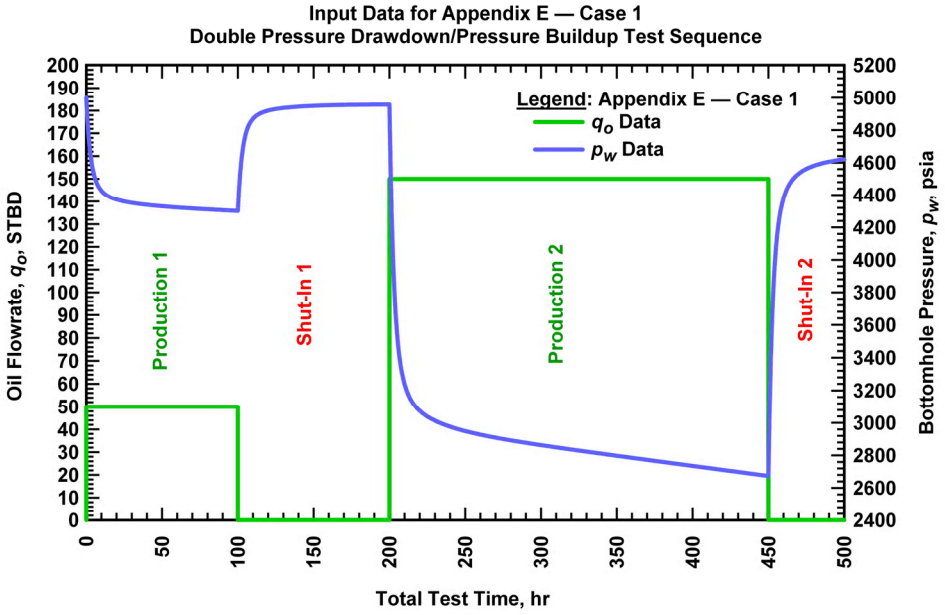

Figure E.1 – Input data for Appendix E Case 1 (Basic case, well with wellbore storage and skin).

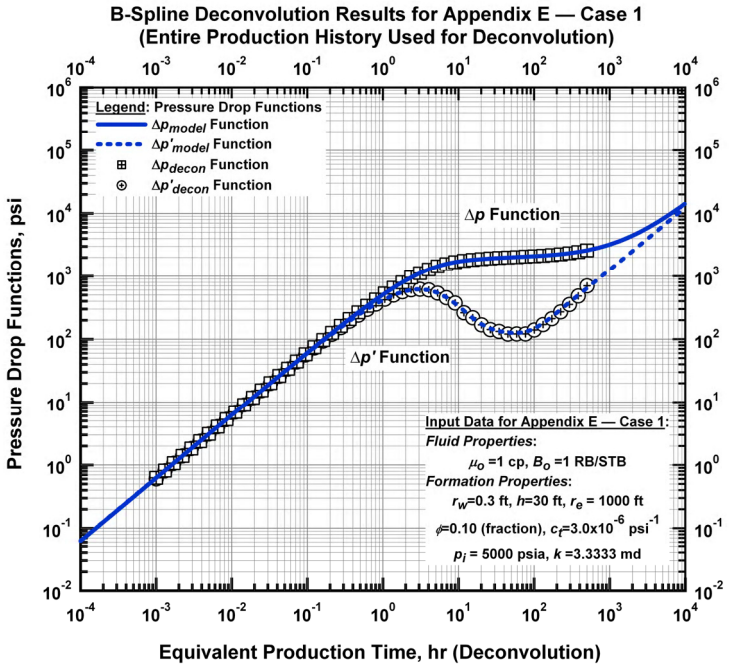

Figure E.2 – Appendix E Case 1: B-Spline deconvolution results for the first case — deconvolved pressure functions for the entire test sequence.

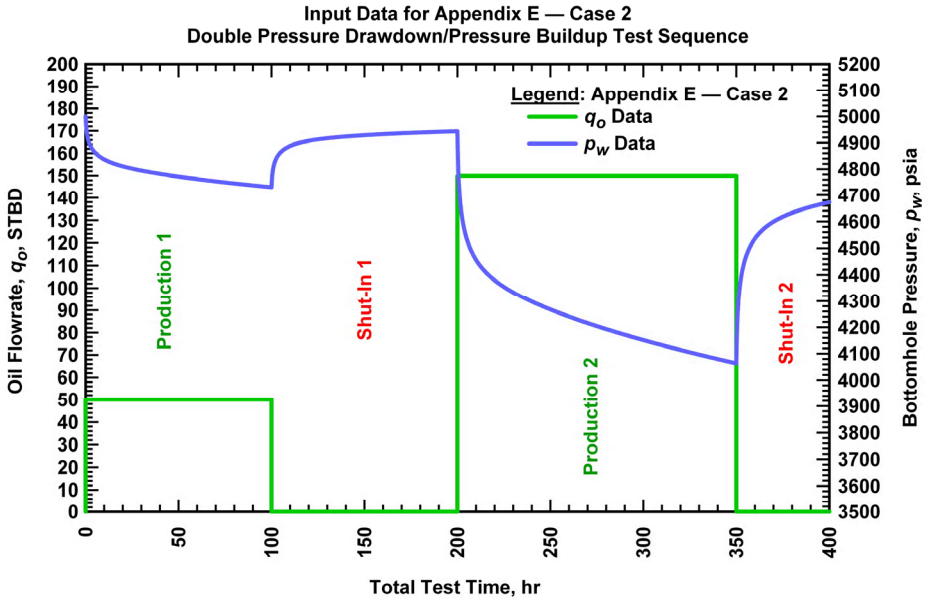

Figure E.3 – Input data for Appendix E Case 2 (well with a vertical fracture in a reservoir having parallel faults).

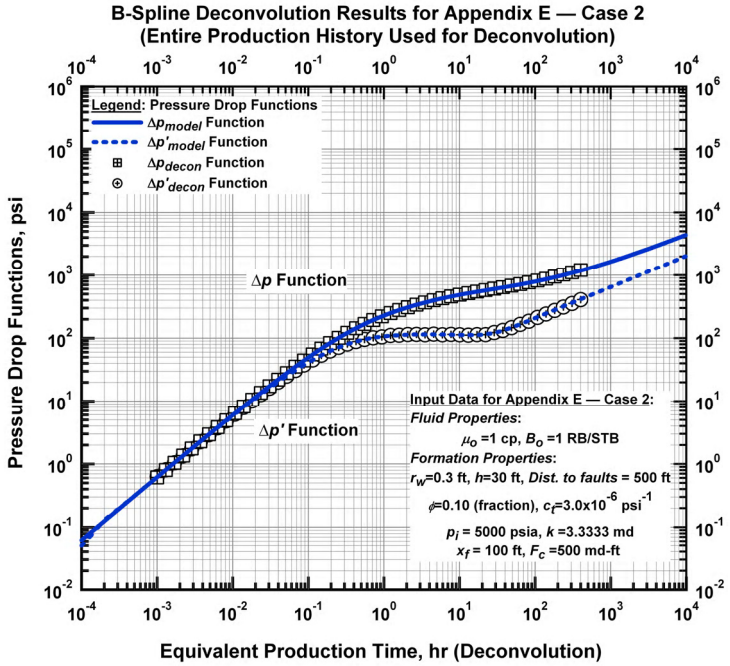

Figure E.4 – Appendix E Case 2: B-Spline deconvolution results for the second case — deconvolved pressure functions for the entire test sequence.

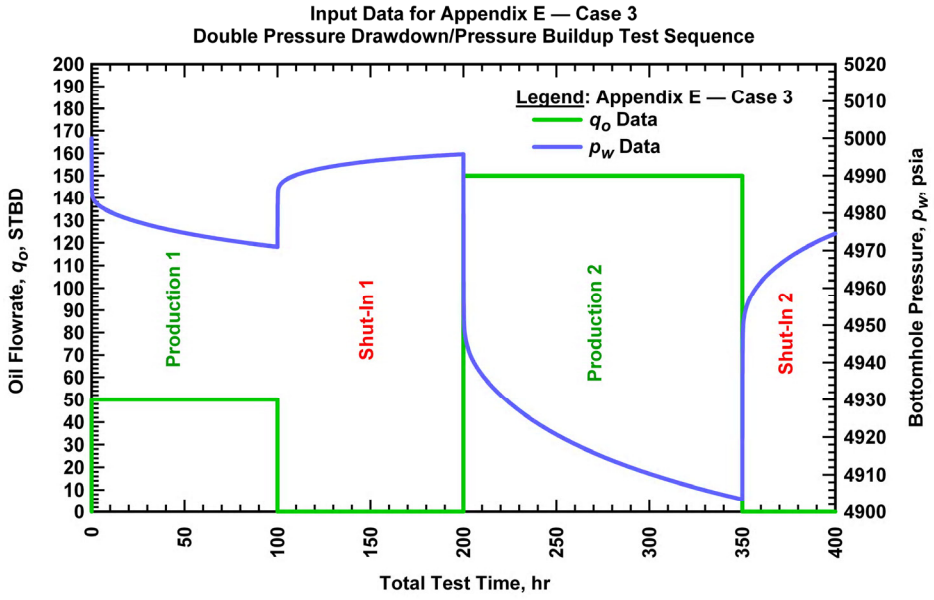

Figure E.5 – Input data for Appendix E Case 3 (horizontal well).

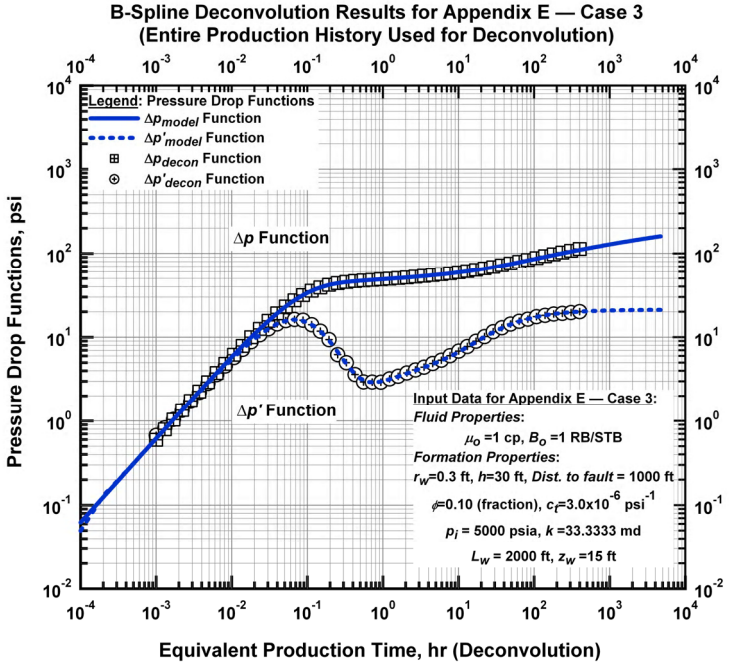

Figure E.6 – Appendix E Case 3: B-Spline deconvolution results for the third case — deconvolved pressure functions for the entire test sequence.

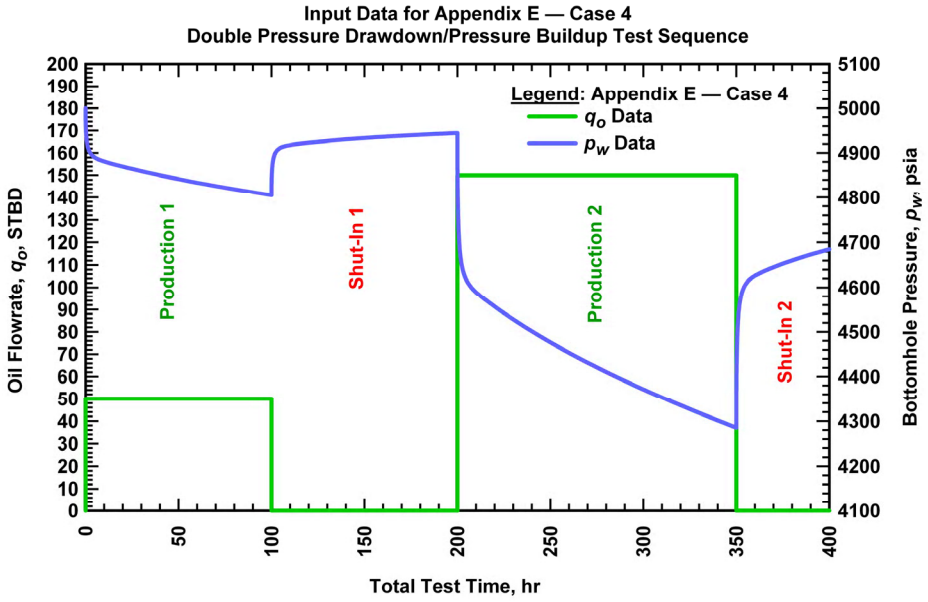

Figure E.7 – Input data for Appendix E Case 4 (well with a vertical fracture in a dual porosity reservoir).

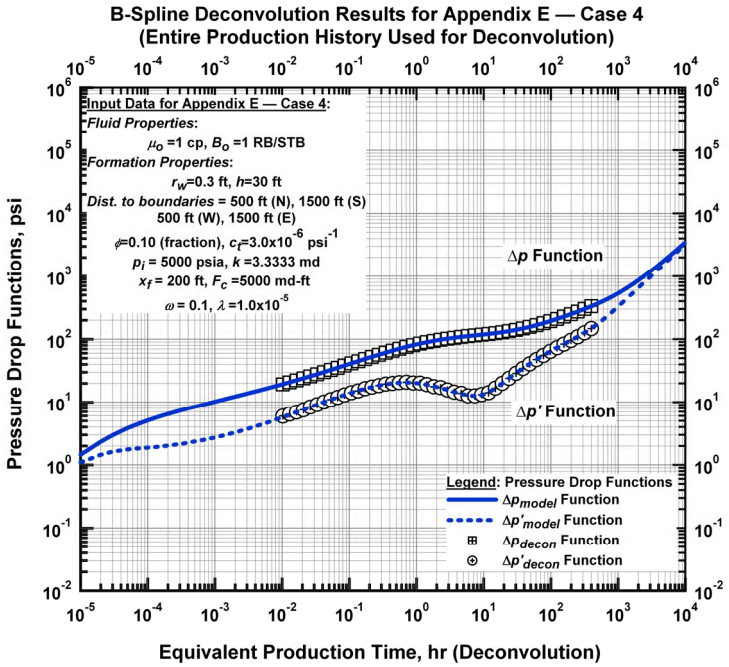

Figure E.8 – Appendix E Case 3: B-Spline deconvolution results for the fourth case — deconvolved pressure functions for the entire test sequence.

Table E.1 – Reservoir and fluid properties for Case E.1 — Wellbore Storage + Skin.

Reservoir Properties:		
Wellbore radius, r_w	=	0.3 ft
Net Pay Thickness, h	=	30 ft
Formation permeability, k	=	3.333334 md
Total compressibility, c_t	=	$3x10^{-6}$ 1/psi
Porosity, ϕ	=	0.10 (fraction)
Outer boundary radius, r_e	=	1000 ft
Initial reservoir pressure, p_i	=	5000 psi
Wellbore storage coefficient, C	=	0.01 RB/psi
Skin factor, s_x	=	2 (dim.less)
Fluid Properties:		
Fluid viscosity, μ	=	1 cp
Formation volume factor, B	=	1 RB/STB
Production Parameters:		
Production rate 1, q_1	=	50 STB/D
Production rate 2, q_2	=	150 STB/D

Table E.2 – Reservoir and fluid properties for Case E.2 — Well with a vertical fracure with parallel faults.

Reservoir Properties:		
Wellbore radius, r_w	=	0.3 ft
Net Pay Thickness, h	=	30 ft
Formation permeability, k	=	3.333334 md
Total compressibility, c_t	=	$3x10^{-6}$ 1/psi
Porosity, ϕ	=	0.10 (fraction)
Distance to fault (North)	=	500 ft
Distance to fault (South)	=	500 ft
Initial reservoir pressure, p_i	=	5000 psi
Wellbore storage coefficient, C	=	0.01 RB/psi
Skin factor, s_x	=	2 (dim.less)
Fracture half length, x_f	=	100 ft
Fracture conductivity, F_c	=	500 ft
Fluid Properties:		
Fluid viscosity, μ	=	1 cp
Formation volume factor, B	=	1 RB/STB
Production Parameters:		
Production rate 1, q_1	=	50 STB/D
Production rate 2, q_2	=	150 STB/D

Table E.3 – Reservoir and fluid properties for Case E.3 — Horizontal well.

Reservoir Properties:		
Wellbore radius, r_w	=	0.3 ft
Net Pay Thickness, h	=	30 ft
Formation permeability, k	=	33.333334 md
Total compressibility, c_t	=	3×10^{-6} 1/psi
Porosity, ϕ	=	0.10 (fraction)
Distance to fault	=	1000 ft
Initial reservoir pressure, p_i	=	5000 psi
Wellbore storage coefficient, C	=	0.01 RB/psi
Skin factor, s_x	=	2 (dim.less)
Well length, L_w	=	2000 ft
Distance to the bottom of formation, z_w	=	15 ft
Ratio of vertical to radial permeability, k_z/k_r	=	1 (fraction)
Fluid Properties:		
Fluid viscosity, μ	=	1 cp
Formation volume factor, B	=	1 RB/STB
Production Parameters:		
Production rate 1, q_1	=	50 STB/D
Production rate 2, q_2	=	150 STB/D

Table E.4 – Reservoir and fluid properties for Case E.4 — Dual porosity reservoir with a vertical fracture having rectangular boundaries

Reservoir Properties:		
Wellbore radius, r_w	=	0.3 ft
Net Pay Thickness, h	=	30 ft
Formation permeability, k	=	3.333334 md
Total compressibility, c_t	=	3×10^{-6} 1/psi
Porosity, ϕ	=	0.10 (fraction)
Distance to boundary (North)	=	500 ft
Distance to boundary (South)	=	1500 ft
Distance to boundary (East)	=	1500 ft
Distance to boundary (West)	=	500 ft
Initial reservoir pressure, p_i	=	5000 psi
Wellbore storage coefficient, C	=	1×10^{-5} RB/psi
Skin factor, s_x	=	0 (dim.less)
Fracture half length, x_f	=	200 ft
Fracture conductivity, F_c	=	5000 ft
Storativity ratio, ω	=	0.1
Interporosity flow parameter, λ	=	1×10^{-6}
Fluid Properties:		
Fluid viscosity, μ	=	1 cp
Formation volume factor, B	=	1 RB/STB
Production Parameters:		
Production rate 1, q_1	=	50 STB/D
Production rate 2, q_2	=	150 STB/D

APPENDIX F

ADDITIONAL FIELD EXAMPLES OF THE B-SPLINE BASED DECONVOLUTION METHOD

This appendix illustrates the application of the B-spline based deconvolution method to additional field examples. We are going to present the B-spline based deconvolution results for 3 (three) oil wells and 2 (two) gas wells. We note that all of these cases contain "long term" production history. As we have done before in Chapter V, we perform deconvolution and compare the results with "material balance deconvolution" then we proceed and match the results with an appropriate reservoir model.

All of these cases contain "low-frequency" and "low-quality" type of data which makes it extremely difficult for analysis. In particular, we suspect that two oil cases (oil case 1 and oil case 3) have allocated pressure data. For oil case 1 we do not perform material balance deconvolution, since we do not have the sufficient pressure data available. For the gas cases we perform pseudopressure/pseudotime transformation for theoretical considerations.

Under these circumstances, deconvolution performs very well. Naturally, deconvolved pressure responses have been affected by the noise in the data (apparent anomalies in the well testing derivative functions at early time) but generally, deconvolved pressure response functions show good agreement with the material balance deconvolution results and reservoir model solutions. We conclude that these additional examples can be counted as a stronger confirmation of our methodology.

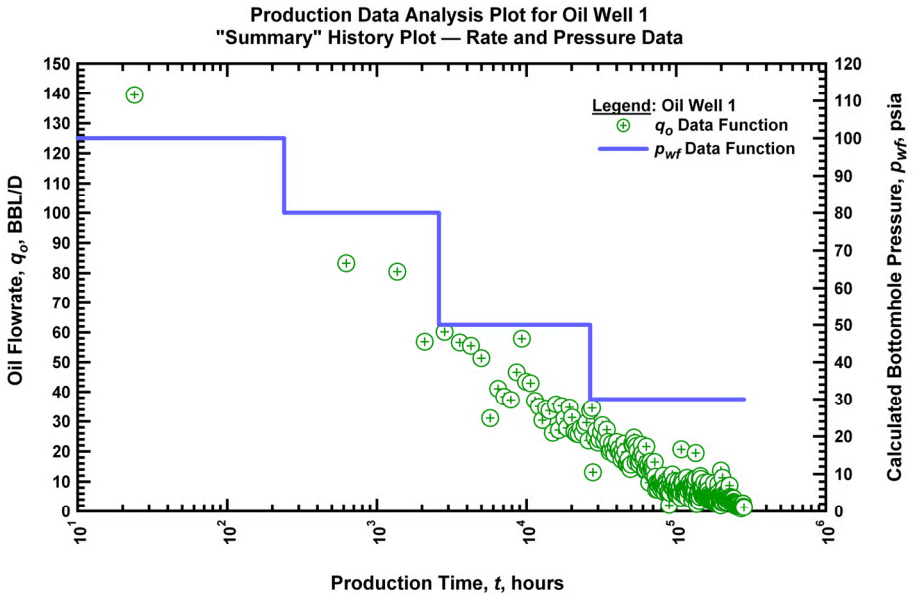

Figure F.1 – Appendix F Case 1 — Production data history plot for Oil Well 1.

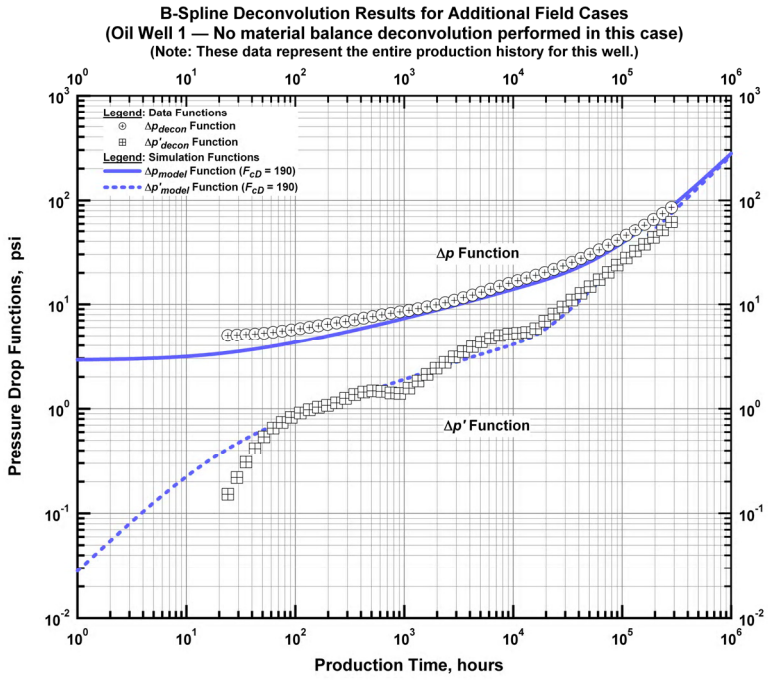

Figure F.2 – Appendix F Case 1 — Deconvolution response functions, and model match (well with a vertical fracture, F_c = 190 md-ft).

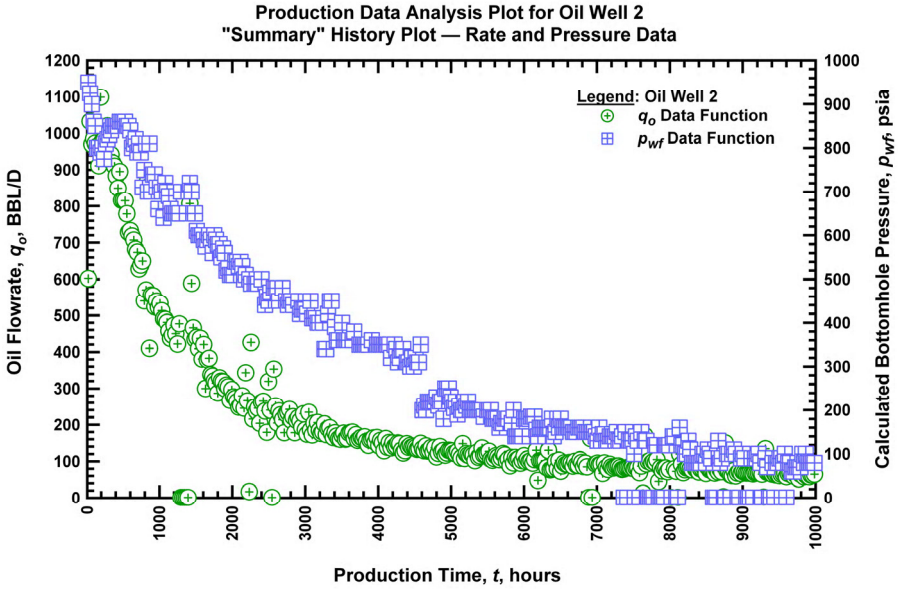

Figure F.3 – Appendix F Case 2 — Production data history plot for Oil Well 2.

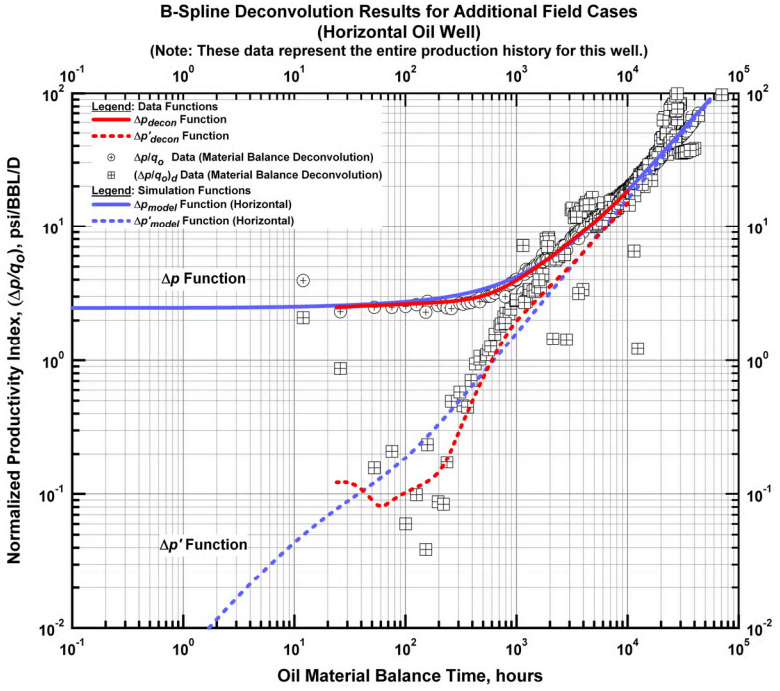

Figure F.4 – Appendix F Case 2 — Deconvolution response functions, model match (horizontal well) and material balance time normalized data.

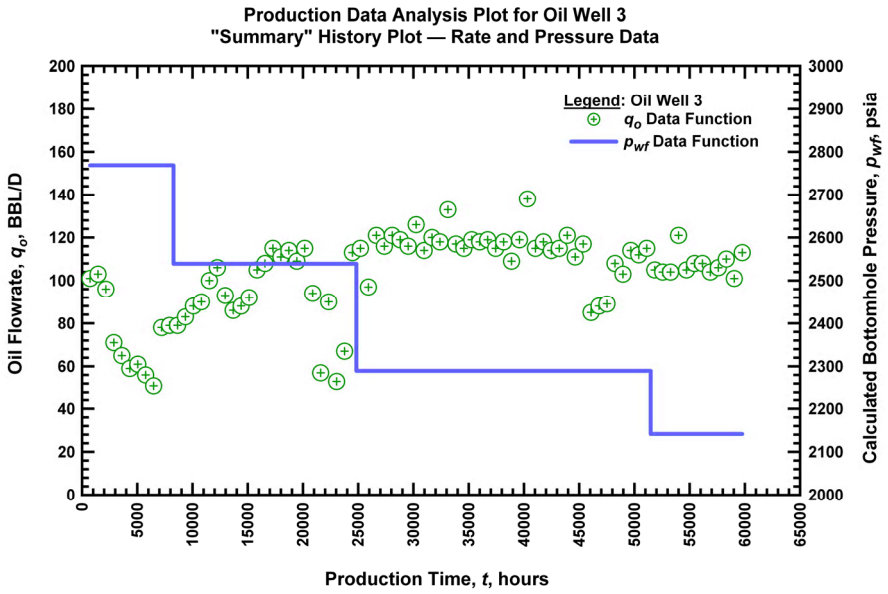

Figure F.4 – Appendix F Case 3 — Production data history plot for Oil Well 3.

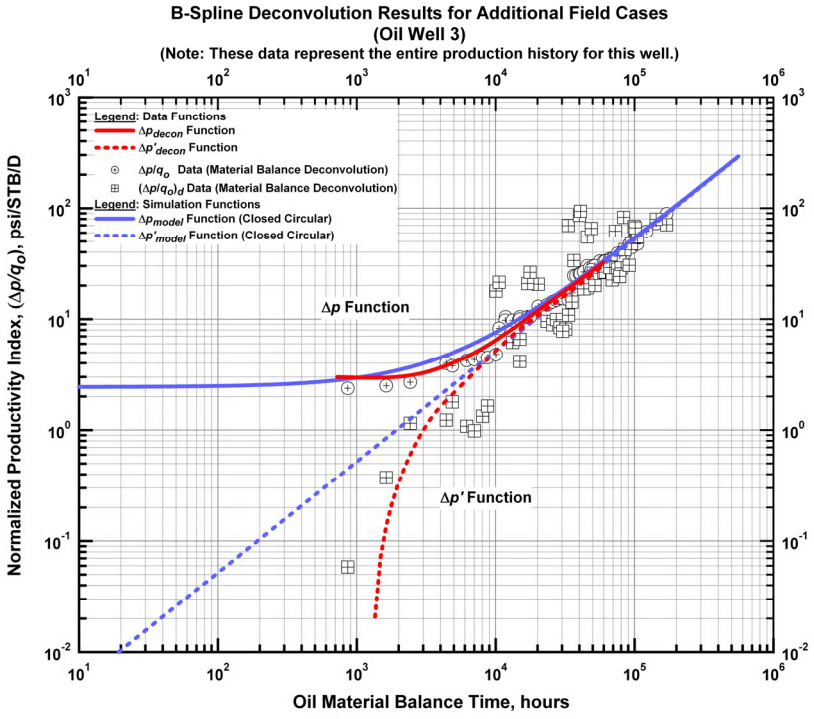

Figure F.5 – Appendix F Case 3 — Deconvolution response functions, model match (homogeneous reservoir with closed circular boundary) and material balance time normalized data.

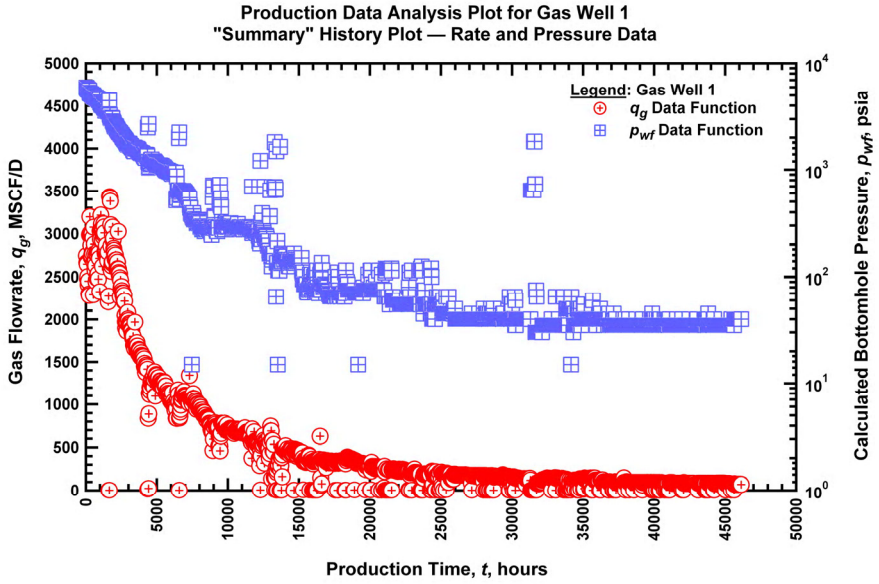

Figure F.6 – Appendix F Case 4 — Production data history plot for Gas Well 1.

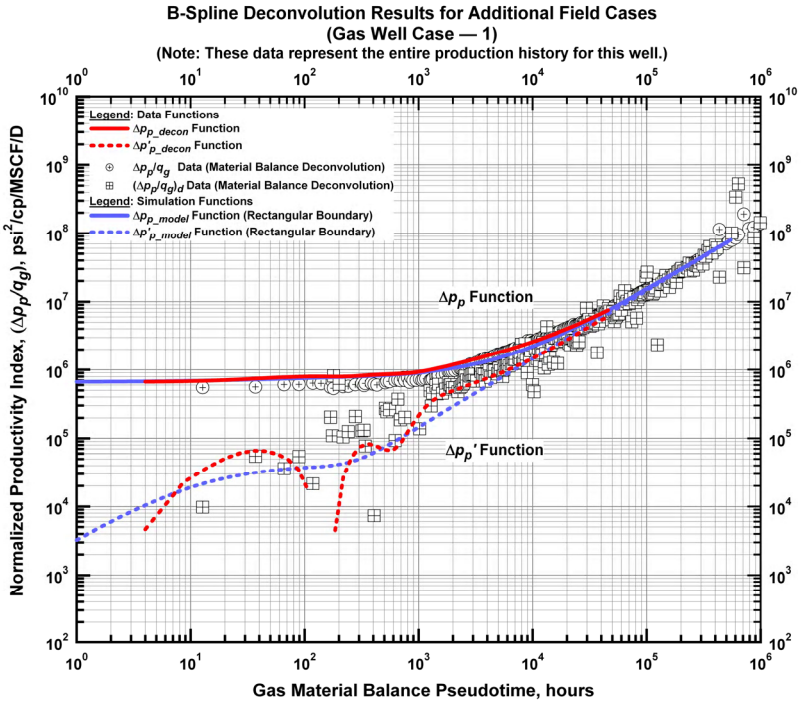

Figure F.7 – Appendix F Case 4 — Deconvolution response functions, model match (homogeneous reservoir with closed rectangular boundaries) and material balance time normalized data.

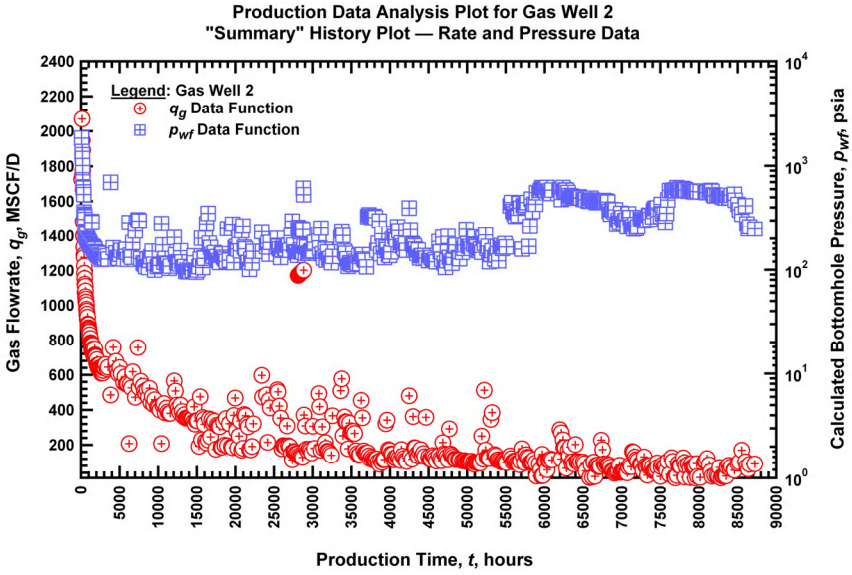

Figure F.8 – Appendix F Case 4 — Production data history plot for Gas Well 2.

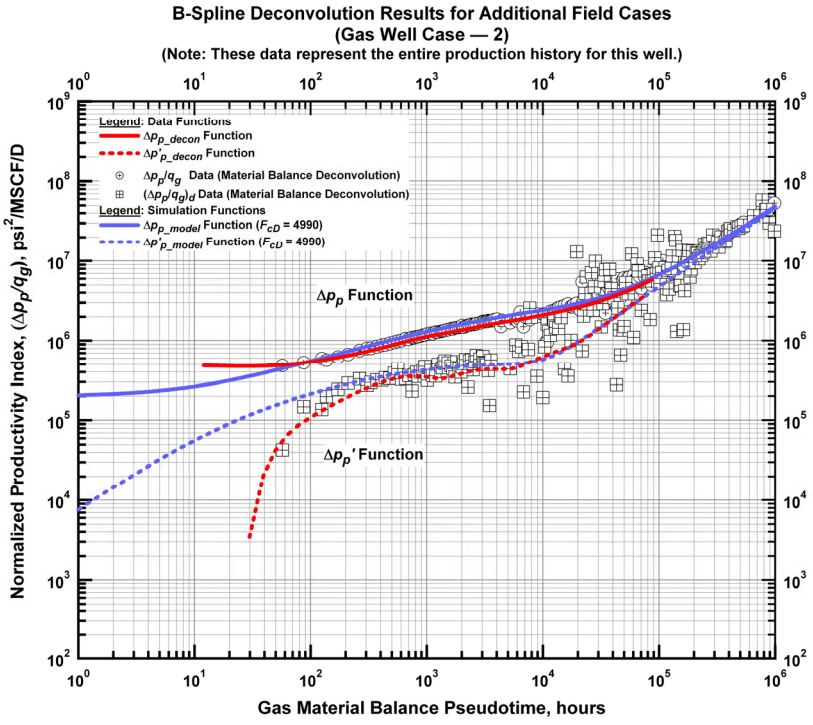

Figure F.9 – Appendix F Case 4 — Deconvolution response functions, model match (well with a vertical fracture, F_c = 4990 md-ft) and material balance time normalized data.

VITA

Name:	Dilhan Ilk
Born:	May 06, 1980 Malkara, Tekirdag, Turkey
Permanent Address:	Acibadem Caddesi, Ibrahimaga Konutlari, A-1 Daire: 15, Acibadem, Kadikoy 34718 Istanbul, Turkey.
Phone:	090-216-3275528
E-mail Address:	dilhan@tamu.edu dilhan@spemail.org
Education:	Texas A&M University, College Station, Texas, USA Master of Science Degree in Petroleum Engineering December 2005 Istanbul Technical University, Istanbul, Turkey Bachelor of Science Degree in Petroleum Engineering June 2003
Affiliations:	Society of Petroleum Engineers